Photoinduced Change in Refractive Index of Functional Polymers for Ophthalmic Applications

Dissertation

zur Erlangung des Doktorgrades
der Naturwissenschaften
(Dr. rer. nat.)

dem
Fachbereich Chemie
der Philipps-Universität Marburg
vorgelegt von

Jens Kristian Träger

aus Sandhausen

Marburg/Lahn 2009

Vom Fachbereich Chemie der Philipps-Universität Marburg
als Dissertation am 20. 04. 2009 angenommen.

Erstgutachter: Prof. Dr. Norbert Hampp
Zweitgutachter: Prof. Dr. Marcus Motzkus

Tag der mündlichen Prüfung (Disputation) am 30. 04. 2009

I have learned to use the word "impossible" with the greatest caution.

Wernher von Braun, 1912 – 1977

Abstract

A cataract is a clouding of the eye's lens that affects vision, causing images to look blurred or fuzzy. It is the leading cause of blindness worldwide with an estimated 50 million people suffering from this illness. Approximately 1.5 million (3%) of cataract patients are children under the age of 16 years. In industrialized countries, about half of the population older than 65 have some degree of clouding of the lens, and after the age of 75 as many as 70% have cataracts. Although the exact causes of cataract formation are still a topic of intense research, it is thought that most cataracts are related to aging and are usually caused by the denaturing of lens proteins, resulting in crystallization of the lens. At present, there are neither scientifically proven measures for prevention of cataracts nor proven pharmaceutical treatments that could heal or at least stop cataract progression. The only way to treat cataract is to surgically remove the cloudy lens. The natural lens is then replaced with an artificial polymeric lens, a so-called intraocular lens (IOL). Cataract surgery is one of the safest, most effective and most common procedures and is performed tens of millions of times every year. However, there are some specific related postoperative problems.

The aim of this work is to overcome one major drawback of IOLs. A typical postoperative complication in cataract surgery is that the refractive power of the implanted IOL is often not sufficient for optimal vision, requiring the patient to use prescription eye wear. This is mainly because the eye is a complex optical system and the biometric data required for the calculation of the IOL's shape cannot be determined with sufficient precision before surgery. In particular, vision is strongly influenced by the radius of curvature of the cornea and the length of the eye ball. In addition, the exact location of the IOL in the capsular bag may change unpredictably during surgery or afterwards while the wound is healing, making the initial IOL design no longer optimal. Analysis of clinical trials indicates that about 80% of cataract patients have post-surgery vision that is within one diopter of the perfect vision (a diopter is a measure of the refractive power of a lens given by the inverse of its focal length), whereas another 10% have an even greater deviation of two or more diopters. In other words, most patients treated with IOLs need prescription eye wear for optimal vision following cataract surgery or the IOL needs to be explanted and changed to a more suitable one in another surgery.

This thesis develops a solution to this problem of poor imaging performance. The focal length of an IOL is tuned postoperatively in a non-invasive manner by changing the refractive index of the implanted lens through a photochemical process. Polymers, sui-

table for the fabrication of an IOL, were synthesized and characterized. These polymers have a specific photo-active linker group attached to the polymer backbone. The linker group mainly used in this work was the coumarin molecule. The carbon-carbon double bonds in the lactone ring of two coumarin molecules readily undergo a $[2\pi + 2\pi]$ cycloaddition reaction to yield a four-membered cyclobutane ring upon irradiation with a suitable UV wavelength. Using a shorter wavelength the photo-dimer may also be cleaved to yield single coumarin molecules again. Photo-induced cross-linking of these photo-active linker molecules leads to a decrease in the IOL's refractive index. This is because the polarizability of the linker molecule, that is related to the refractive index of the polymeric material, is decreased as a result of the formation of the cyclobutane ring. The maximum change in refractive index of the polymers synthesized here is more than 0.03, enabling a fine-tuning of more than 2.5 diopters in a standard IOL. With such postoperative treatment nearly all patients should not need viewing aids after cataract surgery.

Two important steps in the fabrication of polymers actually suitable for IOL manufacturing were successfully developed. First, the insertion of an alkyl spacer molecule between the photo-active coumarin and the methacrylate moiety used to build up the polymer backbone. Second, the free radical bulk polymerization of the molten monomers, which are all solid at room temperature, with an acrylic crosslinker to obtain flexible materials. By alteration of the alkyl spacer length, flexibility of the final material may be tuned. Having a material that is flexible enough to produce an IOL that can be rolled or folded is very important because this allows the insertion of the IOL through a relatively small cut in the eye. This technique does not require any stitching resulting in an accelerated healing process, while reducing the risk of infections. Inside the capsular bag the IOL then needs to relax back to its initial shape.

Owing to the spatial resolution provided by the optical process connecting two linker molecules or cleaving the bonds between them, further advantages arise that will be of great benefit in the future. Spatial controlled alteration of the refractive index not only paves the way to correct aberrations such as astigmatism but also a multifocal lens could be created. Compared with other approaches for tuning the refractive power of an IOL, the system presented here offers further advantages since the focal length change is induced with virtually no delay. This makes a direct analysis and control of the achieved visual acuity possible. Photo-controlled tuning may be performed more than once and even a change back towards the initial value is possible by using another irradiation wavelength.

Zusammenfassung

Die Katarakt oder der „Graue Star“ ist eine Erkrankung des Auges, in deren Verlauf sich die ursprünglich klare Augenlinse trübt. Die Umwelt erscheint dem Betroffenen unscharf, matt, verschleiert und verzerrt. Katarakt ist weltweit die häufigste Ursache für Blindheit. Schätzungen gehen davon aus, dass mehr als 50 Millionen Menschen auf Grund einer Katarakt erblindet sind, von denen etwa 1,5 Millionen (3%) Kinder unter 16 Jahren sind. In den Industrieländern zeigt etwa die Hälfte der mehr als 65 Jahre alten Bevölkerung eine mehr oder weniger starke Trübung der Augenlinse. Unter den über 75 jährigen leiden sogar 70% an einer Katarakt. Obwohl die genauen Ursachen der Entstehung einer Katarakt nach wie vor Gegenstand intensiver Forschung sind, so gilt doch als gesichert, dass es sich meist um einen alterungsbedingten Effekt handelt, bei dem denaturierte Proteine der Augenlinse kristallisieren und so die Trübung verursachen. Es gibt weder eine wissenschaftlich abgesicherte Prävention der Katarakt noch gibt es eine belegte medikamentöse Therapie, die den Krankheitsverlauf stoppen oder gar die Trübung zurückbilden könnte. Die einzige Möglichkeit die Katarakt zu behandeln, ist die chirurgische Entfernung der getrübten Linse gefolgt vom Einsetzen einer Kunststofflinse, einer sogenannten Intraocularlinse (IOL), in das Auge. Die Kataraktoperation ist heute eine der sichersten, effektivsten und am häufigsten durchgeführten Operationen überhaupt. Sie wird jedes Jahr an mehreren zehn Millionen Patienten durchgeführt. Jedoch kann es zu gewissen spezifischen postoperativen Komplikationen und Problemen kommen.

Das Ziel dieser Arbeit ist es, eine Lösung für ein Hauptproblem der Behandlung mit IOLs zu bieten. Eine typische postoperative Komplikation der Kataraktchirurgie ist, dass die Brechkraft der implantierten IOL oftmals nicht den Wert hat, der für eine optimale Sehschärfe erforderlich wäre. Der Patient ist dann nach der Kataraktoperation auf das Tragen von Sehhilfen angewiesen. Der Hauptgrund für diese Abweichung ist, dass das Auge ein aus mehreren brechenden Grenzflächen bestehendes komplexes optisches System darstellt. Die für die Berechnung der optimalen IOL Form benötigten biometrischen Daten können vor der Operation oft nicht mit der erforderlichen Präzision gemessen werden. Insbesondere wird das Sehvermögen vom Krümmungsradius der Hornhaut, die den größten Beitrag zur Fokussierung des Lichts im Auge leistet, sowie der Länge des Augapfels bestimmt. Weiterhin kann die exakte Lage der IOL im Kapselsack nicht vorhergesagt werden, insbesondere da sich die IOL während des Heilungsprozesses in den ersten Wochen und Monaten nach der Operation noch etwas in Richtung der optischen Achse sowie senkrecht dazu verschieben kann. Die zuvor

berechnete und implantierte IOL Form stellt dann nicht mehr das Optimum für den Patienten dar. Die Auswertung klinischer Studien hat ergeben, dass etwa 80% der Kataraktpatienten nach der Operation eine Abweichung im Bereich von einer Dioptrie um das angestrebte Refraktionsziel haben. Bei weiteren 10% der Patienten ist die Abweichung mit zwei oder mehr Dioptrien sogar noch größer. Die meisten der mit IOLs behandelten Patienten benötigen also nach der Operation eine Sehhilfe oder die IOL muss in einer weiteren Operation explantiert und durch eine andere ersetzt werden.

Im Rahmen dieser Arbeit wurde eine Lösung für das beschriebene Problem, der bei vielen Patienten unzureichenden Sehleistung nach der Implantation einer IOL, entwickelt. Die Brennweite der IOL wird postoperativ und nicht-invasiv gezielt verändert, indem der Brechungsindex des Linsenmaterials mittels eines photochemischen Prozesses modifiziert wird. Im Rahmen dieser Arbeit wurden Polymere, die für die Herstellung einer IOL geeignet sind, synthetisiert und charakterisiert. Diese Polymere tragen photoaktive Linkergruppen entlang ihres Rückgrats. Das Cumarinmolekül fand im Rahmen dieser Arbeit hauptsächlich als Linkermolekül Anwendung. Zwei Cumarinmoleküle gehen über die im Lactonring befindliche Kohlenstoff-Kohlenstoff Doppelbindung recht einfach eine $[2\pi + 2\pi]$ Cycloadditionsreaktion unter Bildung eines Cyclobutanrings ein, wenn sie mit UV-Licht geeigneter Wellenlänge bestrahlt werden. Ebenso ist es möglich, durch Verwendung einer anderen, kürzeren Wellenlänge diese Photodimere wieder zu spalten und wieder einzelne Cumarinmoleküle zu erhalten. Die photoinduzierte Verknüpfung der photoaktiven Linkermoleküle führt zu einer Erniedrigung des Brechungsindex der IOL. Der Grund dafür ist, dass die Polarisierbarkeit der Linkermoleküle, die direkt mit dem Brechungsindex des polymeren Materials verknüpft ist, als Resultat der Bildung des Cyclobutanrings erniedrigt wird. Die maximal mögliche Brechungsindexänderung der im Rahmen dieser Arbeit synthetisierten Polymere beträgt gut 0,03, was eine Brechkraftänderung von etwas mehr als 2,5 Dioptrien bei einer Standard-IOL ermöglicht. Mittels einer solchen postoperativen Behandlung benötigten also fast alle Kataraktpatienten nach der Operation und anschließender Feineinstellung der IOL keine Sehhilfe mehr.

Zwei wichtige Entwicklungsschritte für die Synthese von Polymeren, die für die Herstellung von IOLs geeignet sind, wurden erfolgreich durchgeführt. Erstens wurde eine Alkylkette, ein sogenannter Spacer, zwischen das photoaktive Cumarin und die Polymerhauptkette eingefügt. Zweitens wurden durch freie radikalische Substanzpolymerisation der geschmolzenen Monomere, die alle bei Raumtemperatur als Feststoff vorliegen, und unter Zugabe eines Quervernetzers flexible Polymermaterialien erhalten. Hauptsächlich durch Veränderung der Länge des Spacers können sowohl starre als auch elastische Materialien hergestellt werden. Es ist sehr wichtig über ein Material zu verfügen, das flexibel genug ist, die daraus hergestellte IOL falten bzw. rollen zu können. Dies ermöglicht das Einsetzten der IOL in den Kapselsack des Auges durch einen vergleichsweise kleinen Schnitt, der nicht vernäht werden muss. Dadurch wird die Heilung beschleunigt und das Infektionsrisiko gesenkt wird. Die IOL muss sich dann im Kapselsack selbständig in ihre ursprüngliche Form entfalten.

Dank der räumlichen Adressierbarkeit, die das optische Verfahren der Verknüpfung zweier Linkermoleküle bzw. die Spaltung der Bindungen zwischen zwei Linkermolekülen ermöglicht, ergeben sich weitere höchst interessante Ansätze für die Zukunft. Durch die räumlich kontrollierte Änderung des Brechungsindex können nicht nur Abbildungsfehler wie Astigmatismus korrigiert werden, es könnten auf diese Weise auch multifokale Linsen hergestellt werden. Verglichen mit anderen Ansätzen, die Brechkraft einer IOL postoperativ zu verändern, bietet die hier vorgestellte Lösung den weiteren Vorteil, dass die Änderung der Brechkraft praktisch ohne zeitliche Verzögerung eintritt. Dies ermöglicht eine direkte Messung und Kontrolle der erreichten Sehschärfe. Die photoinduzierte Änderung der Brechkraft kann mehrmals durchgeführt werden und es ist auch eine Änderung zurück in Richtung des Ausgangswerts möglich, wenn eine entsprechend andere Wellenlänge verwendet wird.

Publications

The majority of the work presented here has been published:

Jens Träger, Hee-Cheol Kim, Martin Schraub, Norbert Hampp,
„Photo reactions induced by two-photon absorption“
in *Lasers in Chemistry: Probing and Influencing Matter* (Ed. Maximilian Lackner), Volume 2, Wiley-VCH, Weinheim, **2008**.

Jens Träger, Sebastian Härtner, Jasmin Heinzer, Hee-Cheol Kim, Norbert Hampp,
„Two-photon-induced cycloreversion reaction of chalcone photodimers“,
Chemical Physics Letters **2008**, *455*, 307-310.

Jens Träger, Hee-Cheol Kim, Norbert Hampp,
„Polymers for *in vivo* Tuning of Refractive Properties in Intraocular Lenses“,
Macromolecular Bioscience **2008**, *8*, 177-183.

Hee-Cheol Kim, Jens Träger, Matthias Zorn, Niko Haberkorn, Norbert Hampp,
„Ophthalmic drug delivery utilizing two-photon absorption: A novel approach to treat posterior capsule opacification“
in *Therapeutic Laser Applications and Laser-Tissue Interactions III*
(Ed. Alfred Vogel), *Proceedings of SPIE* **2007**, *6632*, 66321E/1-66321E/8.

Jens Träger, Jasmin Heinzer, Hee-Cheol Kim, Norbert Hampp,
„Materials for intraocular lenses enabling photo-controlled tuning of focal length in vivo“
in *Therapeutic Laser Applications and Laser-Tissue Interactions III*
(Ed. Alfred Vogel), *Proceedings of SPIE* **2007**, *6632*, 66321F/1-66321F/10.

Jens Träger, Hee-Cheol Kim, Norbert Hampp,
„Opthalmology: Two-Photon Treatment“,
Nature Photonics **2007**, *1*, 509-511.

Jens Träger, Hee-Cheol Kim, Norbert Hampp,
„Polymers for refractive index change in intraocular lenses: A novel approach for photoinduced tuning of focal length“,
in *Ophthalmic Technologies XVI* (Ed. Fabrice Manns, Per G. Söderberg, Arthur Ho),
Proceedings of SPIE **2006**, *6138*, 61381D/1-61381D/9.

Table of Contents

1 Introduction

Cataract is a clouding of the lens of the eye which impedes the passage of light (Fig. 1.1). Most cases of cataract are related to the aging process. However, children can be born with a cataract or develop it in teenage. Furthermore a cataract may develop after eye injuries, inflammation, and some other eye diseases. According to studies of the World Health Organization more than 50 million people suffer from cataract worldwide which makes cataract the cause for about half of all worldwide cases of blindness. Although cataracts can be surgically removed, in many countries surgical services are inadequate, and cataract remains the leading cause of blindness. As the average life expectancy, the number of people suffering from cataract is growing. Cataract is thus an important cause of bad vision in both developed and developing countries (Fig. 1.2). Comprehensive prevention of cataract development is not known yet. The treatment of cataract is an operation, which is very successful in restoring sight. The opaque lens is removed and replaced by an artificial intraocular lens (IOL).[1] Even though the first successful implantation of an IOL was accomplished already in 1950 by *Sir Harold Ridley*[2–7] some significant drawbacks related to IOL surgery still exist today. A typical postoperative complication is posterior capsule opacification (PCO), the so-called secondary cataract. PCO is caused by proliferation and migration of retained lens epithelial cells into the optical axis, and leads to a progressive deterioration and disturbances in visual activity.[8–14]

Another typical problem related to the implantation of an IOL is that the result obtained, as far as optimal vision is regarded, is far less than optimal in most cases. Biometric data of the eye before IOL implantation, among them curvature radii of the cornea and length of the eye-ball, cannot be determined with the desired precision. Positioning of the IOL during surgery, unpredictable effects from wound healing, and post-operative migration of the IOL occuring within weeks and months after cataract surgery are hard to predict. The great variety of approaches and formulas to predict the IOL power before cataract surgery shows that an optimal solution has not been found yet.[15–25] Clinical

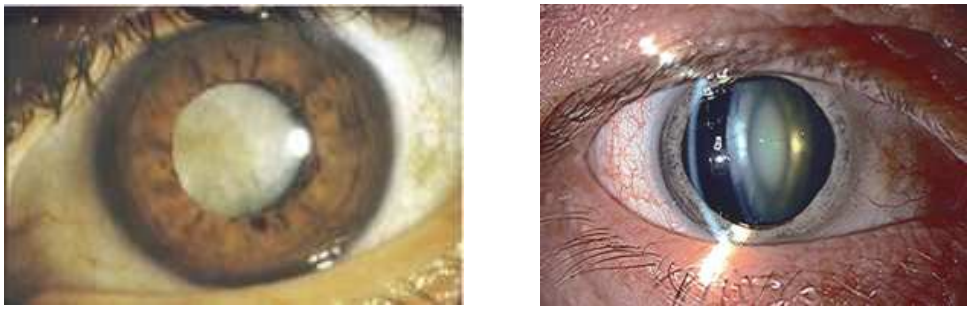

(a) (b)

Figure 1.1: Photographs of cataracts in adult lenses. (a) Cataract in a very advanced state and (b) slit lamp illumination of a cross-section through the opaque lens.

trials dealing with the outcome of cataract surgeries have shown that more than 80% of the patients are within 1 diopter (D) of the desired refraction and require some correction to provide for the best level of vision.[26] Even most recent works show that refractive errors after cataract surgery are practically unavoidable even though a trend of reduction of the magnitude of the refraction error is evident.[27–30] Even greater problems arise if certain conditions of the eye exist, for example, if the axial length of the eye is significantly longer[31] or shorter[32] than average. Pediatric cases are generally prone to complications associated with refractive power prediction.[33,34] Intraocular lens power errors due to production tolerances[35] may contribute significantly to the total error, particularly for high-power IOLs. Despite some manufacturers claiming to produce IOLs with very low tolerance, the applicable ISO 11979 standard allows tolerances of ± 0.33 D in the corneal plane for an IOL above 25.00 D and even ± 0.66 D for an

(a) (b)

Figure 1.2: Simulation of the visual perception of a person (a) with optimal vision (b) suffering from cataract. (Bayerischer Blinden- und Sehbehindertenbund e.V.)

IOL above 30.00 D. This is especially a problem because the ophthalmic surgeon usually has no means to assess the focal length of an IOL before implantation. A very important issue also is IOL calculation for patients which have undergone refractive surgery like the popular laser-assisted in situ keratomileusis (LASIK). Due to the unnatural shape of the cornea caused be LASIK, accurate prediction of the optimal IOL for such eyes is even more complicated than in a surgically untreated eye.[36–43] Since LASIK seems to become more and more popular, a great number of patients having undergone that procedure might need an IOL in the forseable future creating new challenges for cataract surgery and IOL calculation that will be difficult to address.

The objective of this thesis is to provide a solution for the almost unavoidable refractive errors after cataract surgery. Polymers suitable for an IOL are to be developed whose optical properties, in particular their focal length, can be altered in a non-invasive manner post-operatively. To tune the optical properties of the implanted IOLs the refractive index of the lens polymers has to be changed in a photoinduced process. Prototype IOLs shall be manufactured and characterized with respect to their photoinduced focal length change to proof the effectiveness of this concept. The change in refractive power should be at least 1 D to be suitable for the proposed application. Furthermore, it should be shown that elastomeric polymers employing this concept can be made to allow manufacturing of foldable IOL which are state of the art in cataract surgery.

The aim of this introductive chapter is to give a brief outline of the formation and treatment of cataract as well as the concept of altering the refractive index of a polymer by a photochemical reaction. Special attention will be payed to the photochemistry of the most promising molecule – coumarin – that is used to realize the described idea.

1.1 Cataracts and their Treatment

1.1.1 Historical Overview

The eye is one of the oldest fields of interest in medical science. As early as 1550 BC comprehensive studies of eye diseases were written down in the “Papyros Ebers.” There are numerous references to cataracts and their treatment in the literature of many ancient civilizations. Perhaps the first is in the “Code of Hammurabi” (1750 BC). This includes

a schedule of payments for the surgeon, should sight be restored, along with the penalty of the removal of the surgeon's fingers should the patient die or lose their eye.[44,45] Cataract derives from the Latin cataracta meaning "waterfall" and the Greek kataraktes and katarrhaktes, from katarassein meaning "to dash down." As rapidly running water turns white, the term may have been used later metaphorically to describe the similar appearance of mature ocular opacities. In Latin, cataracta bore the alternate meaning "portcullis." Therefore, it is also possible that the name came about through the sense of "obstruction." Early Persian physicians called the term "descent of the water," vulgarized into waterfall disease or cataract. It was believed that such blindness is caused by an outpouring of corrupt humor into the eye. It was not until the middle of the 17th century that the true cause for cataract became known. The French surgeon *Pierre Brisseau* was the first to write down the finding that cataract is caused by an opacification of the eye lens in 1705.[46]

Prior to 1750 AD, cataract was treated by dislocation into the vitreous cavity using a lance, a process known as couching (Fig. 1.3). Reference to this technique can be found in Hindu manuscripts dating from 600 BC. Lancing instruments such as the one used for couching have been found in Greece dating from 1000 to 2000 BC. It is unclear whether these cultures developed couching independently or whether the technology was handed on. Certainly couching was common during the Roman Empire around the time of Christ and thereafter. The procedure is described in the work "De Re Medicina" of the Latin encyclopedist *Aulus Cornelius Celsus*, which is the oldest Greco-Latin medical document after the Hippocratic writings. It appeared around 29 AD.[47] Prior to the establishment of ophthalmology as a specialty, aside from mainstream surgery, general surgeons treated cataractous lenses by couching. However, cataract treatment also attracted others. In the 18th century, traveling quacks were common. They attracted patients through vigorous self-promotion and operated cataracts, and other common maladies, in town centers and marketplaces. As a result of this operation formerly blind people were at least able to distinguish between light and dark. Sometimes, if the patient was myopic, he could even recognize faces. The outcome from the patient's point of view, however, lagged well behind the claims of the cataract lancer. The treatment was not successful in the long run. Very often irrevocable blindness was caused by an inflammation of the eye or absolute glaucoma soon after the couching. This was due to the irritation caused by the lancing or dissolution of lens fragments in the eye. This is the reason why cataract lancers never returned to the location of their former work.

Figure 1.3: Historical woodcut sketching of early cataract treatment (G. Baritsch, Dresden 1583). A tool was used to dislocate the opaque natural lens from the visual axis.

The advent of more subtle methods to treat cataract came with the Age of Enlightenment when another French, *Jacques Daviel* pursued an alternative to couching after one of his patients suffered bilateral blindness following the procedure (Fig. 1.4). He conducted the first planned surgical extraction of an opaque eye lens in 1753.[46,48] Development and improvement of the extraction procedure occurred throughout the 19th century (Fig. 1.5). The German ophthalmologist *Albrecht von Graefe*, who was an Ordinary Professor at the Humboldt-University of Berlin, developed a new operation technique for cataract. He suggested a small linear scleral incision for extra-capsular surgery rather than a large limbal corneal incision.[49] The benefits were a lower rate of infection, less post-operative astigmatism and more rapid post-operative recovery. These goals drive improvement of cataract treatment up to the present.

Two other 19th century developments were also important to cataract surgery. The English surgeon *Joseph Lister* promoted the idea of sterile surgery and successfully introduced phenol to sterilize surgical instruments and to clean wounds in 1867. The second was the introduction of cocaine as a local anesthesia. The Austrian ophthalmologist *Karl Koller* became aware of the anesthetic properties of cocaine through recreational use and introduced it for eye surgery.[50] During the second half of the 19th century, surgeons became interested in removing the complete lens within its capsule. *Georg Joseph Beer* introduced the flap operation for cataracts. He invented a specially designed knife with a narrow blade, which was exceptionally sharp and long, permitting superi-

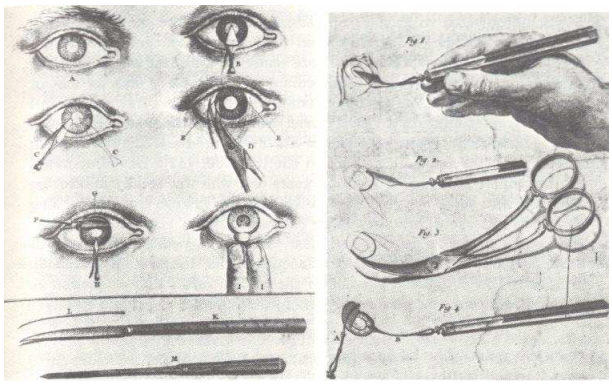

Figure 1.4: Daviel's method of cataract extraction.

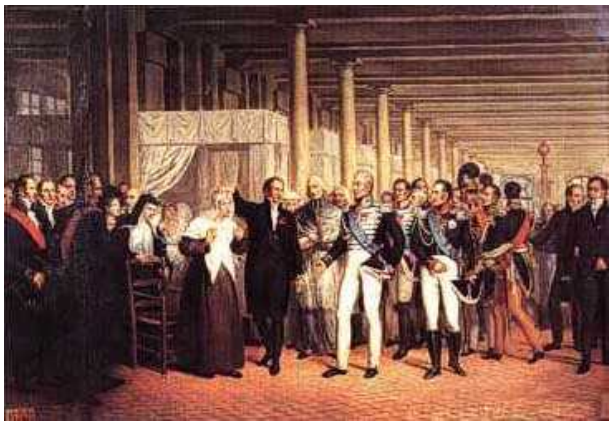

Figure 1.5: Cataract surgery of a female patient. 19th century painting of an unknown artist.

or incisions. The advantages of this operation, known as Beer's operation, were quicker healing, better post-operative vision and the absence of capsular thickening and proliferation.[51,52] All surgeons did not immediately adopt this advance and therefore it was not until the early 20th century that intra-capsular surgery was firmly established as a preferable method over extra-capsular surgery. Further developments in anesthesia and the introduction of sutures greatly assisted the progress of intra-capsular surgery. The next important advance for cataract surgery was the introduction of the operating microscope by *Ken Swann* in 1948 starting the era of ophthalmic microsurgery. This was closely followed by surely one of the most important advances in cataract surgery, the invention of the IOL. Detailed information about the IOL is given in section 1.3.1.

1.1.2 Modern Methods of Cataract Surgery

There are two types of eye surgery that can be used to remove cataracts, intra-capsular cataract extraction (ICCE) and extra-capsular cataract extraction (ECCE). ICCE surgery involves removing the entire lens of the eye, including the lens capsule, but it is rarely performed in modern practice. The nucleus can be manually expressed from the eye, with a technique similar to that described by *Daviel*.[46] Later on several methods were developed to remove the hard nucleus effectively out of the capsular bag. The Spanish ophthalmologist *Ignacio Barraquer* designed an erisophake controlled by an electric pump and later used alpha-chymotrypsin to enzymatically dissolve the zonules for removal of the lens.[53,54] An adhesive bowl was used to extract the lens until cryo-surgery was introduced by *Tadeusz Krwawicz* of Poland in 1961 to remove the lens with a tiny probe that could attach by freezing a small area on the surface of the cataract.[55] With this method the healing time is shortened and the ocular fundus can be immediately examined for areas that pose the risk of a retinal detachment. However, the main disadvantage of ICCE is the lack of a sealing in form of a membrane against the vitreous body.

Extra-capsular (ECCE) surgery consists of removing the lens but leaving the majority of the lens capsule intact. In late 1967 *Charles Kelman* developed a technique for emulsifying the lens' contents using ultrasonic vibrations and aspirating the emulsified cataract.[56] An ultrasonic probe emitting high frequency (44 kHz) sonic energy is used to disrupt the hard lens nucleus. This is achieved through cavitation, a phenomenon in which a flowing liquid forms vaporous bubbles in a region where the pressure of the liquid falls below its vapor pressure.[57] Aspirated fluids are replaced by irrigation with a balanced salt solution, thus maintaining the anterior chamber, while cooling the handpiece used for this procedure. This method is called phacoemulsification (Fig. 1.6). However, the procedure did not achieve widespread acceptance until the late 1980s and 1990s. It is still the method of choice today. The technique has evolved to use low enough amounts of energy to split the nucleus into fragments without damaging the neighboring structures of the eye. Phacoemulsification can be done through a comparatively small wound of approximately 3 mm length. In contrast, manual expression of the nucleus demands a larger wound of approximately 9 mm length.[44] Internal wound architecture has been important in the evolution of cataract surgery. Paying careful attention to wound construction can create wounds that need not be sutured. Separating the external and internal wounds by making these incisions of partial thickness and

splitting along the eye wall to create a tunnel creates a structure where an application of force to the eye will not result in wound gape and loss of intraocular contents. Nowadays phacoemulsification is the procedure of choice for cataract extraction in the Western world. The reasons why are rooted in an improved outcome for the patient. The main advantage is reduced corneal astigmatism after cataract surgery. Since the cornea is the major refracting surface of the eye, minor disturbances to its shape may result in marked astigmatism with serious consequences for vision. Corneal surgery generally has the tendency to produce astigmatism. But with less invasive techniques less distortion is produced than with more disruptive procedures. Small cataract incisions produce less astigmatism than large incision cataract surgery, but the difference is short lived.[58] However, there is also some dispute over the advantages of phacoemulsification.[59,60]

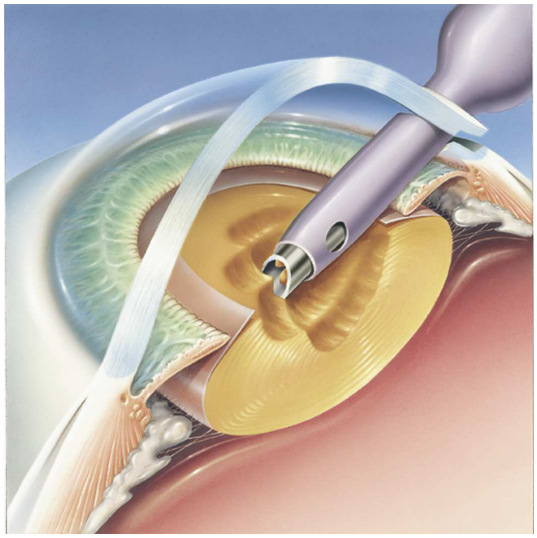

Figure 1.6: In phacoemulsification the eye's internal lens is emulsified utilizing an ultrasonic handpiece, and aspirated from the eye.

Phacoemulsification leaves the lens capsule intact enabling it to act as a sealing. New lens fibers are build up all the time at the posterior capsule leading to a complication called posterior capsule opacification (PCO) or secondary cataract that disturbs the vision yet again.[9,10,61–75] The main treatment of PCO is Nd:YAG laser secondary posterior capsulotomy, a sometimes dangerous procedure.[76–97] Furthermore, residues of the capsule might shrink and also disturb vision. Phacoemulsification is more expensive to perform requiring the use of sophisticated machinery. The most serious ocular complication of phacoemulsification lens extraction is dropping the nucleus into the

vitreous cavity. This may result in visual loss due to inflammation and retinal detachment. Fortunately, this complication is unlikely to arise for experienced surgeons and sight loss can be prevented by vitrectomy and nucleus removal. Conversely, the risk of expulsive haemorrhage, a rare but devastating complication of cataract surgery, is thought to be less with phacoemulsification. This is because the eye with phacoemulsification may be maintained as a closed system during surgery. That is, through the use of viscoelastic materials and infusion of a physiological salt solution, the intraocular pressure is maintained at normal levels. Unlike with extra-capsular lens expression, where once the eye is opened the intraocular pressure falls to atmospheric pressure and haemorrhage from leaky intraocular vessels is encouraged. One of the most recent development in cataract surgery are Erbium:YAG laser emulsifiers which allow for incisions as small as 1.25 mm.[98] The Er:YAG laser, which emits at 2940 nm, relies on its wavelength in the infrared for cataract surgery. At this wavelength, the laser produces cavitation bubbles that collapse slowly in the cataract and very quickly in water. This leads to propagated energy within the lens, allowing the laser to emulsify the material efficiently without producing thermal energy. The laser can be used with a prechopper to reduce the operating time.

1.1.3 Causes and Epidemiology of Cataract

The causes for cataract are numerous and a great number of studies have been published claiming a wide variety of reasons. Sometimes those studies contradict each other. However, the undisputed major risk factor for lens opacification is aging causing about 90% of all cataracts.[99] A bewildering array of etiologic factors have been postulated of being responsible for age-related cataracts.[100–113] Studies have focused on genetic factors,[114–120] environmental influences[121–130] and on the metabolic and biochemical changes in the crystalline lens.[114,115,120,121,131–136] Many investigators believe that an important factor in the pathogenesis of cataracts is exposure to ultraviolet radiation.[130,137–148] To give just a few examples, in a study conducted in Australia a strong positive association of occupational sun exposure between the ages of 20 and 29 years with nuclear cataract was found. Exposure later in life resulted in weaker associations.[137] Also a positive correlation between cataract prevalence and sunlight in Nepal has been found.[139] A high prevalence of cataract was detected in Northern India in a population living in the plains compared to an adjacent population living at high altitudes in the Himalayas showing a lower prevalence.[149] Several reports have noted an

increased risk of cataract among cigarette smokers.[150–163] Some researchers suggested that severe diarrhea may be a major risk factor for the development of cataract,[164,165] but other studies have not supported this hypothesis. Several studies have correlated nutritional status with cataractogenesis where both malnutrition in developing countries as well as supernutrition, expressed by an increased body mass index (BMI), often found in industrialized countries are risk factors.[166–168] The role of a suboptimal supply of vitamins and trace elements has also been investigated.[131,133,135,169,170] At first sight these studies might suggest that regular intake of antioxidants such as vitamin A, C, and E is theoretically helpful. But it has been shown that taking such vitamins as a dietary supplement has no benefit.[171] Others have implicated alcohol as well as some illegal drugs as a factor.[152,156,172–176] Pre-existing medical conditions, such as diabetes mellitus[134,177–180] and glaucoma,[178] may cause cataract, but in most cases of cataract, there is no known pre-existing disease factor.[99] This complex and confusing list of causes may be simplified to the "Seven Ds," which are listed in Table 1.1.

Table 1.1: Simplified summary of cataract risk factors – The "Seven Ds"[99]

Major Risk Factors	
Diabetes	
Drug	Smoking, alcohol, steroids, others
Daylight	Exposure to UV radiation
Dehydrogenase deficiency	Glucose-6-phosphate dehydrogenase
Minor Risk Factors	
Dehydration	Severe diarrhea, uremia
Diet	General deficiency and/or micronutrients
Don't know	Unknown factors

Recent research suggests that statins, substances which are rather known for their ability to lower lipids in the blood but are also believed to have antioxidant qualities, could help to prevent cataract. It is believed that oxidative stress plays a role in the development of nuclear cataracts, which are the most common type of age-related cataract. To explore the relationship between nuclear cataracts and statin use, a group of patients who were at risk of developing nuclear cataracts were partially treated with statins. The results suggest that statin use in an at-risk population may be associated with a lower risk of developing nuclear cataract disease.[181] Lutein and zeaxanthin are xanthophyll carotenoids found particularly in dark-green leafy vegetables and in egg yolks. They are widely distributed in tissues and are the principal carotenoids in the eye lens and macular region of the retina. Epidemiologic studies indicating an inverse relationship

between xanthophyll intake or status and both cataract and age-related macular degeneration suggest these compounds can play a protective role within the eye. Even though research in this field is scant and mixed there seems to be a weakly positive effect offered by nutrients lutein and zeaxanthin.[182–185] Bilberry extract[186,187] and grape seed extract[188] show promising results in rat models supposedly due to the antioxidants contained therein. There is also one clinical study that suggests a beneficial effect of bilberry for cataract prevention in humans.[189] In the past few years, eye drops containing acetyl-carnosine have been used by several thousand cataract patients across the world. The drops are believed to work by reducing oxidation and glycation damage in the lens, particularly reducing crystalline cross-linking.[190,191] The use of these drops remains controversial due to the lack of large and properly designed trials.

In summary, it can be said that cataracts are difficult to prevent due to the numerous and often unclear causes. Although there is no scientifically proven effective pharmaceutical that could prevent, retard or even reverse the formation of cataracts, there are some behavioral patterns that might be helpful to prevent or rather delay the development of cataract. Reduction of smoking cigarettes, exposure to ultraviolet light by wearing sunglasses, and alcohol consumption should be considered. Diabetes mellitus, hypertension and a high body mass index are identified as additional risk factors.

Surgical treatment is the only way to treat the blinding condition caused by cataract and the only way to meet the need for cataract service is to increase the number of operations.[192–202] One measurement of the quantity of cataract service is termed the cataract surgery rate (CSR) which is defined as the number of cataract operations per year per 1 million people.[200,203,204] Whereas access to cataract surgery in industrialized countries is usually not a problem in many remote parts of the developing world, people remain blind from cataract. A CSR of about 5000 is common in most developed countries, whereas rates as low as 300 are seen in some developing countries of Africa and, in some areas of China the CSR is probably less than 200.[205–217] In developing countries a lack of access to quality eye care at an affordable price exists. Even where surgical services are available, low vision associated with cataract may still be prevalent, as a result of the long period spent waiting for operations and barriers to surgical uptake. As populations age, the number of people with cataracts is growing. This has lead to a worldwide cataract backlog, i.e. the number of people being blind or visually impaired is growing more rapidly than the number of surgeries that can be performed. The four main barriers to obtaining cataract surgery are lack of patient awareness, poor quality

of service, cost of surgery, and transportation problems or distance to the surgical site. To increase the CSR, these factors have to be minimized.[99]

1.2 Synopsis of Refractive Errors

A refractive error, is an error in the ability to focus light by the eye and a frequent reason for reduced visual acuity. An eye having no refractive error when viewing a distant object is emmetropic. An eye that has a refractive error when viewing a distant object is said to be ametropic. Refractive errors are frequently categorized as spherical and cylindrical. Spherical errors occur when the optical power of the eye is either too large or too small to focus light on the retina (Fig. 1.7). People suffering from a refraction error have blurry vision. Myopia, also called near- or short-sightedness, is a refractive defect of the eye in which collimated light produces an image focus in front of the retina when accommodation is relaxed. Those with myopia see nearby objects clearly but distant objects appear blurred. With myopia, the eyeball is too long, or the cornea is too steep, i. e. the optics are too powerful for the length of the eyeball. So images are focused in the vitreous inside of the eye rather than on the retina at the back of the eye. Hyperopia, also known as farsightedness or longsightedness, is a defect of vision caused by an imperfection in the eye. When the optics are too weak for the length of the eyeball, causing inability to focus on near objects, and in extreme cases causing a sufferer to be unable to focus on objects at any distance. As an object moves toward the eye, the eye must increase its optical power to keep the image in focus on the retina. If the power of the cornea and lens is insufficient, as in hyperopia, the image will appear blurred.

Astigmatism is an optical defect whereby vision is blurred due to the inability of the optics of the eye to focus a point object into a sharp focused image on the retina. This may be due to an irregular or toric curvature of the cornea or lens. There is a difference in the degree of curvature refraction of the two different meridians i.e., the eye has different focal points in different planes (Fig. 1.8). For example, the image may be clearly focused on the retina in the horizontal plane, but not in front of the retina in the vertical plane. People with this refraction error see contours of a particular orientation as blurred, but see contours with orientations at right angles as clear. Astigmatism causes difficulties in seeing fine details, and in some cases vertical lines (e. g. walls) may appear tilted to

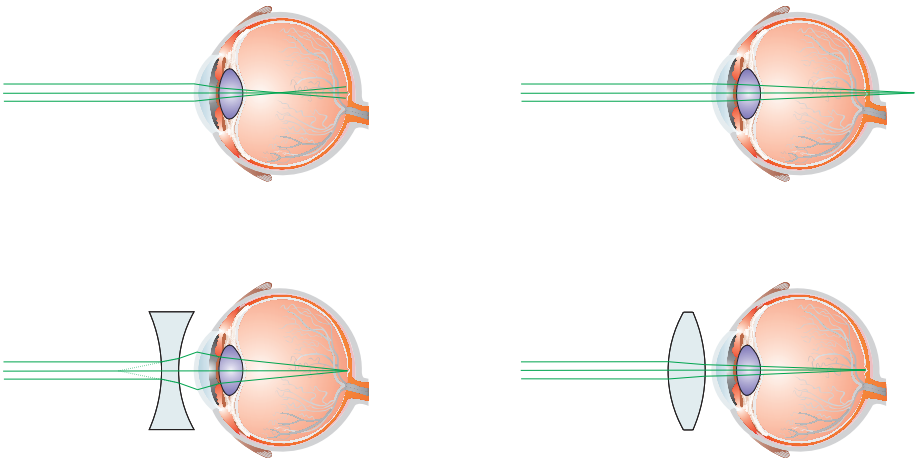

Figure 1.7: (a) Myopia (top) and the compensation for myopia using a concave corrective lens (bottom). (b) Hyperopic eye (top), and the correction of vision with convex lens (bottom).

the patient. The astigmatic optics of the human eye can often be corrected by spectacles, hard contact lenses or contact lenses that have a compensating optic.

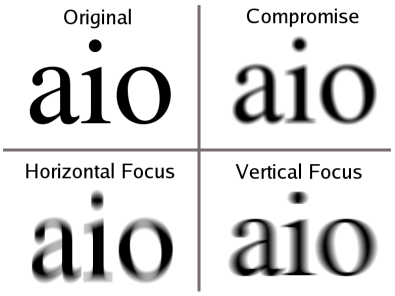

Figure 1.8: Blur from astigmatic lens at different distances. There is no distance at which an overall sharp image can be achieved.

To determine the visual acuity usually an eye chart is used. The most popular eye chart is the Snellen chart (Fig. 1.9) named after the Dutch ophthalmologist *Herman Snellen* who developed it in 1862. Eye charts usually display several rows of test symbols called optotypes, each row with a different size. The patient is asked to identify the numbers or letters of each row of the chart, usually starting with large optotypes and continuing to rows with smaller ones until the optotypes cannot reliably be identified anymore. Technically speaking, testing visual acuity utilizing an eye chart is a psychophysical

measurement that attempts to determine a sensory threshold. The traditional Snellen chart is made up of eleven lines of capitalized letters. The first line consists of one very large letter, which may be one of several letters, for example E, H, N, or A. Subsequent rows have increasing numbers of letters that decrease in size. The row containing the smallest optotypes that can be read accurately indicates the patient's visual acuity of that eye. The optotypes have the appearance of capitalized letters, and are intended to be seen and read as letters. They are not, however, letters from any ordinary typographer's font. They have a particular, simple geometry in which the thickness of the lines equals the thickness of the white spaces between lines and the width of the gap in the letter "C" and the height and width of the optotype is five times the thickness of the line. Only the ten letters C, D, E, F, L, N, O, P, T, Z are used in the traditional Snellen chart. The minimum illumination for externally illuminated charts should be 480 lx, however this very important parameter is frequently ignored by physicians, making many test results invalid.

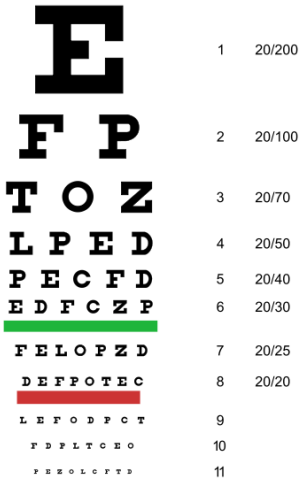

Figure 1.9: A typical Snellen chart to estimate visual acuity. When printed out at correct size, the E on line one will be 88.7 mm tall and when viewed at a distance of 20 ft (6.1 m), the visual acuity can be estimated based on the smallest line one can read.

Snellen defined "standard vision" as the ability to recognize one of his optotypes when it subtended five minutes of arc. Thus the optotype can only be recognized if the person viewing it can discriminate a spatial pattern separated by a visual angle of one minute of arc. In the most familiar acuity test, a Snellen chart is placed at a standard distance, twenty feet in the US. At this distance, the symbols on the line representing "normal"

acuity subtend an angle of five minutes of arc, and the thickness of the lines and of the spaces between the lines subtends one minute of arc. This line, designated 20/20, is the smallest line that a person with normal acuity can read at a distance of twenty feet. Three lines above, the letters have twice the dimensions of those on the 20/20 line. The chart is at a distance of twenty feet, but a person with normal acuity could be expected to read these letters at a distance of forty feet. This line is designated by the ratio 20/40. If this is the smallest line a person can read, the person's acuity is 20/40. Simply speaking this person needs to approach to a distance of twenty feet to read letters that a person with normal acuity could read at forty feet. Speaking in an even more simplified way, this person could be said to have "half" the normal acuity. Outside of the US, the standard chart distance is six meters, normal acuity is designated 6/6, and other acuities are expressed as ratios with a numerator of six. In Europe, the value is often given in the decimal system where one minute of arc is the reference value that is correlated with the individual visual acuity. The visual acuity is the better the greater this value is. For example, if the smallest optotype a person can resolve corresponds to two minutes of arc or 20/40 the value would be 0.5 or 50%. The largest letter on an eye chart represents an acuity of 20/200, the value that is considered "legally blind" if a person cannot read that letter even with the best possible glasses. Some people with refractive errors have the misconception that they have "bad vision" because they cannot even read the E at the top of the chart without glasses. But in most situations where acuity ratios are mentioned, they refer to best corrected acuity. Many people with moderate myopia cannot read the first line without glasses, but have no problem reading the 20/20 line or 20/15 line with glasses.

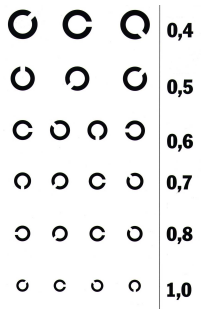

Figure 1.10: A visual acuity test chart comprised of Landolt C optotypes in various sizes and orientations.

Snellen charts have been the target of some criticism. The fact that the number of letters increases while the size decreases introduces two variables, rather than just one. Some

people may simply or unconsciously memorize the Snellen chart before being tested, or between tests of one eye and the other, to give the impression that their vision is good. Several studies indicate that the crowding together of letters makes them inherently more difficult to read. One approach to overcome this problem is an optotype called the Landolt C (Fig. 1.10). It consists of a ring that has a gap, thus looking similar to the letter C. The gap can be at various positions, usually left, right, bottom, top, and the 45° positions in between and the task of the tested person is to decide on which side the gap is. The Landolt C has the advantage of being more difficult to guess and to memorize than the traditional letters on the Snellen chart. The size of the C and the break are reduced in size until the subject makes a random rate of errors. The minimum angle of the break is judged as the visual acuity.

1.3 Correction of the Refractive Error after Cataract Surgery

The absence of the lens of the eye is called "aphakia". Even though aphakic people can see at least nearby objects the quality of vision is greatly affected. The lens is responsible for much of the converging power of the optical system of the eye having a typical value of about 20 D in a healthy eye. Patients with their eye lens removed are highly myopic. Without optical correction they cannot even see the largest letter on the Snellen chart. The traditional method was to provide the patient with spectacles to overcome the loss of converging power and treat the optical deficiency of the aphakic eye (Fig. 1.11). Such spectacles allow the patient to read the bottom line of the Snellen chart, but there are serious disadvantages. The thick converging lenses provide the retina with a magnified image of about 25%. This magnification could cause diplopia, commonly known as double vision, which is the simultaneous perception of two images of a single object. These images may be displaced horizontally, vertically, or diagonally in relation to each other. Diplopia was especially a problem when there was a long time gap between surgery on both eyes because diplopia is very likely to occur when the images on the respective retinas of the two eyes differ significantly in size. Also, these high refracting lenses cause spherical aberration, i.e. straight lines away from the optical center of the lens appear curved, an effect that is exaggerated by movement. The reduced visual field caused by the lenses is responsible for the so-called "jack-in-the-box" phenomenon where objects suddenly appear in the field of vision from the periphery. The spectacles are quite uncomfortable to wear due to their heavy weight. For such patients, one form

of visual disability, which was due to cataracts, was replaced by another, that associated with aphakia. The frustration for aphakic patients was considerable. In a worst case scenario, breakage or loss of the glasses, occurring quite often, may condemn the patient in a rural setting to a visual acuity as bad or worse than the acuity present with the primary cataract. The limitations of aphakic spectacle vision drove the search for effective prosthetic correction.[218–229]

Figure 1.11: Spectacle aphakic correction for an "only" eye in Uganda.[230]

Contact lenses were an option for the correction of aphakia. They are optically much more desirable since the image magnification is less and the field of vision is greater. However, lens handling is a real difficulty for the elderly with poor vision and possibly limited hand strength or flexibility. Although contact lens correction of aphakia represents an improved outcome for the aphakic patient, success rates for contact lens wear in aphakia are limited.[231] In effect, the cataract operation without an IOL is, as *Harold Ridley* first noted, "only half an operation."

1.3.1 Intraocular Lenses

The suggestion of using an optical aid implanted in the eye is attributed to *Giacomo Casanova* and dates back to the 18th century.[232] However, it took some time until this concept could successfully put into practice for the first time. During World War II it

was *Harold Ridley* who observed that poly(methyl methacrylate) (PMMA) fragments from canopies were inert in the injured eyes of pilots.[233] Since the PMMA fragments did not trigger rejection, *Ridley* proposed the use of artificial lenses in the eye to correct cases of cataracts. He designed the first ever intraocular lens and had it manufactured using an identical plastic – Perspex CQ™ made by ICI. *Ridley* achieved the first implant of an intraocular lens on November 29th 1949 at St Thomas' Hospital, London, although it was not until 1950 that he left an artificial lens permanently in place in an eye. The IOL was placed on the posterior lens capsule after extra-capsular removal of the natural lens. *Ridley* was an exceptional surgeon, and achieved success in this approach, although not all surgeons could reproduce his results with the heavy prototype. Others later capitalized on this material to make lighter anterior chamber lenses. *D.P. Choyce*, a former assistant to *Ridley*, carried this idea through a period of great hostility,[234–236] being joined by *Binkhost*, and *Boberg Ans* in Europe, and *Tennant* in the USA. *Choyce's* Mark IX was moderately successful, having four rigid feet in the angle of the anterior chamber. This lens occasionally caused attrition of the corneal endothelium and decompensation edema. *Danheim's* lens, with flexible nylon loop supports, was particularly prone to this complication. At the same time surgical techniques were improving with very thin sutures having a diameter of only 0.02 mm on atraumatic needles. In the early 1960s the Dutch ophthalmologist *Cornelius Binkhorst* made implants to clip onto the iris sphincter, sometimes aided by pilocarpine miosis.[237,238] Initial results were good though the technique was difficult. Typical post-operative refractions showed high astigmatism resulting from the large wound. It was at this time that many UK surgeons began to feel that implants were a "respectable" method of treatment. However, problems still existed among them pupil dilatation that allowed lens dislocation into the vitreous gel, long term miosis that cheesewired the iris, and lenticulodonesis that caused corneal endothelial damage.

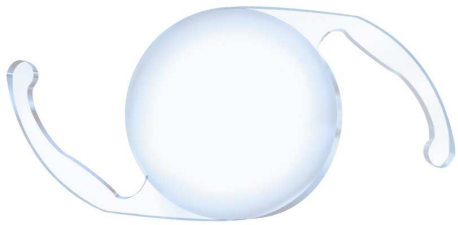

Figure 1.12: Modern three piece acrylic intraocular lens.

Meanwhile, in the 1970s *John Pearce* developed a new reduced incision microsurgery, with implantation of the IOL in the posterior chamber (Fig. 1.12). Later on this procedure was refined to "endocapsular" implantation, i.e. into the natural place, the capsular bag, which affords better optical outcomes. There was one disadvantage, the capsular epithelial regeneration could cloud the pupil later causing PCO. To treat this Nd:YAG laser capsulotomy was developed and is still the common method today. However, this method has some serious disadvantages (Sec. 1.1.2). In recent decades, there has been a rapid evolution of designs, materials, and implantation techniques for intraocular lenses, making them a practical way to restore normal vision at the time of surgery. With the advance of foldable IOLs, lenses can be implanted through the same small incision that is created in the phacoemulsification procedure. These IOLs are made of a flexible material allowing them to be folded for implantation. A foldable IOL can be implanted through a much smaller incision than a nonfoldable, rigid IOL. This type of incision is about 3 mm and does not require sutures for wound closure. Once inside the eye, the lens unfolds and returns to its original shape (Fig. 1.13). The advantages of foldable IOLs and the smaller incision required include less trauma to the eye, little discomfort during or after the surgery, no need for stitches, reducing astigmatism and provide better vision, providing a faster postoperative recovery period and quicker return to normal activity. Therfore, foldable IOLs are state of the art in industrialized countries today rendering rigid IOLs a phased-out model.

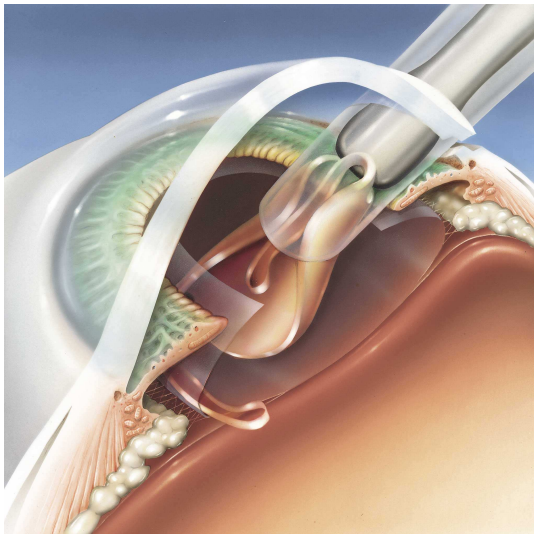

Figure 1.13: Implantation of a foldable intraocular lens through a micro incision.

The IOL is immersed in the liquid of the eye chambers. Its optical effective part has a diameter between 5 mm and a maximum of 7 mm. At the edges of the optic part of the IOL elastic loops or brackets are attached depending on the particular model. These loops, called the haptics, are responsible for centering the lens in the capsular bag and safely holding it in place. The overall diameter of an IOL is about 12 mm, its thickness is dependent on its refraction power and normally varies between 0.7 mm and a maximum of 2 mm. The weight of an IOL is on the order of 50 mg.[99,239,240] The polymers which are used to make modern foldable IOLs may be divided into two subgroups. The IOLs may either be made of (1) acrylic or methacrylic or (2) of silicone based polymers.[241,242] To simplify matters, polymers synthesized from esters of acrylic or methacrylic acid will be called acrylics. Acrylic as a lens material was approved by the U. S. Food and Drug Administration (FDA) in December 1994 and an increase in use in the USA from 2% to 9% between 1994 and 1995 was observed.[243] Acrylic IOLs have a refractive index of around 1.55 and the hardness of the acrylic is temperature dependent. The high refractive index gives acrylic lenses the lowest edge thickness of all available lens materials. At low temperatures the lens feels almost like PMMA and folding is facilitated by warming the lens. Acrylic lenses fold and unfold slowly and can be handled when wet. If the lens is too warm it can become sticky and unfolding can be difficult. Condensations occur less frequently on acrylic lenses than PMMA and silicone lenses following fluid-air exchange.[244] Common lens design is three piece, with a foldable acrylic optic and PMMA haptics. However, one piece acrylic lens have also been manufactured. Hydrogel, a soft hydrophilic material has a long history of use as a biomedical material[245] and is now used in folding IOLs. The material used is poly(hydroxyethyl methacrylate) (PHEMA) with a water content varying from 18% to 30% and a refractive index of 1.47. The material is quite hard at room temperature when completely dry and can therefore be easily milled and turned to produce an IOL. When immersed in water the lens takes up the predetermined amount of liquid, swells and becomes flexible. Of course the amount of volume increase due to the water uptake has to be taken into account when machining the lens out of the dry polymer. Hydrogel lenses fold and unfold faster than acrylic ones and are more controllable than silicone. Because of their water content they must be kept hydrated until implantation, making lens presentation in the operating theater slightly more difficult. Hydrogel lenses are available with a hydrogel optic bonded to PMMA haptics and as single piece lenses. Results of acrylic lens implantation have been published by *Oshika et al.*[246] who found that 96.9% of patients had a corrected visual acuity of 20/40 or better at day one and at 2 years post-operatively 100% had 20/40 or better and 86.3% 20/20 or better. The

measured flare intensity was less than with other types of IOLs and no other postoperative complications were encountered. Hydrogel one piece lenses have produced good visual results. *Percivals* and *Jafree* reported 100% of patients seeing 6/9 or better.[247,248] The only adverse reaction reported was asymptomatic decentration in two cases. The author has obtained good results from clinical trials on a hydrogel lens with PMMA haptics with 97.1% of eyes seeing 20/40 or better at 12 to 14 months post-operatively and no sight threatening complications.

Silicone has been in use as an IOL material since the early 1980s with FDA approval obtained in 1990 for a three piece silicone lens. Silicone in IOLs is a biologically inert polymer, polydimethylsiloxane (PDMS), which cannot leach out unlike silicone in breast implants. The earlier lenses had a refractive index of 1.41 making folding of three piece lenses over 22 D difficult. The refractive index of most three piece silicone IOLs is now 1.47 reducing thickness and facilitating folding. However, having thicker lenses with a refractive index of 1.41 and plate haptic could be advantageous because it fills out the capsular bag better, reducing the chance of posterior capsular opacification. Silicone folds easily but springs open unless delivery is controlled. The unfolding of a silicone IOL may damage structures inside the eye if it is not carefully controlled. Silicone IOLs are difficult to handle when wet as the material becomes slippery. They should not be used in the presence of silicone oil in the vitreous cavity, or if silicone oil may be required in the future, as condensations will occur on the lens, in particular in the presence of a posterior capsulotomy.[244] Therefore acrylic lenses are a better choice for people who have a history of uveitis, have diabetic retinopathy requiring vitrectomy with replacement by silicone oil or are at high risk of retinal detachment. Silicone lenses are currently the most popular foldable IOLs[243] with two styles in use – a three piece design with a silicone optic and polypropylene or PMMA haptics and a one piece plate haptic lens. Silicone has the longest track record of surgical results with millions of silicone lenses implanted worldwide and many published results. *Cumming* compared the results of 503 patients implanted with plate haptic silicone lenses with 253 patients implanted with three piece silicone lenses.[249] Visual results in both groups were excellent with 97.5% of patients with plate haptic lenses seeing 20/40 or better but he found a higher incidence of cystoid macular edema with a visual acuity of less than 20/40 in the three piece group than in the plate haptic group. Complications were reported in 10% of eyes implanted with a three piece lens compared with 3% of eyes implanted with the plate haptic lens. The three piece lens in this study did have polypropylene loops which are known to have a higher complication rate.

A new category of intraocular lenses was created with the advent of multifocal and accommodating lenses. An accommodative IOL technology with the potential to provide over 10 D of accommodative power was proposed.[250] With an IOL that sits on top of the collapsed capsular bag, this accomodative IOL may be the first intraocular lens to provide real, comfortable, and lasting accommodation for near, intermediate and far distances. Other recent IOL developments include blue light filtering IOLs which include an absorber to filter UV as well as high-energy blue light present in natural and artificial lighting, both of which can cause vision problems. With toric IOLs astigmatic vision can be corrected.

Special types of phakic IOLs (PIOLs) are available for patients requiring IOL implantation without removal of the crystalline human lens, particularly useful in refractive surgery for high myopia. PIOLs can be either spheric or toric – the latter is used for astigmatic eyes. The difference is that toric PIOLs have to be inserted under a specific angle, or the astigmatism will not be fully corrected, or it can even get worse. Additionally the eye surgeon has to determine the correct size of the PIOL for each patient individually. If the lens is of incorrect length, it can rotate inside the eye, causing astigmatism, and/or damage to the natural lens. It can also block the natural flow of fluid inside the eye, causing glaucoma. According to placement site in the eyes PIOLs can be divided into two groups. (1) Angle supported PIOLs which are placed in the anterior chamber. They are notorious for their negative impact on the corneal endothelial lining, which is vital for maintaining a healthy dry cornea. (2) Iris supported PIOLs are gaining more and more popularity. The IOL is attached by claws to the mid peripheral iris by a technique called enclavation. It is believed to have a lesser effect on corneal endothelium. Sulcus supported PIOLs are placed in the posterior chamber in front of the natural crystalline lens. They have special vaulting so as not to be in contact with the normal lens. The main complications with this type is their tendency to cause cataracts and/or pigment dispersion. Also aphakic IOLs are implanted via clear lens extraction and replacement (CLEAR) surgery for correcting larger errors in myopic, hyperopic, and astigmatic eyes. During CLEAR, the crystalline lens is extracted and an IOL replaces it in a process that is very similar to cataract surgery and involves lens replacement. CLEAR has a 90% success rate, the risks include wound leakage, infection, inflammation, and astigmatism. CLEAR can only be performed on patients with ages of 40 and older. This is to ensure that eye growth, which disrupts IOLs, will not occur post-surgery.

In summary, the advancement of IOL technology has brought by a very sophisticated mean to restore vision after removal of the natural eye lens. However, problems and complications that need to be solved are still persistent. We have not yet achieved *Charles Kelman's* aspiration for the millennium, saying "We must restore the patients vision at 90 to that which they enjoyed at 19 – including accommodation."[251]

1.3.2 Prediction of the Technical Specifications of an IOL

The prediction of the refraction power after a cataract surgery is often a great challenge and inaccurate.[26] Thinking that since the fundamental work of *Helmholtz* and *Gullstrand*,[252] the human eye was completely understood with regards to its optical properties often proofs to be wrong. An eye consists of different not perfectly spherical interfaces and contains liquid media having refractive indices different from air. Hence the eye represents a complex optical system.[15] For the calculation of the perfect IOL for a patient's eye a great number of formulas and approaches can be found in the literature.[15–25] These empiric formulas give more or less satisfying results. The more the optical properties of an eye deviate from the average values of the probands collective that has been employed during formula development, the more likely unsatisfying results are to be expected. One of the best theoretical approaches are so called ray tracing models. This technique allows calculations with an error of less than 0.001 D, a value that the patient cannot perceive.[15] However, the most serious problem is not the theoretical ability to calculate an optical system but the errors in the biometric data that need to be collected before cataract surgery. It is still quite a difficult task to measure the curvature radii of the cornea, the length of the eye ball, or the refractive power with the required precision. Even with state of the art biometric measuring equipment errors can be minimized but not prevented. Therefore, the input data for the calculation of an ideal IOL is already erroneous.

Aside from the errors due to the measurement of biometric data an exact prediction of the postoperative refraction is almost impossible. This is mainly due to unpredictable effects which may occur during the healing process within the weeks or months following the cataract surgery. These may include (but are not limited to) effects on the pseudophakic anterior chamber depth, which is the notional distance between the vertex of the cornea to the effective principal surface of the IOL and changes in the cornea shape.[16] The exact value of those changes depends on a variety of factors including

originalities of the eye, the IOL type, as well as the surgeon and the instruments utilized.[26] Last but not least uncertainties in the specifications of the IOL chosen have to be mentioned.[16] The applicable ISO 11979 standard allows tolerances of ± 0.33 D in the corneal plane for an IOL above 25.00 D and even ± 0.66 D for an IOL above 30.00 D. Despite some manufactures claiming to produce IOLs with lower tolerance, the ophthalmic surgeon usually has no means to check the refractive properties of an IOL before implantation. In summary, the main sources of errors are not the computational method but the measuring tools of the biometric data and the individually unique healing process.

According to clinical trials slightly more than 80% of the patients are typically in a range of ± 1 D around the desired refraction. A significantly higher precision seems not to be feasible with methods currently available.[26] Most recent work shows a trend toward smaller post-operative refractive errors related to cataract surgery. However, refraction errors are practically inevitable.[27–30] Even greater problems arise when certain conditions of the eye persist, for example, if the axial length of the eye is significantly longer[31] or shorter[32] than average. In general, pediatric cases of cataract are complicated because the eye is still growing.[33,34] The growth of the eye is not finished until the age of about 25. A very important issue also is IOL calculation for patients which have undergone refractive surgery like the popular laser-assisted in situ keratomileusis (LASIK). The procedure uses an excimer laser (193 nm) to remodel the corneal stroma by vaporizing tissue in a finely controlled manner. When using LASIK to correct myopia the cornea gets an oblate shape. Correction of myopia is by far the most common case for the application of LASIK.[253,254] IOL power calculation after excimer laser surgery can be difficult, especially when pre-refractive keratometry values are not available. Due to the unnatural shape of the cornea accurate prediction of the ideal IOL for such eyes is even more complicated than in a surgically untreated eye.[36–43] Since LASIK seems to become more and more popular, a great number of patients that have undergone that procedure in recent years might also suffer from cataract and need an IOL in the next ten or twenty years. This creates a new challenge for cataract surgery and especially IOL calculation that will be difficult to address. Since it is unavoidable today that a great number of patients treated with IOLs will need prescription eyewear for ideal vision other concepts need to be developed to gain optimal vision after cataract surgery.

1.4 Changing the Focal Length of a Lens

Since there are shortcomings in preoperative IOL refractive power prediction which can not be overcome in the near future the aim of this work is to provide a solution for non-invasively changing the refractive power of an already implanted IOL. The idea is to create polymers suitable for the fabrication of IOLs whose refractive index may be changed non-invasively later on. The change in refractive index shall be large enough that a change in focal length of at least 1 D of a typical IOL can be achieved. Thus with IOLs made from these polymers the great majority of patients would not need any additional prescription eyewear. Furthermore, a postoperative variation of the lens optical power would also be economically favorable. A set of standard lenses could be used and the refractive power could be fine tuned post-operatively to gain perfect vision. Also, aberrations such as astigmatism could be corrected for. In the following section the theoretical background of the focal length alteration of an IOL through refractive index tuning will be outlined.

1.4.1 Parameters Determining the Focal Length of a Lens

A lens is an optical device with perfect or approximate axial symmetry which transmits and refracts light, converging or diverging the beam. A simple lens, like an IOL, is a lens consisting of a single optical element. Most lenses are spherical lenses: their two surfaces have the shape of parts of the surfaces of spheres, with the lens axis ideally perpendicular to both surfaces. Each surface can be convex, concave, or planar. An IOL is usually biconvex just like the natural lens of the eye. The line joining the centers of the spheres making up the lens' surfaces is called the axis of the lens. Typically, the lens axis passes through the physical center of the lens, because of the way they are manufactured. Toric lenses have surfaces with two different radii of curvature in two orthogonal planes. They have a different focal power in different meridians enabling the correction of astigmatism.

If the lens is biconvex or plano-convex, a collimated beam of light pasing through the lens, traveling parallel to the lens axis will be focused to a spot on the axis, at a certain distance behind the lens known as the focal length f (Fig. 1.14). In this case, the lens is called a positive or converging lens. The focal length f is positive for converging lenses,

and negative for diverging lenses. The value $1/f$ is known as the optical power of the lens, measured in diopters (D), which are expressed in units of one over meters (m^{-1}). The physical reason for the refraction of light at the surface of the lens is that the speed of light in the two adjacent media is different. The refractive index n of a given medium is a measure of how much the speed of light in that particular medium c_m is reduced compared to the speed of light in vacuum c_0 which is a natural constant.

$$n = \frac{c_0}{c_m} \tag{1.1}$$

Snell's law, named after the Dutch mathematician *Willebrord Snellius*, states that the ratio of the sines of the angles of incidence θ_1 and refraction θ_2 is equal to the ratio of velocities in the two media c_1 and c_2, respectively. Also, the ratio of the sines of the angles of incidence is equal to the inverse ratio of the indices of refraction.

$$\frac{\sin\theta_1}{\sin\theta_2} = \frac{c_1}{c_2} = \frac{n_2}{n_1} \tag{1.2}$$

This makes Snell's law the mean to determine the paths of light rays through refractive media with varying indices of refraction. As light passes the interface between different media, depending upon the relative refractive indices of the two media, the light will either be refracted to a smaller, or greater angle. These angles are measured with respect to the normal, perpendicular to the interface. In the case of a biconcave lens light traveling from the surrounding medium into the lens material, which has a higher refractive index, light would be refracted towards the normal. This is because the light is slowed down inside the lens. Due to the convex curvature of the lens the light is focused in one spot (Fig. 1.14). Refraction between two surfaces is also referred to as reversible because the angles would be the same for light propagating in the opposite direction, if all other parameters were identical.[255] Of course, the focal length of a lens dependens upon the refractive index of the material the lens is made of, or more precisely the difference between the lens material's refractive index and the refractive index of the surrounding medium. For example, the refractive index of air can be approximated by the refractive index of vacuum which is by definition 1. The aqueous liquids inside the human eye have a refractive index of 1.336[252,256] meaning that the speed of light in that medium is only about 75% of the speed of light in vacuum. Therefore, the material of an IOL needs to have a refractive index greater than 1.336.

The focal length of a lens is also heavily dependent upon the two curvature radii r_1 and r_2 and to a lesser extent dependent upon the center thickness t_c of the lens. All these

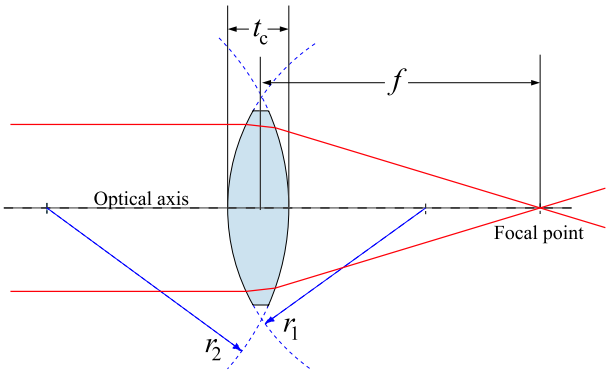

Figure 1.14: Sketch of a converging biconvex lens defining the curvature radii and the focal length.

parameters affecting the focal length are taken into account in the paraxial formula for lenses in arbitrary media. This formula allows for the calculation of the lens constant k

$$k = \frac{n' - n}{r_1} + \frac{n'' - n'}{r_2} - \frac{t_c\,(n' - n)\,(n'' - n')}{n'\,r_1\,r_2} \tag{1.3}$$

where n and n'' are the refractive indices of the media adjacent to the front and the back of the lens an n' is the refractive index of the lens material. The signs of the lens' radii of curvature indicate whether the corresponding surfaces are convex or concave. The sign convention used is defined as follows: if r_1 is positive the first surface is convex, and if r_1 is negative the surface is concave. The opposite holds true for the back surface of the lens: if r_2 is positive the surface is concave, and if r_2 is negative the surface is convex. Naturally, if either radius is infinite, the corresponding surface is flat. This means that in our example of a biconvex IOL r_1 is always positive and r_2 is always negative. Finally the effective focal length

$$f = \frac{n}{k} \quad \text{and} \quad f'' = \frac{n''}{k} \tag{1.4}$$

on both sides of the lens can be calculated.[257,258] In our case f is always equal to f'' because the media surrounding both sides of the lens have the same refractive index. The change in focal length of an IOL or a lens in general, when only its refractive index is changed, is dependent on the initial focal length. In order to estimate how large the change in refractive index of the IOL material has to be to provide an useful change in focal length, average IOL data must be used. For example, if a lens would have curva-

ture radii of 14.5 mm and −14.5 mm, a center thickness of 1 mm, and a refractive index of 1.55, the refractive power would be 22 D. This is an average value for commercial IOLs. To lower the refractive power by 2 D to 20 D the refractive index would have to be lowered by 0.02 to 1.53. This example shows that a change in refractive index of about 0.02 must be achieved to accomplish a change in refractive power that is large enough to correct the refractive errors of most patients treated with IOLs.

1.5 Methods for Changing the Refractive Index of a Polymer

The approach taken in this work, to achieve the described change in focal length of an IOL shall be mainly an alteration of the refractive index of the polymer the lens is made up of. Since the IOL is to be tuned non-invasively once implanted the change in refractive index must be induced by light. Due to the absorption properties of the cornea (Fig. 1.15) restrictions to the wavelength, that can be used, apply.[259–261] Biocompatibility of the material also plays an important role, making polymers with the highest possible similarity to existing polymers used for IOLs, generally favorable. Furthermore, no substances of low molecular mass should be contained within the polymer at the time of manufacturing or be released as a result of the light induced lens tuning process. The requirements on a non-invasively tunable IOL are summarized in Table 1.2. The following sections aim to provide the physical background of refractive index change, give a brief overview of refractive index change in polymers and explain the approach for refractive index change used in this work.

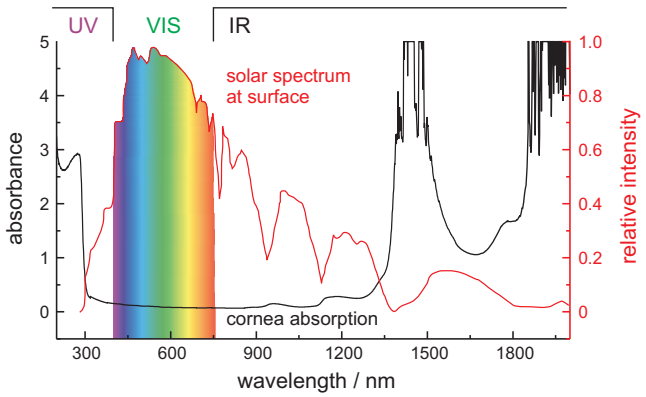

Figure 1.15: Absorption spectrum of the human cornea (black line) and the solar irradiance spectrum at the surface (red line) for reference. The IOL cannot be irradiated with shorter UV wavelengths due to the absorption of the cornea.

Table 1.2: Requirements for the polymer for non-invasively refractive index tunable IOLs.

Transparent	The polymer may not be opaque. Otherwise scattering will be caused by the polymer or embedded particles generating glare.
Colorless	The material should be without color. Only a slight yellowish tone caused by an absorption of blue light can be tolerated. Colored materials are not suitable.
Photo tunable	The refractive index of the material needs to be tunable by light to make the process non-invasive. Furthermore, the wavelength used must not be absorbed by the cornea.
Reversible	The change in focal length and thus the refractive index should be reversible to allow for a correction of a previous optical tuning even after a prolonged period of time.
Immune to sunlight	The overall IOL must be designed in such a way that light from the sun or other common light sources cannot change the refractive power even after extended periods of time.
Elastomeric	The material should have elastomeric properties to obtain a foldable IOL and avoid plastic deformation.
Cross-linked	To afford elastomeric properties the polymer must be a cross-linked network. A cross-linking procedure that does not involve a photochemical process is favorable to avoid undesired changes in refractive index.
Bulk polymerizable	The corresponding monomer should be polymerizable to a plate in a bulk polymerization. Bulk polymerization is the conversion of monomer into a polymer without the aid of a solvent.
Suitable for turning	The mechanical properties of the polymer must allow the fabrication of IOLs by diamond turning.
Biocompatible	The polymer must not have any toxic or injurious effects on the eye.
Non-degradable	Despite being biocompatible the polymer should not be bio-degradable. Otherwise, the IOL would degrade over the long time it needs to stay in the eye.

1.5.1 Polarizability and Index of Refraction

The speed of light in vacuum c_0 is a fundamental constant and describes the speed of an electromagnetic wave in vacuum. From the solutions of *Maxwell's* equations the speed of light in vacuum can be related to the electric constant ε_0 and the magnetic constant μ_0. They are also fundamental constants.[262,263]

$$c_0^2\,\varepsilon_0\,\mu_0 = 1 \quad \text{or} \quad c_0 = \frac{1}{\sqrt{\varepsilon_0\,\mu_0}} \tag{1.5}$$

The speed of light when passing through a transparent medium c_m, is less than it is in vacuum. With regard to Eqn. 1.5 the electric constant needs to be substituted by the permittivity ε and the magnetic constant by the permeability μ.

$$c_m = \frac{1}{\sqrt{\varepsilon\,\mu}} = \frac{1}{\sqrt{\varepsilon_0\,\varepsilon_\mathrm{r}\,\mu_0\,\mu_\mathrm{r}}} = \frac{1}{\sqrt{\varepsilon_\mathrm{r}\,\mu_\mathrm{r}}} \cdot c_0 \tag{1.6}$$

The relative permittivity ε_r (also called dielectric constant) is a dimensionless, material dependent quantity that gives the permittivity relative to the electric constant. The relative permittivity of vacuum is therefore $\varepsilon_\mathrm{r} = 1$ which can also be seen by comparing Eqn. 1.5 and Eqn. 1.6. The actual permittivity is then calculated by multiplying the relative permittivity by ε_0

$$\varepsilon = \varepsilon_\mathrm{r}\,\varepsilon_0 = (1 + \chi_\mathrm{e})\,\varepsilon_0 \tag{1.7}$$

where χ_e is the electric susceptibility of the material, a value closely related to ε_r and defined as

$$\chi_\mathrm{e} = \varepsilon_\mathrm{r} - 1. \tag{1.8}$$

The relative permittivity describes how the electric field strength is lowered if the material, also referred to as a dielectric, is placed in an electric field. Relative permittivity is determined by the ability of a material to be polarized in response to the field, and thereby reduce the total electric field within the material. The relative permittivity of most materials is between 1 and 100, however dielectrics with ε_r of up to 10000 are known. To give a few examples the relative permittivities of polystyrene, cellulose and water are 2.5, 4.5 and 81, respectively. The relative permittivity of air can be regarded as 1 to a good approximation. In general, the relative permittivity is not a constant, as

it can vary with the frequency of the field applied, humidity, temperature, and other parameters. In a nonlinear medium, the permittivity can depend on the strength of the electric field.[264] Therefore, the outdated term "dielectric constant" for ε_r is ambiguous and should not be used anymore.

For a magnetic field the values μ_0, μ_r and μ are defined analogous to the corresponding values of the electric field. The permeability is

$$\mu = \mu_0 \, \mu_r \tag{1.9}$$

and the magnetic susceptibility is

$$\chi_m = \mu_r - 1. \tag{1.10}$$

By definition the relative permeability of vacuum is $\mu_r = 1$. The relative permittivity varies with magnetic field strength and is generally a function of frequency. The relative permeability of a substance can also have negative values. One distinguishes diamagnetic substances ($\mu_r < 1$), paramagnetic substances ($\mu_r > 1$) and ferromagnetic substances ($\mu_r \gg 1$). Most organic substances like polymers are diamagnetic and their relative permeability is very close to 1.[262]

The refractive index n is a material constant that characterizes the refractive properties of that medium. As already introduced in section 1.4.1 the refractive index is the ratio of the speed of light in vacuum to the speed of light in a given medium (Eqn. 1.1). Vacuum consequently has a refractive index of 1. The refractive index of water is 1.333. The refractive index of commercially available glassware ranges from 1.4 to 1.9. The refractive indices of most organic polymers are between 1.4 and 1.6, with specially modified high refractive index polymers having an index of refraction of more than 1.7. The refractive index is generally dependent on the frequency of light, a phenomenon called dispersion. Since the refractive index of dry air ($n_{air} \approx 1,0003$) is only slightly different from 1, measurements can be made relative to air to a good approximation. In technical optics the refractive index n' is used. It is defined as

$$n' = \frac{c_{air}}{c_m}. \tag{1.11}$$

By substituting Eqn. 1.5 and Eqn. 1.6 in Eqn. 1.1 we obtain the relation

$$n = \frac{\sqrt{\varepsilon_0\,\varepsilon_\mathrm{r}\,\mu_0\,\mu_\mathrm{r}}}{\sqrt{\varepsilon_0\,\mu_0}} = \sqrt{\varepsilon_\mathrm{r}\,\mu_\mathrm{r}}. \tag{1.12}$$

Since $\mu_\mathrm{r} \approx 1$ for organic polymers at frequencies in the visible part of the electromagnetic spectrum, Eqn. 1.12 may be further simplified to

$$n \approx \sqrt{\varepsilon_\mathrm{r}}. \tag{1.13}$$

This means that the refractive index of a polymer is changed when its relative permittivity ε_r is varied. To understand how relative permittivity and thereby the refractive index of a polymer can be modified we have to take a closer look on what happens when light waves interact with matter. If an electric field, in this case the electric component of a light wave, $\vec{E}$, acts on a medium it induces a dipole moment $\vec{p}$. Polarity $\vec{P}$ is defined as electric dipole density per unit volume.

$$\vec{P} = \frac{\mathrm{d}\vec{p}}{\mathrm{d}V} \tag{1.14}$$

The norm of the vector $\vec{P}$ is the area density σ_p of the polarity charge.

$$\left|\vec{P}\right| = \sigma_\mathrm{p} \tag{1.15}$$

The polarity vector $\vec{P}$ and the outside electric field vector $\vec{E}$ point in the same direction. The lines of electric flux of the electric field induced by the polarity charges $\vec{E}_\mathrm{pol}$ run from the positive to the negative surface charges of the dielectric. Hence, the electric flux lines inside the dielectric run into the opposite direction as those of the exterior electric field $\vec{E}$. The polarity $\vec{P}$ within the electric field is given by

$$\vec{P} = (\varepsilon_\mathrm{r} - 1)\,\varepsilon_0\,\vec{E} = \chi_\mathrm{e}\,\varepsilon_0\,\vec{E}. \tag{1.16}$$

The electric susceptibility is defined in Eqn. 1.8. Two types of polarity need to be distinguished: displacement polarity and orientational polarity. Displacement polarity is caused by the displacement of electric charges in neutral atoms or molecules relative to each other. It is the relative tendency of a charge distribution, like the electron cloud of an atom or molecule, to be distorted from its normal shape by an external electric field, i.e. the electric field induces electric dipole moments. Orientational polarity is caused by orienting permanent dipoles along the electric field lines. Those dipoles have been

present in the medium even before the electric field was applied. In the visible spectral range only orientational polarity of the electron shell has to be taken into account. The frequencies of visible light are relatively high in the range of about 10^{14} Hz to 10^{15} Hz. Therefore, factors contributing to the overall polarity caused by displacement of the atoms and orientation of permanent dipoles are so small that they can be neglected. Only the electrons are able to "follow" the quickly oscillating electric field.[265,266] For the displacement polarity the equation

$$\vec{P} = x\,\alpha\,\vec{E} \tag{1.17}$$

provides a relation between the number of particles per unit volume x and the polarity. The constant of proportionality α in this equation is called electric polarizability. Polarizability is a molecular parameter. Quantum particles are not rigidly connected to each other, they are rather bound to their resting position by forces that are, to a first approximation, elastic. Therefore, *Newton's* law $F = -k\,x$ can be applied. An external electric field $\vec{E}$ exerts a force $Q \cdot E$ upon such a charge Q. This force deflects the charge by a distance $x = F/k = Q\,E/k$. This displacement causes an induced dipole moment

$$\vec{p} = Q\,x = \frac{Q^2}{k}\,\vec{E} = \alpha\,\vec{E}. \tag{1.18}$$

By comparison with Eqn. (1.16) we can easily see that α must be proportional to ε_r.

$$\alpha \propto (\varepsilon_\mathrm{r} - 1)\,\varepsilon_0 \tag{1.19}$$

This means that altering the polarizability of molecules comprizing a given medium must cause a change in refractive index of that medium. In other words, we have found a relation between the polarizability which is a molecular or atomic property and the refractive index which is a property of the bulk material. The refractive index of materials depends on the linear polarizability α and the number density of molecules. This is expressed mathematically by the *Lorentz–Lorenz* equation that relates the refractive index n to the molar refraction R.

$$R = \frac{n^2 - 1}{n^2 + 2} \cdot \frac{M}{\varrho} = \frac{n^2 - 1}{n^2 + 2} \cdot V_\mathrm{m} \tag{1.20}$$

Sometimes the letter A instead of R is used for the molar refraction to avoid confusion with the universal gas constant. M is the molar mass, ϱ the density and V_m the molar

volume which is molar mass divided by density. The molar refraction is the volume of a substance taken up by each mole of that substance. In SI units R has the unit $m^3\ mol^{-1}$. The already deduced relation between the refractive index and the polarizability becomes more obvious in an alternate diction of the *Lorentz–Lorenz* equation where N is the number density of molecules.[267–269]

$$\frac{n^2-1}{n^2+2}\cdot\frac{M}{\varrho}=\frac{4}{3}\,\pi\,N\,\alpha \tag{1.21}$$

The refractive index does change with the polarizability but also with the number density of molecules. If the reaction that is utilized to control the refractive index, changes the molar volume of the material this may also contribute to the alteration of optical properties. In the case of reactions that break π conjugation, the linear polarizability significantly decreases, but the change in density is usually considered negligible.[270] For most transparent saturated organic compounds, the molar refraction, which is largely independent of temperature and physical state, can be calculated by summation of atomic and structural constants.[271] If the density is also known the refractive index can be calculated. In terms of group contribution to the refractive index, the molecular polarizability is expressed as the sum of the polarizabilities of the constituent functional groups.[267,272,273] Alternatively and equivalently, the polarizability is usually expressed as the sum of the molar refraction of functional groups of the organic molecules and polymers

$$\frac{n^2-1}{n^2+2}\cdot V_\mathrm{m}=\sum_i R_i \tag{1.22}$$

in which R_i is the molar refraction of a functional group i. For a polymer, V_m and i are the molar values corresponding to the polymer repeat unit.[274] There is a large body of experimental data on the refractive index for many classes of organic non-conjugated polymers. Reliable predictions of the refractive indices of non-conjugated polymers can be obtained by using semi-empirical group-contribution models derived from the refractive indices of liquid organic compounds as well as organic polymers.[267,272] These group-contribution calculations are based on the molar refraction as an additive function and different models of the refractive index such as those by *Lorentz–Lorenz*[268,269], *Gladstone–Dale*[275,276], *Vogel*[277,278] and *Looyenga*[275]. The molar refraction values corresponding to these group-contribution models can be found in the respective literature[267] and have been found to predict the refractive index of non-conjugated polymers in good agreement with experimental data. The fundamental assumption of the

semi-empirical group-contribution formalisms is the additivity of properties of functional groups such as molar refraction. Therefore, problems arise when significant cooperative effects among functional groups invalidate the additivity principle. It is difficult or impossible to accurately predict the refractive index of conjugated polymers when cooperative effects due to π-electron delocalization are neglected. It has been found experimentally that the refractive index estimate of all these models is bad for conjugated polymers.[279–282] An accurate theoretical prediction is difficult still today because π-electron delocalization effects on the refractive index of polymers are not taken into account in the currently available molar refraction values of functional groups.

1.5.2 Synopsis of Refractive Index Change in Polymers

Polymers capable of refractive index changes have gained increased attention not only due to their potential application as media in optical data storage devices. Such materials also have applications in optics and photonics with distributed feedback lasers and optical waveguides. Numerous mechanisms for refractive index modulation in polymers have been reported. One of the simplest approaches is to modify the refractive index of PMMA by UV laser light. Photons of suitable wavelengths initiate a side chain cleavage from the main polymer chain as shown in Fig. 1.16 Considering the UV laser assisted modification mechanism of PMMA one has to distinguish between two cases.[283] Using 248 nm radiation, a complete side chain scission occurs while at 193 nm only an incomplete side chain scission is observed. Usually the carbon–carbon and carbon–hydrogen bonds of an aliphatic organic polymer have a dissociation energy of about 7.9 eV which corresponds to 160 nm irradiation.[284,285] however, similar to other photochemical reactions of Norrish I type the carbonyl in the side chain plays a crucial role.[286–288] The oxygen atom in the carbonyl group attracts all electrons of the double bond because of its high electronegativity. This leads to a weakening of the bonds adjacent to the carbonyl group. Therefore, the carbon–carbon bond and the carbon–oxygen bond attached to the carbonyl group have reduced dissociation energies. For the cleavage of the carbon–oxygen bond, a photon energy of 6.3 eV (corresponding to 193 nm) is necessary whereas for the cleavage of the carbon–carbon bond a photon energy of only 4.1 eV (corresponding to 248 nm) is sufficient (Fig. 1.16). In both cases the UV laser irradiation results in a side chain scission of different types leading to an increase of the mechanical density due to *van-der-Waals* interactions and thus an increase of the optical refractive index.[289,290] Refractive index increases accompanied by

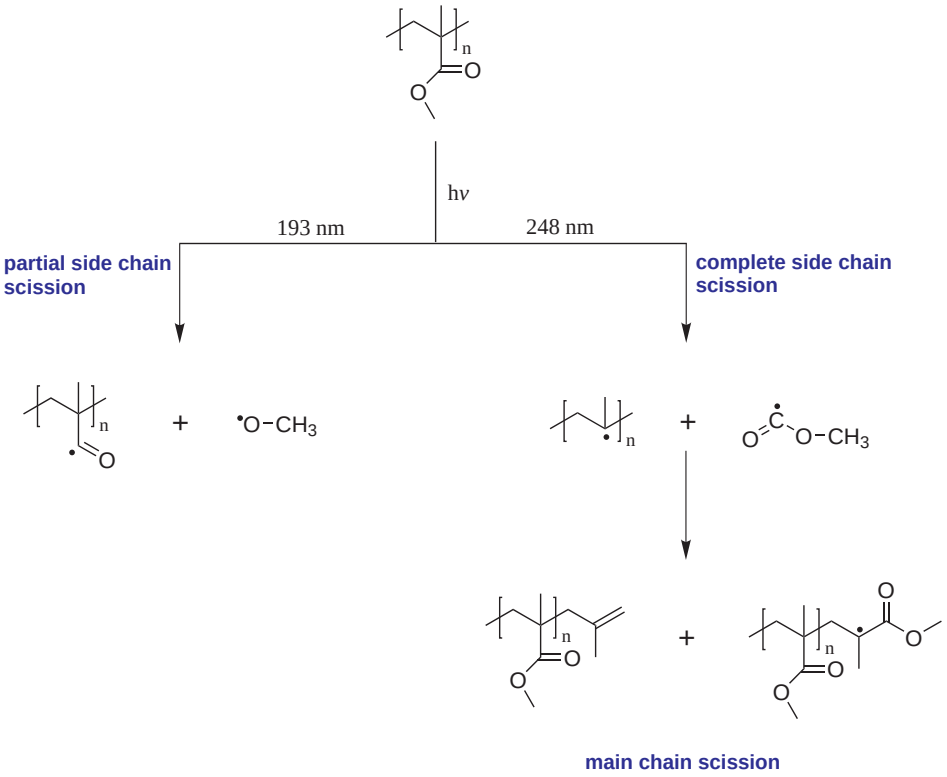

Figure 1.16: UV-photon induced photochemical modification mechanisms of PMMA at different wavelengths. Depending on the wavelength an incomplete side chain scission (left) or a complete side chain scission (right) occurs.

thickness reduction has also been detected in PMMA thin films when irradiated with a conventional UV lamp.[291–294] For most samples, especially thicker films in the range of several microns the refractive index change was below 0.01. Thickness of the PMMA films was also reduced upon UV irradiation due to the mass loss originating from the escape of volatile molecules generated during the UV irradiation process.[291] In similar experiments, a decrease in refractive index was observed for poly(ethylene terephthalate) (PET) films when irradiated with 15 ns pulses from excimer lasers at both 193 nm and 248 nm. However, the mechanisms are not known in such detail as it is the case for PMMA.[295] Laser induced refractive index change was reported in poly(isopropyl acrylamide) gels via a photo-thermal conversion process. The refractive index change is caused by the thermal expansion of the gel. The thermal expansion of the solvent as well as its mobility, which is restricted by the polymer chains, determins the magnitude of the refractive index change. Even though the refractive index change occurs within 10^{-2} s, the magnitude was as low as 10^{-3}.[296] Large refractive index changes induced

in silicone and acrylate based hydrogel polymers induced by femtosecond laser micromachining were also reported. The hydrogels exhibit water contents between 36% and 80% and were kept in a hydrating solution throughout the experiments. A Ti:Sapphire laser operating at 800 nm, emitting pulses with 30 fs width, and 1.3 nJ energy was used to micro-machine optical gratings inside several hydrogel based polymers. By measuring the diffraction efficiency of the grating at 632.8 nm the authors found refractive index changes up to 0.06 within the irradiated area.[297] The index of refraction changes observed in these hydrogels are much larger than those that have been observed in other polymer materials or ordinary glasses. It is believed that the action of the femtosecond pulses could cause a phase separation.[298,299] This phase separation means that water is locally excluded from the irradiated regions leading to a densification of the polymer material thus causing the refractive index change.

A simple method of changing the refractive index upon light radiation is a formulation comprised of a polymerizable compound and a radiation sensitive polymerization initiator dispersed in a polymer matrix. It is possible to make polymers containing a remainder of radical-polymerizable side-chain vinyl group. The polymer can then be irradiated with UV light in order to bring the vinyl groups to reaction. The refractive index change is mostly caused by a density change associated with the reaction of the remaining vinyl groups in the polymer. Due to its simplicity, this straightforward approach seems to have found some commercial interest and is the subject of some patents.[300–302]

Almost all methods for changing the refractive index in plain, undoped polymers are not suitable for the manufacturing of IOLs. The most significant drawbacks are the release of low molecular mass side products (Fig. 1.16) which is not tolerable in a medical implant, the magnitude of refractive index change being too low in most cases to be useful for IOL tuning and the comparatively high energies required to induce the change bearing the risk of ocular damage. For the sake of completeness it should be mentioned that humidity induced refractive index changes in poly(ethylene glycol) (PEG) thin films were reported.[303] Furthermore it is possible to change the refractive index of PMMA films by applying an electric field on the order of 10 kV cm^{-2} when the sample is heated above the glass transition or fluid temperature. A change in refractive index of about 0.015 can be achieved when the film is heated above 250 °C whereas slight changes occur above 80 °C.[304] It is quite obvious that those two approaches are not suitable for post-operative refractive index changes of an IOL.

Many researchers studied the change in refractive index of organic photochromic dyes, such as azobenzenes, fulgides, and diarylethenes.[305–320] Many fused ring bridge structures of π-conjugated bonds in benzene-, naphthalene-, or anthracene-derived ring systems that connect donor and acceptor groups and often contain heteroatoms are useable for refractive index change in polymers. The polarization characteristics of the dye molecules are stabilized since the bonds in the fused ring bridge are not susceptible to rotation, reducing the opportunity for photoisomerization. The dyes are compatible with polymeric compositions and are electrically neutral. But these dyes have charge transport, electronic and orientational properties such that upon illumination the dye facilitates refractive index modulation.[321] There are some reports[316–320] for appreciable changes of the refractive index in the visible region during irradiation of light. UV irradiation largely decreases the refractive indices of PMMA films containing photochemically active nitrones as dopants with high transmittance.[316] The two-dimensional refractive index patterns fabricated by use of these photochemical reactions may be considered for memory, switching, and waveguide applications.[316]

The photoinduced refractive index change of a polyester with covalently bonded side groups of the azo dye disperse red was studied. The polymer shows an absorption peak at 470 nm and is transparent from 640 nm to the near infrared region. Under the exposure of light at or near the absorption peak the refractive index decrease of more than 0.03 at a wavelength of 633 nm. The reason for the photoinduced change in refractive index is the *trans–cis* photoisomerization of the azo groups.[322,323] The refractive index change of azo dye doped polymers was also studied by a number of researchers.[324,325] Sometimes azobenzene groups with heterocyclic sulfonamide functionalities were used. However, this did not lead to significant improvements in terms of refractive index change.[326,327] Refractive index modulation by change in alignment of liquid crystals by photochemically induced phase transitions was found. The liquid crystalline polymers had photochromic dyes like azobenze in the side group.[328] Also, other dyes were investigated with respect to their photoinduced refractive index change. Diarylethene derivatives dispersed in a polymer matrix show a change in refractive index on the order of 10^{-3}. Among these chromophores, bis(thiophen-3-yl)ethene (BTE) derivatives have attracted particular interest for their photochromic efficiency and thermal stability. These molecules can be switched between a closed and an open ring configuration using light of 350 nm, and 500 nm, respectively (Fig. 1.17).[329,330] BTE derivatives were functionalized with a methacrylic moiety to allow the formation of copolymers with styrene and butyl methacrylate (BMA) via free

radical polymerization. This affords a photochromic polymer in which photochromophores are attached to polymer chains by covalent bonding.[331]

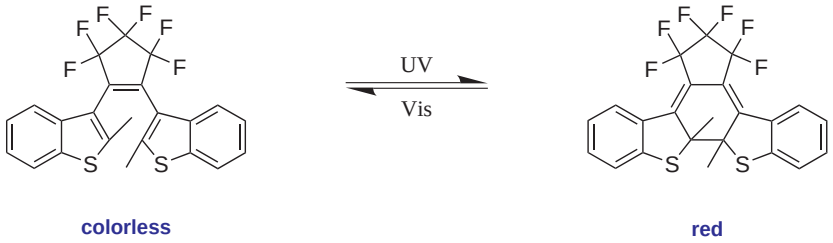

Figure 1.17: Chemical structure of (1,2-bis(2-methylbenzothiophen-3-yl) hexafluorocyclopentene (left) and the photochromic ring closure/opening process. Note the chromic change from colorless to red.

In a similar fashion, the refractive index of polymers doped with spiropyran dyes can be switched very fast using two different wavelengths. Spiropyrans undergo a UV light induced ring opening reaction that leads to a colored photomerocyanine. The photomerocyanine can react back to the spiropyran by either irradiating the dye with visible light or by heating.[332,333] Some papers report refractive index changes in polymer films doped with nitrone derivatives. These molecules form an oxaziridine when irradiated with UV light.[270] In some cases further rearrangements starting from the oxaziridine were observed.[334] The refractive index changes reported were up to 0.028 for PMMA doped with 23% (4-*N*,*N*-dimethylaminophenyl)-*N'*-phenylnitrone (Fig 1.18).

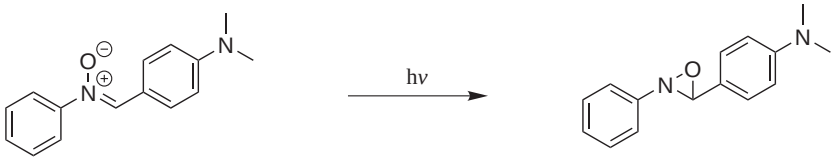

Figure 1.18: Chemical structure of (4-*N*,*N*-dimethylaminophenyl)-*N'*-phenylnitrone and the photochemical reaction to from an oxaziridine.

Phthalocyanines are macrocyclic compounds having an alternating nitrogen carbon ring structure and often coordinate a metal ion in the center. They were also proposed as a dopant for refractive index change in polymer films.[335,336] Polyfluorenes are a class of electroactive and photoactive polymeric materials where the main chain is composed of the dye molecule itsself (Fig 1.19). These polymers can be made by various coupling reactions like the *Yamamoto*, *Suzuki*, or *Stille* coupling using sufficient bifunctional monomers.[337] It has been found that the refractive index of the β-phase

which contains extended rigid chains is appreciably larger than that of the glassy polymer. Therefore this offers a way to change the refractive index.[338] Complex refractive index changes in composite materials composed of a high and a low refractive index polymer with a fluorene group in the main chain were also reported.[339]

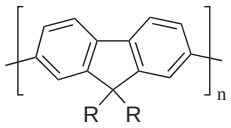

Figure 1.19: Poly(9,9-dialkylfluorene) is the lead structure of a class of polymers that has received a lot of attention owing to the fact that it can also be used to develop all plastic, full-color, light-emitting diodes. R is usually an alkyl chain with a length on the order of six to eight carbon atoms.

A photoinduced refractive index change as large as 0.014 at 633 nm in transparent polymer films was realized by using photoirradiation of polyimide precursor films containing a phenylazide and successive imidization. The phenylazide fragment forms a charge-transfer complex with imide moiety.[340] A rather special method uses polymer films with acid-responsive chromic dyes like rhodamine B or coumarin 6. Electron beam acid generators like phenyl *p*-toluenesulfonate, triphenylsulfonium triflate or 1,2,3-tris(methanesulfonyloxy)benzene generate acid by irradiation with an electron beam. That acid protonates the dye affording a color change due to the different absorption spectra of the unprotonated and protonated dye. Electron beam irradiation with doses of about 50 µC cm^{-2} gave refractive index changes of about 0.013 at 633 nm.[341] Small refractive index changes were observed in films formed of poly(3-octylthiophene) or poly(phenylene vinylene) derivative blended with fullerenes. However, it is difficult to process these blends due to the tendency of the fullerene to phase separate and crystallize. Despite apporaches to overcome this problem by using methanofullerenes the absorption in the visible spectral range is a further disadvantage.[342,343] ORMOCER® polymer which are inorganic-organic hybrid materials can show a refractive index change of up to 0.03 with relatively low exposure using a standard mecury lamp. To yield the UV-sensitivity of the material and to initiate a free radical polymerization process an α-amino acetophenone photo-initiator must be added to the polymer.[344]

Refractive index changes were also detected in PMMA films containing various compounds which release nitrogen molecules during photolysis with suitable wavelength. The obtained changes in refractive index were about 0.015. For α-diazoketone derivatives it could be shown that the refractive index changes were on the same order of ma-

gnitude regardless of the types of substituents even in the case of highly electronically delocalized species. This suggests that the release of nitrogen molecules mainly contributes to the refractive index change.[320] The refractive indices in the visible wavelength region of PMMA films containing various mesoionic phenyloxatriazolone compounds decreased after photoirradiation in correlation to the decrease in absorption in the ultraviolet region. However, the changes were comparatively small with a maximum value for Δn of 0.006.[345] Also, mesoionic main chain polymers were synthesized but the changes in refractive index were not higher as for other mesoionic compounds.[346]

All methods for changing the refractive index of polymers described in the paragraphs above use dyes or dye like molecules and all have therefore the serious disadvantage that at least one form shows an absorption in the visible spectral range rendering them unsuitable for IOL manufacturing. It is not only intolerable to have a colored IOL, but ambient light could also cause unintentional refractive power changes. Furthermore, many materials described contain an active low molecular mass compound that is mixed in the polymer matrix. This bears the risk of a diffusion controlled release of those possibly toxic low molecular mass substances from the implanted IOL.

Polymers containing aromatic ester groups which undergo a photo-Fries rearrangement from aryl esters to hydroxyketones display large changes in their refractive index (Fig. 1.20). The polymers under investigation were poly(4-actoxystyrene) and derivatives of polynorbornene. The photolytic reaction, the so-called photo-Fries rearangement, is induced upon irradiation with UV light ($200 - 250$ nm) and causes refractive index increases btween 0.03 and 0.05.[347] Owing to the fact that the photo-Fries rearrangement proceeds via a radical mechanism, different isomers are produced. Furthermore, the carbonyl radical may undergo a side reaction and may not recombine with the aromatic system. Also, decarboxylation via a concerted mechanism was observed affording the release of CO_2. Because of these reasons and the fact that very hard UV light must be used, this reaction seems not to be suitable for IOL polymer tuning.

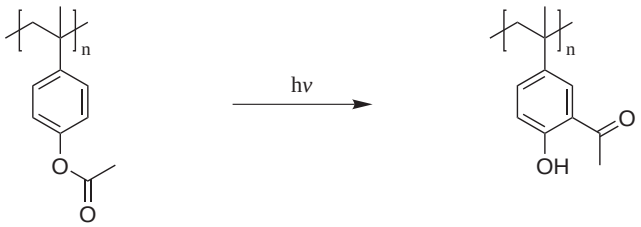

Figure 1.20: Poly(4-acetoxystyrene) and its photo-Fries rearrangement.

A copolymer containing pendant norbornadiene moieties was reported to show a refractive index change of about 0.01 at 633 nm.[317] The refractive index change here is caused by the photoisomerization of norbornadiene to quadricyclane induced by UV irradiation (Fig 1.21). Disadvantageous is that quadricyclane is highly toxic and there is no known way to convert quadricyclane back to norbornadiene in a defined way.[348]

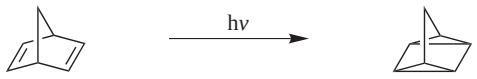

Figure 1.21: Quadricyclane (right) is a highly toxic norbornadiene (left) isomer that can be obtained from norbornadiene by a photochemical reaction

Certain low molecular mass pseudohalides (R−XCN with X = O, S, Se) undergo a photoinduced refractive index change as a result of the photoisomerization to the corresponding iso-compound (R−NCX). Consequently, polymers bearing SCN substituents like poly(4-vinylbenzyl thiocyanate) were synthesized (Fig. 1.22). Upon UV irradiation with a high pressure mercury lamp, the refractive index increases up to 0.03 as a result of the photoisomerization. Further modification of the UV irradiated polymer accompanied by slight additional refractive index changes was carried out with gaseous amines to give derivatives of thiourea.[330,349–351] The procedure is prone to side reactions because the photoisomerization occurs via a free radical intermediate step. Side reactions are the recombination of R−$CH_2^{\bullet}$ radicals which lead to crosslinking of the polymer as well as the release of the corresponging dipseudohalide (e.g. NCS−SCN). Also, the isothyocyante can release sulfur in a second photochemical step to give the isocyanate. Given all these undesired side reactions and the fact that the reaction is not reversible this polymer seems not suitable for IOL manufacturing.

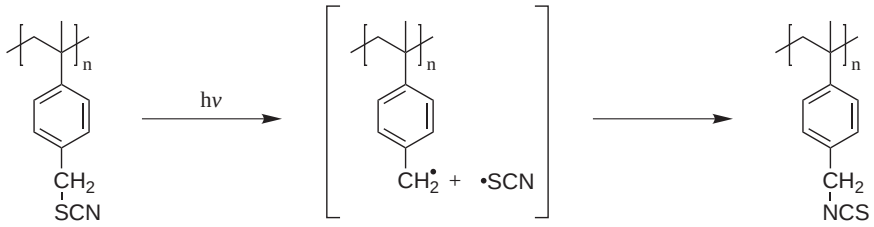

Figure 1.22: Photoisomerization of SCN substituents in poly(4-vinylbenzyl thiocyanate) to give isothiocyanates

A rather exotic way of changing the refractive index uses polymer electrolytes. Polymer electrolytes have received much attention because of their potential for achieving high ionic conductivities combined with enhanced mechanical properties. Materials with significant room temperature ionic conductivity can be obtained by dissolving organo-tin halides and quaternary ammonium salts in poly(vinyl chloride), poly(ethyl methacrylate) or polyethyleneoxide. It was found that the optical properties are dependant on the electric field applied. Refractive index changes of up to 0.6 were reported when a voltage as low as 16 V was applied.[352] Refractive index changes induced by an electric field were also found in polyimide varnishes containing a nonlinear chromophore in the side chain. Application of about 140 V gave relativley large refractive index changes, however, only in the wavelength region of absorption.[353] The refractive index of liquid crystaline polymers can not only be changed in a photochemical way as described above but also by means of an electric field. However, the change of refractive index is below 10^{-3}.[354,355]

1.5.3 Photoinduced Dimerization

In the work presented here the change in refractive index is to be realized by the $[2\pi + 2\pi]$ cycloaddition of two carbon-carbon double bonds to form a cyclobutane ring (Fig. 1.23). Due to the vanishing of the double bonds as a result of the dimerization process the polarizablitiy of the molecule is changed which in turn causes a change in refractive index (Sec. 1.5.1). Especially at least one of the moieties R at each double bond should prefearably be an aromatic π-conjugated system. It can then be expected that the polarizability of the molecule in the direction of the double bond decreases significantly after the dimerization because the resonance with the aromatic system is not longer possible. The final effect would be a decrease in refractive index. If all moieties R were π-conjugated systems they would form an overall conjugated system which includes the dimerizable double bond. The change in refractive index could be even greater when this conjugated system is destroyed because the resonance of the double bond with the two moieties is suspended.

$[2\pi + 2\pi]$ Cycloaddition reactions belong to the group of the pericyclic reactions that mostly progress in a concerted fashion. The most famous of this group of reactions is the *Diels-Alder* reaction which can be found in every organic chemistry textbook and has found widespread application in the synthesis of natural materials. The *Diels-Alder* re-

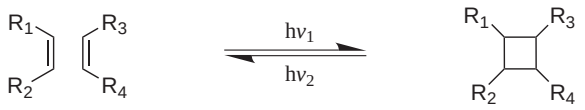

Figure 1.23: Schematic of the photoinduced $[2\pi + 2\pi]$ cycloaddition, and cycloreversion, respectively.

action is a $[4\pi + 2\pi]$ reaction induced by thermal heat with all reactants in their respective electronic ground state.[356–359] On the contrary a $[2\pi + 2\pi]$ cycloaddition reaction leads to a four membered ring by forming of two new σ-bonds. The stereochemistry of pericyclic reactions is predictable by a set of rules known as the Woodward-Hoffmann rules. They were devised by *Robert Burns Woodward* and *Roald Hoffmann* based on orbital symmetry. By taking the energy and symmetry of every molecular orbital which is involved in the reaction into account the course of the reaction and the resulting products can be predicted. Organic reactions that obey these rules are said to be symmetry allowed. Reactions that take the opposite course are symmetry forbidden and require a lot more energy to take place if they take place at all.[360] *Hoffmann* was awarded the 1981 Nobel Prize in Chemistry for this work, shared with *Kenichi Fukui* who developed a similar model, while *Woodward* had died two years before he could win a second Nobel Prize for Chemistry.

The highest occupied molecular orbital (HOMO) of one of the reactants always interacts with the lowest unoccupied molecular orbital (LUMO) of the other reactant. However, a binding interaction is only possible if the approaching ellipsoids of the π-orbitals have the same sign. In this case the reaction is symmetry allowed. When looking at the π-orbitals involved one can see that as far as the $[2\pi + 2\pi]$ cycloaddition is concerned the reaction is symmetry forbidden if thermally induced (Fig. 1.24).

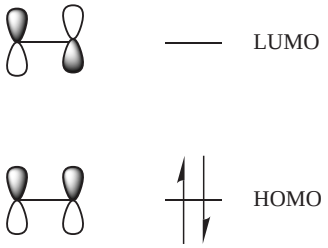

Figure 1.24: Highest occupied molecular orbital (HOMO) and lowest unoccupied molecular orbital (LUMO) of the reacting alkenes in a $[2\pi + 2\pi]$ cycloaddition.

When the reactants approach each other suprafacial, which means at the same side of the π-bond, an antibonding interaction results. In the case of an antrafacial approach, which means an approach to different sides of the π-bond a bonding would result, but this reaction pathway is impossible for geometric reasons (Fig. 1.25).

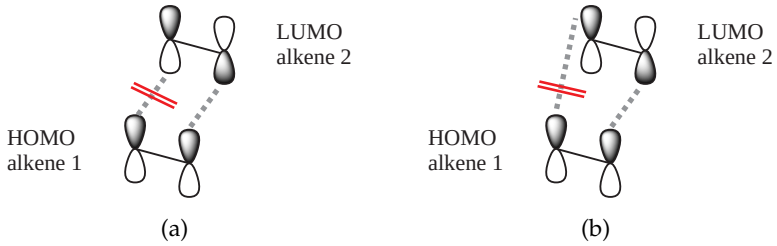

Figure 1.25: Suprafacial (a) and antrafacial (b) for a thermally induced $[2\pi + 2\pi]$ cycloaddition. Both reaction pathways shown do not lead to the product.

The $[2\pi + 2\pi]$ reaction becomes symmetry allowed if an electron of one of the reactants is excited from the HOMO to the LUMO. This excitation is done with a photon of the right energy corresponding to the energy gap between HOMO and LUMO. In most cases the photon must have a UV wavelength. Therefore the reaction is called photochemically allowed (Fig. 1.26).

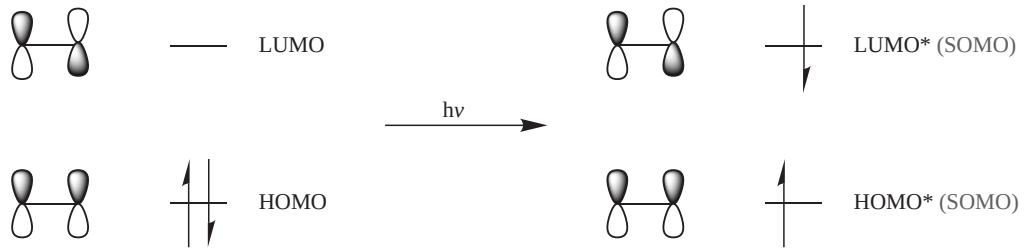

Figure 1.26: Photonic excitation of an electron from the HOMO to the LUMO of the alkene.

Considering the symmetry of the electronically excited state of one alkene and the ground state of the other advantageous orbital interactions become feasible. The HOMO of the alkene in ground state can interact with the former HOMO* [†] of the excited

[†]The HOMO* and the LUMO* of the excited alkene may more precisely be called single occupied molecular orbital (SOMO) because they are occupied with only one electron as can be seen from Fig. 1.26. However, the denomination HOMO and LUMO is contained here with an asterisk added to symbolize the electronically excited state. This notation was chosen because when using the term SOMO in this case it would be ambigous which orbital is meant.

alkene and a bonding orbital interaction that leads to the product comes into effect. Also the single ocupied former LUMO* of the excited reactant can go into a bonding interaction with LUMO of the ground state alkene (Fig. 1.27).[361]

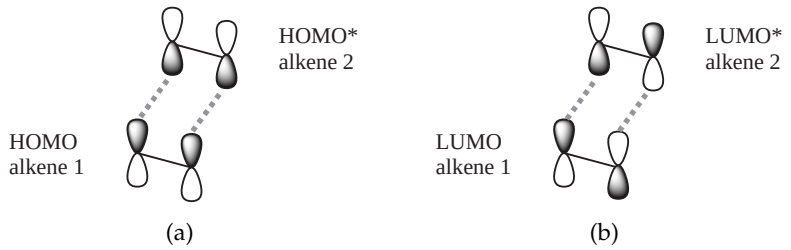

Figure 1.27: Molecular orbital interactions during the course of the photoinduced $[2\pi + 2\pi]$ cycloaddition. (a) The HOMO of the ground state reactant interacts with the former HOMO* of the excited alkene or (b) the LUMO of the alkene in ground state interacts with the former LUMO* of the excited alkene.

It has been found that the photochemically induced $[2\pi + 2\pi]$ cycloaddition in numerous cases will not follow a concerted reaction pathway and therefore will not be stereoselective. This can be explained by the formation of a 1,4-biradical intermediate in its triplet state (Fig. 1.28). The reaction via the 1,4-biradical is no longer stereospecific with respect to the ring formation and various isomers are observed. The dimer of which the greatest amount is generated will be the thermodynamically most favorable one. Which isomers are preferentially formed is dependant on the number of substituents on the alkenes as well as the sterical demand of those substituents.

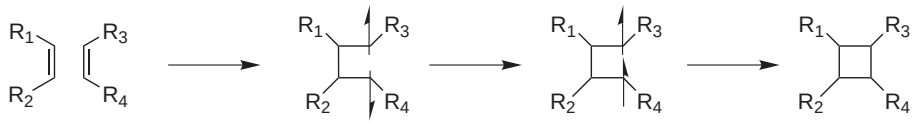

Figure 1.28: $[2\pi + 2\pi]$ Cycloaddition that involves a triplet 1,4-biradical intermediate.

The formation of an excited triplet state from a singlet ground state by absorption of a photon is normally forbidden because the quantum mechanical principles demand the spin multiplicity to remain constant. However, it is possible that the excited singlet state undergoes an intersystem crossing to a triplet state. This is markedly possible for molecules with a strong angular momentum coupling through spin-orbit interaction. For most alkenes and the 1,4-biradicals formed by them the possiblity for an intersystem crossing is quite low. Triplet sensitizers like benzophenone, acteophenone, or acetone

can be used to facilitate the intersystem crossing. The triplet sensitizers have a high intersystem crossing quantum yield and can pass their triplet energy to the reactants via collisions.[362–364]

1.5.3.1 Common Molecules used for Dimerization

One of the most famous and longest known molecules that relatively easy undergoes a $[2\pi + 2\pi]$ cycloaddition is *trans* cinnamic acid and its esters.[365–368] But it has to be noted that the cycloaddition only takes place to a significant extent under well chosen conditions. In diluted solutions the intramolecular process of *cis-trans* isomerisation is by far favored over the intermolecular process of dimerization (Fig. 1.29). It could experimentally be shown that in dilute solutions of ethyl cinnamate isomerization is the only photochemical reaction, at least in the initial stage of the reaction.[369–371] In the solid state and in polymers though, the situation is reversed.[371,372] Crystalline ethyl cinnamate forms almost exclusively dimers upon UV irradiation and the isomerization is negligible. The explanation for this finding is the absence of free volume in the solid state that would allow the rotation of the bulky phenyl group. Dimerization is also observed in films of polymers containing cinnamic acid side groups like the well known poly(vinyl cinnamate) (PVCi). The polymer mainly shows crosslinking between the polymer chains under UV irradiation which makes the irradiated areas insoluble. This property made PVCi one of the first photoresists for microelectronics.[373,374] The isomers formed can be either head-to-head or head-to-tail depending on the relative orientation which two dimerizing molecules approach each other at (Fig. 1.30). Also *syn* and *anti* diastereomers can occur. In the case of molecules like cinnamic acid that can undergo a *cis-trans* isomerisation before dimerization, also dimers between the *trans* and *cis* species are observed.[372,375]

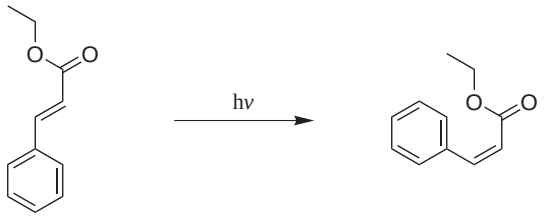

Figure 1.29: Photoinduced *cis-trans* isomerisation of ethyl cinnamate in dilute solution.

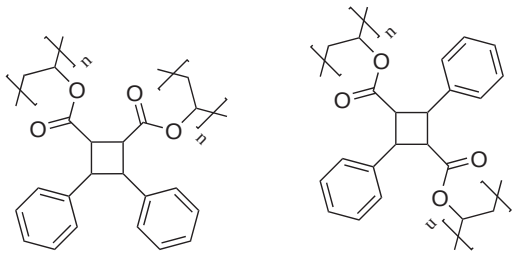

Figure 1.30: Head-to-head (a) and head-to-tail (b) isomers of poly(vinyl cinnamate).

Similar to the photodimerisation of cinnamic acid that of chalcones has been known for over eighty years and yields cyclobutane derivatives of different stereochemistry (Fig. 1.31). The first work on this subject was conducted by *Stobbe* and *Bremer* of Germany in 1929.[376] In the following time chalcone dimers and their derivatives have received considerable attention.[377–381] In a recent work the nonlinear two-photon properties of chalcone dimers were investigated.[382]

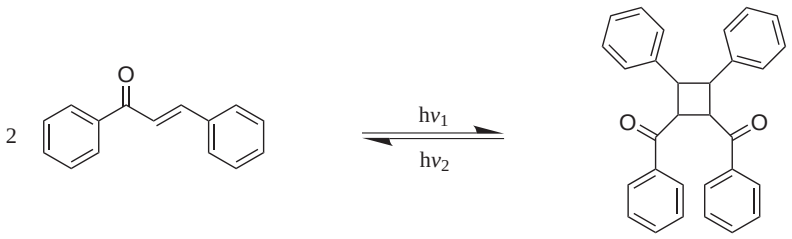

Figure 1.31: Reversible photodimerization of chalcone under irradiation with UV light.

Another class of substances very similar to the chalcones are stilbenes. Since stilbenes have a very high tendency for *cis-trans* isomerisation[383] dimerization reactions were mostly observed in cases were the stilbene is bound to some sort of high molecular mass backbone.[384,385]

The coumarin molecule and its derivatives play the most important role as a photodimerizable system in this thesis (Fig 1.33). This is because an isomerization of the photosensitive double bond of the coumarin molecule is not possible. The double bond is incorporated in a lactone ring and thereby protected from being isomerized offering the advantage that no photons are "wasted" for a *cis-trans* isomerisation. Furthermore the axes of the coumarin photodimer stay aligned with the axes of the monomeric cou-

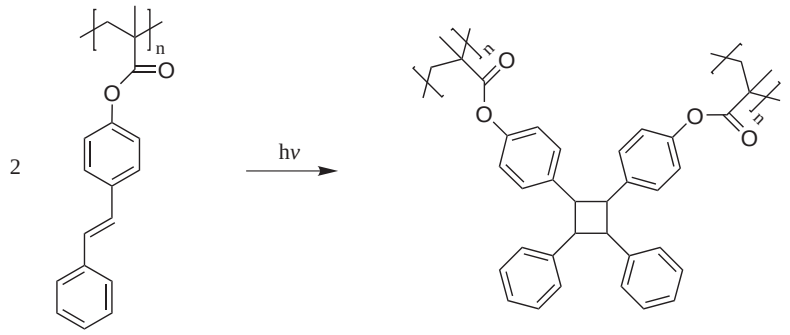

Figure 1.32: Photodimerization of polymer attached stilbene molecules.

marins. A reorientation with respect to the bond angles of the coumarin chromophore is therefore not necessary which should faciliate the dimerization process (Fig 1.34).

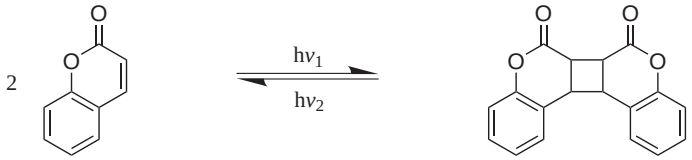

Figure 1.33: Reversible photodimerization of coumarine under irradiation with UV light.

The fact the coumarin can be photochemically dimerized was first reported by *Ciamician* and *Silber* in 1902.[386] The photochemical properties of coumarin and many of its derivatives have since been investigated in more detail and are well known today.[387–392] In principle four isomers can be formed: *syn*-head-to-head (*syn*-hh), *anti*-head-to-head (*anti*-hh), *syn*-head-to-tail (*syn*-ht), and *anti*-head-to-tail (*anti*-ht).[364] The dimerization of coumarin in the solid state was not possible but many of its derivatives are dimerizable in the solid state.[393] The dimerization of polymer bound coumarins like poly(7-methacryloyloxycoumarin) (PMAOC) can be described according to *Perny* and coworkers analogous to the above schema.[394]

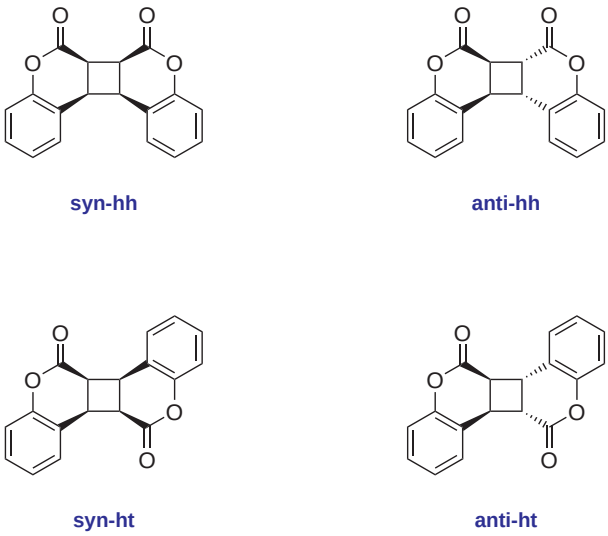

Figure 1.34: Possible isomers of coumarin photodimers.

2 Methods and Materials

2.1 Chemicals

7-Hydroxycoumarin (Acros), 3-bromo-1-propanol (Chempur), 1,8-octandiol (ABCR), 1,10-decandiol (Sigma-Aldrich), 1,12-dodecandiol (Sigma-Aldrich), 5-bromo-1-pentanol (TCI Europe), 7-bromo-1-heptanol (TCI Europe), 8-bromo-1-octanol (Sigma-Aldrich), 9-bromo-1-nonanol (Sigma-Aldrich), 10-bromo-1-decanol (Alfa Aesar), 11-bromo-1-undecanol (Sigma-Aldrich), methacryloyl chloride (Lancaster), ethylene glycol dimethacrylate (Aldrich), octandiol dimethacrylate (Acros), benzophenone (Fluka), triethylamine (Riedel-de Haën), *N*,*N*′-dimethylacetamide (puriss., water < 0.01%, Fluka), *N*,*N*′-dimethylformamide (DMF) (extra dry, water < 50ppm; Acros), dichlormethane (gradient grade, Fisher Scientific), acetic anhydride (Fluka), glacial acetic acid (Merck), hydrochloric acid (Fluka), hydrofluoric acid (40%, purum, Riedel-de Haën), nitric acid (65%, Merck), sodium acetate (anhydous, Fluka), pyridine (extra dry, water < 50 ppm, Acros) were used as received. *n*-butyl methacrylate (*n*BMA, Acros), *tert.*-butyl methacrylate (*t*BMA, Acros), and other solvents were purified by distillation prior to use. If necessary, drying of solvents was performed according to standard protocols.[395]

2.2 Characterization Methods

2.2.1 Nuclear Magnetic Resonance (NMR) Spectroscopy

^{1}H-NMR spectra were recorded on an AV-300 (300 MHz, Bruker) or AV-500 (500 MHz, Bruker) spectrometer using either $CDCl_3$, DMSO-d_6, acetone-d_6 or acetonitrile-d_3 as a solvent. ^{13}C-NMR spectra were measured utilizing the same equipment with frequen-

cies of 75 MHz, or 125 MHz, respectively. The δ chemical shift scale was calibrated using the residual solvent peak.

2.2.2 Ultraviolet-visible Spectrophotometry (UV/Vis)

UV/Vis absorption spectra were recorded at room temperature on an UVIKON 922 (Kontron) spectrophotometer. Liquid samples were measured in quartz (QS, Helma) cuvettes with 1 cm path length. Polymer films were cast on $45 \times 12.5\,mm^2$ quartz plates (QX, Helma) and had thicknesses between 100 and 200 nm. All samples had an optical density (OD) of less than 2.5 at the observed wavelength to ensure a linear operation of the spectrometer.

2.2.3 Infrared Spectroscopy

Infrared spectra were recorded on a FT-IR 1600 spectrometer (Perkin Elmer) at room temperature with the dry substances prepared as KBr pellets.

2.2.4 Mass Spectrometry

Mass spectra using electrospray ionization (ESI) were recorded on a LCQ-Duo (Thermo) for low resolution or on a Finnigan LTQ-FT (Thermo) for high resolution mass spectra (HRMS), both operated in positive mode. Mass spectra after electron impact ionization were measured using either an CH7 (Varian) or a MAT 95 (Finnigan) for high resolution mass spectra. The electron energy was 70 eV.

2.2.5 High Performance Liquid Chromatography (HPLC)

Analytic HPLC was performed on an Agilent Technologies 1050 equipped with a diode array detector using a RP-18 column (250 mm $\times$ 4 mm, 3 µm, Nucleosil).

2.2.6 Polymer Analysis

2.2.6.1 Thermogravimetric Analysis

Thermogravimetric analysis was performed using a thermo-balance TGA/SDTA 851^e (Mettler Toledo) in open corundum crucibles under nitrogen atmosphere in a temperature range from 25 to 800 °C at a heating rate of 10 K min^{-1}. Sample weight ranged from 8 to 12 mg.

2.2.6.2 Differential Scanning Calorimetry

Differential Scanning Calorimetry measurements were accomplished on a DSC 821^e (Mettler Toledo). An amount of 8 to 12 mg of the polymers was loaded into aluminum crucibles. Measurements were conducted under nitrogen atmosphere in a temperature range from −70 to 280 °C. Samples were subjected to a cyclic temperature program with a heating and cooling rate of 10 K min^{-1}. Data analysis was performed with the STAR^e Software (Mettler Toledo) using the second heating curve.

2.2.6.3 Size Exclusion Chromatography

Gel permeation chromatography (GPC) analyses were performed using solutions of the polymers (1 g L^{-1}) in *N*,*N*′-dimethylformamide (DMF). Separation was done on a combination of two 600 × 8 mm^2 and one 300 × 8 mm^2 column (PSS SDV, 10 µm, 10^6 Å, 10^4 Å, 10^3 Å, respectively) followed by a differential refractometer (Knauer) and a variable wavelength detector (Knauer) for detection. The molar masses were determined as poly(methyl methacrylate) equivalents (PSS).

2.2.7 Tensile Testing

Stress-strain measurements were conducted on a Zwick/Roell Z0.5 tensometer equipped with a KAF-TC force sensor with a measuring range of up to 200 N. Plates of the

polymer to be tested were die-cut into a dog-bone shape (Fig. 2.1). The bone was linearly extended at a speed of 10 mm min^{-1} and the load extension curve was recorded. The stress-strain curve was calculated from the cross-sectional area and the original effective length of the specimen.

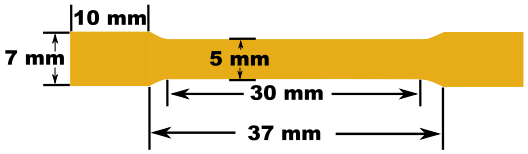

Figure 2.1: Dimensional sketch of the polymer bones used for tensile testing experiments. The thickness of the bone is 2 mm.

2.2.8 Density Determination

Density measurements were conducted in a *Mohr-Westphal* density balance (Gottl. Kern & Sohn) at 20 °C. The sample weight ranged from 5 to 10 g. Deionized water was used as measurement liquid.

2.3 Purification Methods

2.3.1 Column Chromatography

For column chromatography silica gel 60 (230-400 mesh, 40 - 63 µm, Machery-Nagel) was filled into glass columns with a diameter of either 2 or 5 cm at a height of 30 cm and eluted with the given solvent mixture.

2.3.2 Preparative High Performance Liquid Chromatography

The preparative HPLC system consisted of a P680 Pump (Dionex), a RP-18 column (250 mm × 30 mm, 5 µm, YMC) and a 1050 Series fixed wavelength detector (Agilent Technologies). Acetonitrile/water mixtures were used as eluent operating an isocratic flow.

2.4 Thin Film Processing and Characterization

2.4.1 Silicon Wafers

Four inch in diameter, 100 silicon wafers (Siegert Consulting e.K.) were cut into 30 × 30 mm^2 squares. The silicon squares were cleaned with chloroform and acetone using an ultrasonic bath. The silicon oxide layer of about 100 nm on the wafers was removed by etching with a 3:1 mixture of nitric acid and hydrofluoric acid for 15 s followed by etching in pure hydrofluoric acid for 45 s. After each process step the wafers were thoroughly rinsed with deionized water. Prior to use it was checked that the silicon oxide layer was less than 3 nm using a variable angle phase modulation ellipsometer.

2.4.2 Spin Coating

Spin coating is a procedure known for several decades for the application of uniform thin films on flat substrates. Centripetal acceleration will cause the resin to spread to, and eventually off, the edge of the substrate leaving a thin film of material on the surface. Typically spin coating can produce homogeneous films in only a few minutes. The homogeneity of a layer deposited by spin coating is sufficient for optical applications. Spin coating is a well established technique in industry. Main fields of application are the deposition of photoresists for microelectronics, and fabrication of optic components for laser technology and flat screens.[396,397]

A typical process consists of four steps (Fig. 2.2).[398] It involves depositing a small puddle of a polymer solution onto the center of a substrate. The solution or resin may be dispensed on the static substrate or it may be dispensed while the substrate is turning at low speed. A speed of about 500 rpm is commonly used during this step of the process. This serves to spread the fluid over the substrate and can result in less waste of coating material. After the dispense step it is common to accelerate to a relatively high speed to thin the fluid close to its final thickness. Typical spin speeds for this step range from 1500 rpm up to 10000 rpm. This step can take from 10 s to several minutes. Both spin speed and time depend on the properties of the fluid as well as the substrate and define the final film thickness. Film thickness is largely a balance between the force applied to shear the fluid film towards the edge of the substrate and the drying rate

which affects the viscosity of the resin. As the resin dries, the viscosity increases until the radial force of the spin process can no longer appreciably move the resin over the surface. In general, higher spin speeds and longer spin times create thinner films. A separate drying step is sometimes added after the high speed spin step to further dry the film without substantially thinning it. This can be advantageous for thick films since long drying times may be necessary to increase the physical stability of the film before handling.

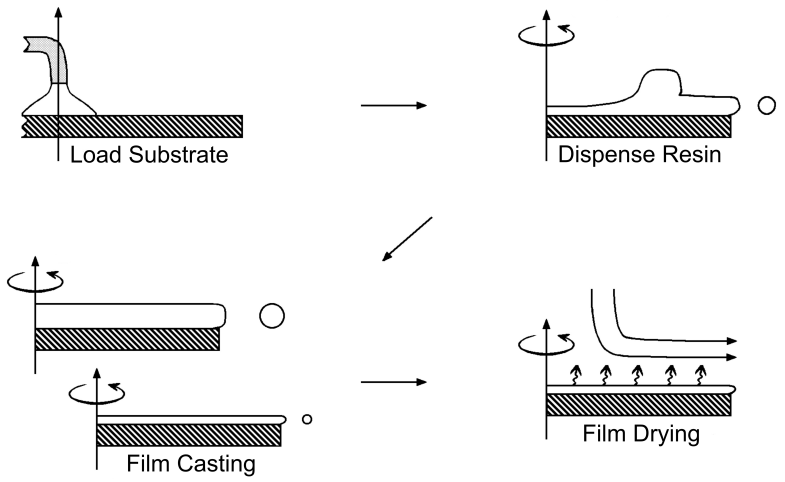

Figure 2.2: The four steps of a typical spin coating process according to *Bornside* et al.[398]

Polymer films on silicon squares were prepared on a SPIN150 spin coater (SPS-Europe B.V.). The spin coater was placed in a laminar flow cabinet and all solutions were filtered through 0.45 µm pore size PTFE syringe filters. About 1mL of a solution of 3% to 8% (w/w) polymer in chloroform was applied to the resting substrate and immediately spun 5 s at 500 rpm, 5 s at 1000 rpm and finally 20 s at 2000 rpm. The wafers were dried at 60 °C for at least 12 h. For UV/Vis measurements films were cast on quartz plates from a 1% (w/w) solution under identical conditions.

2.4.3 Profilometry

Profilometry is a method used for quantitative characterization of a surface's profile. It is also possible to measure the layer thickness and step heights on a surface.[399,400] A

diamond stylus is moved vertically in contact with a sample and then moved laterally across the sample for a specified distance and specified contact force. A profilometer can measure small surface variations in vertical stylus displacement as a function of position. Small vertical features ranging from a few Ångström to some millimeters in height can typically be measured. The height position of the diamond stylus generates an analog signal which is converted into a digital signal, subsequently stored, analyzed, and displayed with a personal computer. The stylus tracking force can range from less than 1 to 50 mg. A microscope objective coupled with a CCD camera allows for visual inspection of the sample and the positioning of the stylus.

The thickness of polymer films was determined by making an approximately 0.5 mm wide scratch into the polymer film. Extreme care was taken that all the polymer along the scratch had been totally removed but the substrate was left undamaged. The average step height was measured with a Dektak^3 ST Profilometer (Sloan) at five randomly selected positions. The stylus force was 5 mg.

2.4.4 Refractive Index Measurement

A prism coupler was used to determine the refractive indices of polymer films on silicon wafers as well as bulk polymer pieces. Since refractive indices of a material depend upon the wavelength of the electromagnetic radiation transmitted, a monochromatic laser is used in conjunction with a prism of known refractive index. The laser beam is directed through one side of the high refractive index prism, bent, and is normally reflected back out on the opposite side into a photo detector. The film to be measured is brought into contact with the prism base by means of a pneumatically operated coupling head. The angle of incidence θ of the laser beam can be varied by means of a rotary table. The prism, the sample, the coupling head, and a photodetector are all mounted upon the rotary table. At certain values of the incident angle θ, the beam is not reflected back out, but instead, is transmitted through the base into the film sample. These angles are called mode angles. At these mode angles, photons violate the total internal reflection criterion, tunnel from the base of the prism into the film and enter into optical propagation modes, causing a sharp drop in the intensity of light striking the photodetector (Fig. 2.3).[401–403]

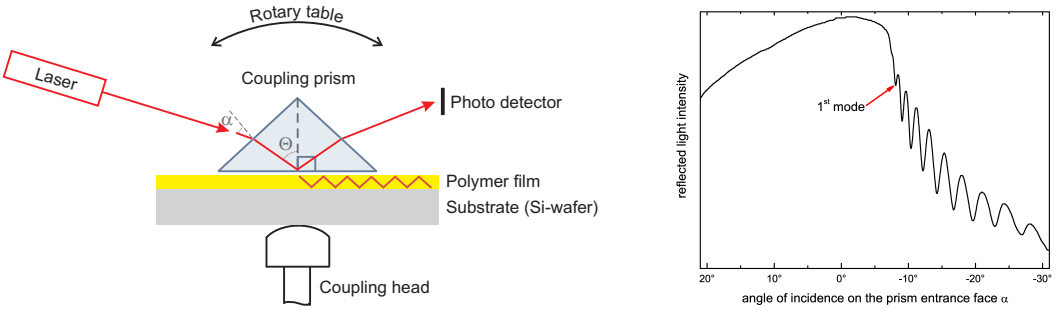

Figure 2.3: (a) Measurement setup of the prism coupler used. The principal components are shown. (b) Plot of a typical prism coupler thin film measurement. The light intensity striking the photodetector is plotted as a function of the angle of incidence.

If the intensity striking the photodetector is plotted as a function of the angle of incidence a characteristic mode pattern will be obtained. For a given substrate type, the angular location of the modes depends only on the film thickness and refractive index. The first mode angle found determines the refractive index, and the angle difference from one mode to the next determines the sample thickness. Thus, as soon as two mode angles are measured, the film thickness and index can be calculated. This is done by the measurement software running on a personal computer attached to the prism coupler. If more than two modes are observed, the problem is overspecified and it is possible to calculate independent thickness and index estimates from each pair of modes. This allows for the calculation of the mean and standard deviation of all estimates and makes the method self-consistant.[402,403]

Prism couplers also allow for coupling light in and out of a waveguide without exposing the cross-section of the waveguide (edge coupling). The coupling of a laser beam by a prism into a planar dielectric light guide is governed by the angle of incidence θ of the light into the prism base (Fig. 2.3).[401,404–406] This angle θ determines the phase velocity in x direction of the incident wave in the prism and in the gap. Strong coupling of light into the film occurs only if we choose θ so that the phase velocity in x direction of the incident wave equals the phase velocity of one of the characteristic modes of propagation in the guide ($m = 0, 1, 2, 3, \ldots$). To achieve this a phase matching condition is

required between the propagation constant of the mth mode in the waveguide β_m and the incident light at an angle θ_m to the normal of the waveguide surface

$$\beta_m = \frac{2\pi}{\lambda_0} \cdot n_p sin\theta_m \tag{2.1}$$

where n_p is the index of refraction of the prism. In the propagating mode m at a discrete beam angle, the wave of the laser beam propagates in the polymer film. At each propagating mode angle, the ratio of the reflected light intensity to the incident light intensity becomes much smaller than the usual total reflected light intensity.

On the other hand, we can calculate theoretical values for the relative propagation constants from the known dispersion equation of a planar dielectric light guide.[403] The refractive index n of the film and the film thickness W can be calculated by

$$n^2 = \frac{N_0^2 \Phi_2^2 - \Phi_0}{\Phi_2^2 - \Phi_0^2} \tag{2.2}$$

and

$$k W \sqrt{n^2 - N_m^2} = \Psi_m (n, N_m) \tag{2.3}$$

with more than three modes observed. The refractive index of the film in question n is obtained as the value of the convergence of the computational iteration. For Eqn. 2.3, N_m is the effective refractive index at mode m. The suffixes 0 and 2 for N in Eqn. 2.2 indicate the number of zero and second propagating modes. Φ_0 and Φ_2 are *Goos-Hänchen* shifts[407] at the film-substrate and film-air interfaces, respectively. In Eqn. 2.3

$$\Psi_m (n, N_m) = m\pi + \Phi_0 + \Phi_2 \tag{2.4}$$

and

$$\Phi_j \equiv \arctan \left[\left(\frac{n}{n_j} \right)^2 \cdot \frac{N_m^2 - n_j^2}{n^2 - N_m^2} \right]^{\frac{1}{2}} \tag{2.5}$$

where the suffix j is 0 or 2 and n_0 is the refractive index of the substrate and n_2 is the refractive index of air. If the calculation is used for three or more modes, the average value and standard deviation of both refractive index and film thickness can be obtained

by the same numerical calculation. The refractive index is calculated to the negative fourth power by the iterativ method.

In summary, the propagation of light into a planar waveguide is governed by a set of parameters. Of these parameters all are known except for the refractive index n and thickness W of the polymer film. Therefore, the problem becomes a solely computational one, where both n and W are iteratively adjusted until the resulting theoretical values for the propagation constant match the experimental values as closely as possible. The values $\bar{n}$ and $\bar{W}$, for which the best match is achieved, are regarded as the results of this method.

The refractive indices of polymer films on Si wafers were determined using a Model 2010 Prism Coupler (Metricon) thin film thickness and refractive index measurement system. Each data point represents the arithmetic mean of five measurements at randomly selected positions around the film center. The wavelength used for measurements was 633 nm from a HeNe-Laser. The refractive index accuracy is ± 0.001.[408] Films for these measurements ranged between 650 nm and about 2 µm in thickness. For the measurement of polymer pieces with a thickness of several millimeters the prism coupler was operated in bulk mode. For bulk material measurements, the principle of operation is quite simple and resembles closely the operation of an *Abbé* refractometer. A material with the refractive index n_m is brought into intimate contact with a prism having the refractive index n_p. In this setup light directed at the base of the prism will be totally reflected at the prism base until the angle of incidence θ becomes less than the critical angle $\theta_\mathrm{c} = \arcsin\left(n_\mathrm{m}/n_\mathrm{p}\right)$. The critical angle of total reflection θ_c can be easily measured since the detector intensity drops off abruptly as θ drops below the critical angle and light starts to leak into the bulk material. Since n_p is known, n_m can be readily calculated. The only drawback of bulk measurement compared to the measurement of thin films on high refractive index substrates is that the refractive index accuracy is worse by a factor of 3 in bulk mode.

2.5 Light Sources

2.5.1 UV Lamps

To expose the polymer films to UV-light a HBO 103 W/2 mercury lamp (Osram), installed in a 60000 Series Q housing (Oriel) and operated with a 68806 Basic Power Supply (Oriel), was used. Band-pass filters for 250 ± 10 nm and 313 ± 10 nm, (313FS 10-25, Oriel) were used to select the ideal wavelengths for dimer cleavage and dimerization, respectively. The light was coupled in a 0.5 m long 77620 Solarization Resistant Fiber (Oriel) with a diameter of 600 µm. The intensity of light on the sample was measured with a S1337-1010BQ silicon photo diode. For photochemical synthesis a Rayonet-type reactor equipped with twelve EVERSUN 40 W/79 25X fluorescent tubes (Osram) in a concentric setup was used.

2.5.2 Lasers

Polymer films and lens prototypes were also irradiated using a diode-pumped, Q-switched, frequency-tripled Nd:YAG Laser (Avia, Coherent) operating at a wavelength of 355 nm and a pulse length of 25 ns. For the experiments described here the laser was operated at a repetition rate of 10 kHz and a pulse energy of about 260 µJ. Two-photon induced cycloreversion experiments were conducted with an Infinity 40-100 q-switched Nd:YAG laser (Coherent). The laser emits pulses of 3 ns length at a wavelength of 532 nm and a repetition rate of 20 Hz. The beam is 5.5 nm and has a flat top profile.

The energy at the location of the sample was measured using a Fieldmaster GS (Coherent) equipped with a power meter head Model 80 (Coherent). The appropriate wavelength was set at the measuring device.

2.6 Calculation of the Induced Change in Focal Length

In order to conclude from the refractive index changes observed with the different polymers to the performance of an actual IOL, a calculation was performed to clarify how the changes convert into optical variations of an implanted lens. For these estimations a homogeneous exposure of the IOL was considered and the change in focal length calculated. It is dependent of both curvature radii and the center thickness of the lens. Typical IOL data was used and the focal length was calculated with paraxial formulas for lenses in arbitrary media to account for the effect that the lens is in contact with the aqueous humour and the vitreous body. The initial focal length of the treated IOLs was 23 D and the change in diopters is calculated assuming that only the refractive index of the IOL is changed.

2.7 Synthetic Procedures

2.7.1 7-Methacryloyloxycoumarin (MAOC)

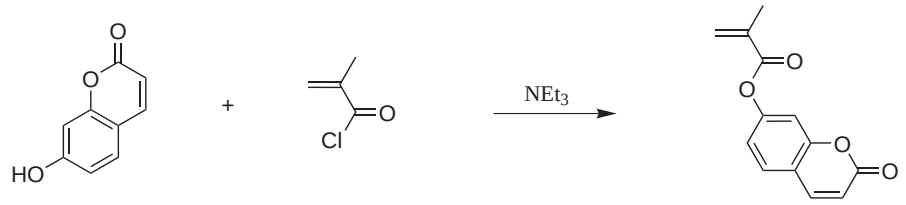

7-Methacryloyloxycoumarin (MAOC) was synthesized as previously described in the literature[394,409,410] by esterification of 7-hydroxycoumarin with methacryloyl chloride in the presence of triethylamine. 7-Hydroxycoumarin (16.2 g, 100 mmol) was suspended in dry tetrahydrofuran. After adding triethylamine (5 eq., 50.6 g, 500 mmol), the mixture was stirred until a clear solution had formed. Methacryloyl chloride (1.5 eq., 15.7 g, 150 mmol) was added dropwise while stirring vigorously. The reaction mixture was heated to 40 °C for 2 h and further stirred for another 18 h at room temperature. The precipitated ammonia salts were filtered off and the solvent was removed under reduced pressure. The solid obtained was recrystallized twice from methanol to give the desired product as white crystals.

Yield 74%

^{1}H-NMR (300 MHz, $CDCl_3$): δ/ppm = 2.07 (s, 3H), 5.82 (s, 1H), 6.38 (s, 1H), 6.40 (d, 2H, J = 13.1 Hz), 7.08 (dd, 1H, J_1 = 12.6 Hz, J_2 = 3.0 Hz), 7.15 (d, 1H, J = 3.0 Hz), 7.50 (d, 1H, J = 12.6 Hz), 7.71 (d, 1H, J = 13.1 Hz).

^{13}C-NMR (75 MHz, $CDCl_3$): δ/ppm = 18.2, 110.3, 115.8, 118.4, 128.2, 128.5, 135.2, 142.8, 153.4, 154.6, 160.2, 165.0.

MS (EI, 70 eV): m/z (%): 230 (10) [M^+], 134 (2), 105 (1), 77 (3), 70 (3), 69 (100), 51 (4), 41 (47), 39 (5), 28 (1).

HRMS (EI): calcd. for $C_{13}H_{10}O_4$ (M^+), 230.0579; found 230.0544.

2.7.2 Bromoalkanols

ω-Bromoalkanols were synthesized starting from the corresponding diols. The synthetic protocol ensures that the ω-bromoalcohol is favored over the dibrominated product.[411,412] Following the typical procedure 171 mmol (1 eq.) of the corresponding diol was dissolved in 500 mL of toluene. After addition of 1.6 eq. hydrobromic acid (9 M, 32.5 mL) the heterogeneous mixture is heated at reflux for 30 h while beeing stirred. The reaction mixture was allowed to cool to room temperature and the phases were separated. The organic layer was washed with brine and the solvent was removed under reduced pressure. The crude product was purified by column chromatography using ether/pentane (1:1) as an eluent to give the desired bromoalkanol as colorless oil.

2.7.2.1 8-bromo-1-octanol

Yield 97%

^{1}H-NMR (300 MHz, $CDCl_3$): δ/ppm = 1.19 - 1.57 (m, 13H), 3.39 (t, 2H, J = 6.8 Hz), 3.46 (t, 2H, 6.8 Hz).

MS (EI, 70 eV): m/z (%): 193 (2), 192 (1), 191 (2), 190 (1), 165 (1), 164 (20), 162 (20), 150 (18), 148 (19), 137 (13), 135 (14), 111 (22), 109 (8), 107 (5), 83 (44), 82 (22), 81 (12) 70 (9),

69 (98), 68 (26), 67 (20), 57 (16), 56 (18), 55 (100), 54 (10), 53 (7), 43 (21), 42 (17), 41 (66), 39 (17), 31 (18), 29 (15), 28 (7), 27 (16).

2.7.2.2 10-bromo-1-decanol

Yield 89%

^{1}H-NMR (300 MHz, $CDCl_3$): δ/ppm = 1.22 - 1.59 (m, 17H), 3.40 (t, 2H, J = 6.8 Hz), 3.64 (t, 2H, 6.8 Hz).

MS (EI, 70 eV): m/z (%): 192 (5), 190 (6), 164 (9), 162 (9), 151 (7), 150, (37), 149 (8), 148 (38), 137 (15), 135 (16), 111 (6), 109 (8), 97 (32), 95 (9), 84 (7), 83 (50), 82 (15), 81 (12), 71 (6), 70 (11), 69 (90), 68 (23), 67 (16), 57 (15), 56 (19), 55 (100), 54 (11), 53 (7), 43 (26), 42 (17), 41 (66), 39 (14), 31 (17), 29 (18), 27 (13).

2.7.2.3 12-bromo-1-dodecanol

Yield 60%

^{1}H-NMR (300 MHz, $CDCl_3$): δ/ppm = 1.23 - 1.61 (m, 21H), 1.85 (q, 2H, J = J = 7.2 Hz), 3.41 (t, 2H, J = 6.9 Hz), 3.63 (t, 2H, 6.6 Hz).

MS (EI, 70 eV): m/z (%): 220 (3), 218 (3), 205 (1), 192 (5), 190 (6), 164 (9), 162 (9), 151 (7), 150, (37), 149 (8), 148 (38), 137 (15), 135 (16), 111 (6), 109 (8), 97 (32), 95 (9), 84 (7), 83 (50), 82 (15), 81 (12), 71 (6), 70 (11), 69 (90), 68 (23), 67 (16), 57 (15), 56 (19), 55 (100), 54 (11), 53 (7), 43 (26), 42 (17), 41 (66), 39 (14), 31 (17), 29 (18), 27 (13).

2.7.3 Alkyl Coumarin Ethers

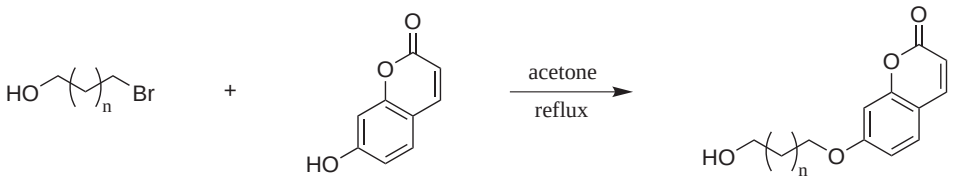

Via a *Williamson* ether synthesis the ω-bromo alcohols were attached to the coumarin molecule. 7-Hydroxycoumarin (25 mmol, 4.05 g), the corresponding bromo alcohol (25 mmol, 1 eq.) and potassium carbonate (137.5 mmol, 19 g, 5.5 eq.) were refluxed in 100 mL acetone for 12 h. The solids was filtered off. After evaporation of the solvent the crude product was re-crystallized from acetone to give white crystals.

2.7.3.1 7-(3-Hydroxypropoxy) coumarin

Yield 70%

^{1}H-NMR (300 MHz, $CDCl_3$): δ/ppm = 1.69 (s, 1H), 2.08 (m, 2H), 3.88 (t, 2H, J = 6.1 Hz), 4.18 (t, 2H, J = 6.0 Hz), 6.25 (d, 1H, J = 9.5 Hz), 6.84 (dd, 1H, J_1 = 9.5 Hz, J_2 = 8.0 Hz), 7.37 (d, 1H, J = 8.0 Hz), 7.63 (d, 1H, J = 9.5 Hz).

^{13}C-NMR (75 MHz, $CDCl_3$): δ/ppm = 31.8, 59.2, 64.5, 104.1, 111.0, 111.9, 113.4, 129.4, 143.6, 156.5, 159.2, 161.0.

2.7.3.2 7-(5-Hydroxypentoxy) coumarin

Yield 93%

^{1}H-NMR (300 MHz, $CDCl_3$): δ/ppm = 1.60 (m, 6H), 1.85 (br s, 1H), 3.69 (t, 2H, J = 6.2 Hz), 4.02 (t, 2H, J = 6.4 Hz), 6.24 (d, 1H, J = 9.5 Hz), 6.81 (m, 2H), 7.35 (d, 1H, J = 8.5 Hz), 7.63 (d, 1H, J = 9.5 Hz).

^{13}C-NMR (75 MHz, $CDCl_3$): δ/ppm = 21.9, 29.6, 32.2, 62.8, 68.7, 104.2, 110.9, 111.9, 113.4, 129.5, 143.4, 156.4, 159.0, 160.9.

2.7.3.3 7-(7-Hydroxyheptoxy) coumarin

Yield 81%

^{1}H-NMR (300 MHz, $CDCl_3$): δ/ppm = 1.46 - 1.75 (m, 10H), 1.78 (br s, 1H), 3.34 (t, 2H, J = 6.5 Hz), 3.94 (t, 2H, J = 6.5 Hz), 6.17 (d, 1H, J = 9.5 Hz), 6.75(m, 2H), 7.29 (d, 1H, J = 8.5 Hz), 7.56 (d, 1H, J = 9.5 Hz).

^{13}C-NMR (75 MHz, $CDCl_3$): δ/ppm = 25.4, 25.6, 25.9, 29.6, 32.2, 62.8, 68.7, 104.1, 111.1, 111.8, 113.4, 129.4, 143.5, 156.5, 159.0, 160.8.

2.7.3.4 7-(8-Hydroxyoctoxy) coumarin

Yield 80%

^{1}H-NMR (300 MHz, $CDCl_3$): δ/ppm = 1.25 - 1.57 (m, 10H), 1.81 (q, 2H, J = 8.1 Hz), 2.63 (br s, 1H), 3.65 (t, 2H, J = 6.6 Hz), 4.01 (t, 2H, J = 6.6 Hz), 6.24 (d, 1H, J = 9.6 Hz), 6.79 - 6.85 (m, 2H), 7.36 (d, 1H, J = 8.4 Hz), 7.63 (d, 1H, J = 9.6 Hz).

^{13}C-NMR (75 MHz, $CDCl_3$): δ/ppm = 25.0, 25.2, 25.4, 28.5, 28.8, 30.5, 32.3, 62.6, 68.2, 112.0, 112.5, 112.6, 128.3, 143.0, 155.5, 160.9, 162.0.

2.7.3.5 7-(9-Hydroxynonoxy) coumarin

Yield 40%

^{1}H-NMR (300 MHz, $CDCl_3$): δ/ppm = 1.26 - 1.59 (m, 12H), 1.81 (q, 2H, J = 7.9 Hz), 2.17 (br s, 1H), 3.64 (t, 2H, J = 6.6 Hz), 4.01 (t, 2H, J = 6.6 Hz), 6.24 (d, 1H, J = 9.5 Hz), 6.79 - 6.85 (m, 2H), 7.36 (d, 1H, J = 8.4 Hz), 7.63 (d, 1H, J = 9.5 Hz).

^{13}C-NMR (75 MHz, $CDCl_3$): δ/ppm = 25.0, 25.2, 25.4, 28.5, 28.8, 29.6, 30.5, 32.3, 62.6, 68.5, 112.0, 112.5, 112.7, 128.6, 143.2, 155.5, 160.9, 162.0.

2.7.3.6 7-(10-Hydroxydecoxy) coumarin

Yield 77%

^{1}H-NMR (300 MHz, $CDCl_3$): δ/ppm = 1.29 - 1.89 (m, 16H), 3.40 (br s, 1H), 3.64 (t, 2H, J = 6.6 Hz), 4.00 (t, 2H, J = 6.6 Hz), 6.24 (d, 1H, J = 9.3 Hz), 6.79 - 6.85 (m, 2H), 7.36 (d, 1H, J = 8.4 Hz), 7.63 (d, 1H, J = 9.3 Hz).

^{13}C-NMR (75 MHz, $CDCl_3$): δ/ppm = 25.6, 25.8, 28.8, 29.1, 29.2, 29.3, 29.4, 32.6, 62.9. 68.5, 101.2, 112.2, 112.8, 112.9, 128.5, 143.3, 155.8, 160.2, 162.3.

2.7.3.7 7-(11-Hydroxyundecoxy) coumarin

Yield 68%

^{1}H-NMR (300 MHz, $CDCl_3$): δ/ppm = 1.24 - 1.60 (m, 18H), 3.48 (br s, 1H), 3.64 (q, 2H, J = 5.1 Hz), 4.01 (t, 2H, J = 6.6 Hz), 6.24 (d, 1H, J = 9.3 Hz), 6.80 - 6.85 (m, 2H), 7.36 (d, 1H, J = 8.7 Hz), 7.63 (d, 1H, J = 9.3 Hz).

^{13}C-NMR (75 MHz, $CDCl_3$): δ/ppm = 25.0, 25.2, 25.4, 28.5, 28.8, 29.1, 29.6, 29.7, 30.5, 32.3, 62.6, 68.5, 112.0, 112.5, 112.7, 128.6, 143.4, 155.3, 160.9, 162.1.

2.7.3.8 7-(12-Hydroxydodecoxy) coumarin

Yield 70%

^{1}H-NMR (300 MHz, $CDCl_3$): δ/ppm = 1.23 - 1.59 (m, 20H), 3.50 (br s, 1H), 3.64 (t, 2H, J = 6.6 Hz), 4.00 (t, 2H, J = 6.6 Hz), 6.24 (d, 1H, J = 9.5 Hz), 6.79 - 6.85 (m, 2H), 7.36 (d, 1H, J = 8.5 Hz), 7.63 (d, 1H, J = 9.5 Hz).

^{13}C-NMR (75 MHz, $CDCl_3$): δ/ppm = 25.0, 25.2, 25.4, 28.5, 28.8, 29.0, 29.1, 29.6, 29.7, 30.5, 32.3, 62.6, 68.5, 112.0, 112.5, 112.7, 128.5, 143.3, 155.5, 160.9, 162.0.

2.7.4 Methacrylate Monomers with Alkyl Spacer Attached Coumarin

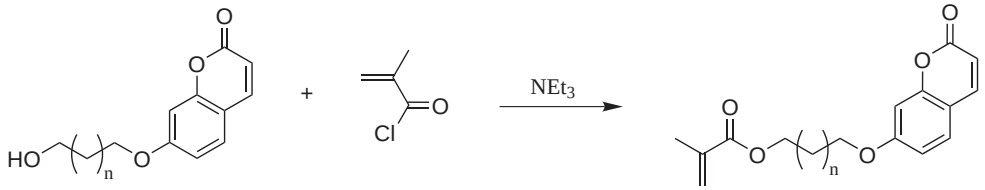

The hydroxy ether of coumarin (100 mmol) was suspended in dry tetrahydrofuran. After addition of triethylamine (5 eq., 50.6 g, 500 mmol) the mixture was stirred until a clear solution had formed. Methacryloyl chloride (1.5 eq., 15.7 g, 150 mmol) was added dropwise while stirring vigorously. The reaction mixture was heated to 60 °C for 2 h and stirred for another 12 h at room temperature. The precipitated ammonia salts were filtered off and the solvent was removed under reduced pressure. For an alkyl spacer length of up to seven carbon atoms a solid was obtained. The respective intermediate product was recrystallized twice from methanol to give the desired final product as white crystals. For spacer lengths of eight or more carbon atoms crystallization of the product was not possible. The crude oil was purified by column chromatography using a pentane/ethyl acetate (5:1) mixture as an eluent.

2.7.4.1 7-(3-Methacryloyloxypropoxy) coumarin (MAOC-C3)

Yield 59%

^{1}H-NMR (300 MHz, $CDCl_3$): δ/ppm = 1.95 (m, 3H), 2.21 (m, 2H), 4.13 (t, 2H, J = 6.1 Hz), 4.36 (t, 2H, J = 6.2 Hz), 5.58 (m, 1 H), 6.11 (m, 2H), 6.26 (d, 1H, J = 9.5 Hz), 6.83 (m, 1H), 7.37 (d, 1H, J = 8.4 Hz), 7.64 (d, 1H, J = 9.5 Hz).

^{13}C-NMR (75 MHz, $CDCl_3$): δ/ppm = 18.1, 28.4, 62.7, 66.4, 76.2, 98.6, 101.2, 111.4, 113.1, 125.3, 128.2, 143.6, 154.1, 156.5, 162.2, 165.7.

MS (EI, 70 eV): m/z (%): 288 (5) [M^+], 203 (10), 161 (7), 145 (4) , 134 (2), 105 (1), 77 (3), 70 (3), 69 (100), 51 (12), 41 (40), 39 (5), 28 (7).

HRMS (EI): calcd. for $C_{16}H_{16}O_5$ (M^+), 288.0998; found 288.0989.

2.7.4.2 7-(5-Methacryloyloxypentoxy) coumarin (MAOC-C5)

Yield 61%

^{1}H-NMR (300 MHz, $CDCl_3$): δ/ppm = 1.43 - 1,76 (m, 6H), 1.87 (m, 3H), 4.03 (t, 2H, J = 6.3 Hz), 4.19 (t, 2H, J = 6.5 Hz), 5.56 (m, 1H), 6.10 (m, 1H), 6.25 (d, 1H, J = 9.5 Hz) 6.82 (m, 2H), 7.36 (d, 1H, J = 8.4 Hz), 7.63 (d, 1H, J = 9.5 Hz).

^{13}C-NMR (75 MHz, $CDCl_3$): δ/ppm = 17.8, 22.1, 29.3, 29.5, 62.4, 66.7, 76.4, 98.1, 101.2, 111.3, 113.1, 125.7, 128.1, 143.3, 154.8, 156.7, 162.3, 165.9.

MS (EI, 70 eV): m/z (%): 316 (4) [M^+], 231 (5) , 203 (5), 161 (7), 145 (4) , 134 (2), 105 (5), 77 (6), 70 (5), 69 (100), 51 (12), 41 (34), 39 (5), 28 (7).

HRMS (EI): calcd. for $C_{18}H_{20}O_5$ (M^+), 316.1311; found 316.1320.

2.7.4.3 7-(7-Methacryloyloxyheptoxy) coumarin (MAOC-C7)

Yield 90%

^{1}H-NMR (300 MHz, $CDCl_3$): δ/ppm = 1.47 - 1.82 (m, 10H), 1.94 (m, 3H), 4.01 (t, 2H, J = 6.4 Hz), 4.15 (t, 2H, J = 6.6 Hz), 5.55 (m, 1H), 6.10 (m, 1H), 6.24 (d, 1H, J = 9.5 Hz), 6.82 (m, 2H), 7.36 (d, 1H, J = 8.4 Hz), 7.63 (d, 1H, J = 9.5 Hz).

^{13}C-NMR (75 MHz, $CDCl_3$): δ/ppm = 18.2, 25.3, 25.7, 25.8, 29.1, 29.6, 65.7, 68.4, 76.2, 98.6, 101.2, 111.4, 113.1, 125.3, 128.2, 143.6, 154.1, 156.5, 162.2, 165.7.

MS (EI, 70 eV): m/z (%): 344 (1) [M^+], 259 (8), 231 (5) , 203 (5), 161 (7), 145 (4) , 134 (2), 105 (5), 77 (6), 70 (100), 69 (3), 51 (16), 41 (25), 39 (15), 28 (13).

HRMS (EI): calcd. for $C_{20}H_{24}O_5$ (M^+), 344.1624; found 344.1639.

2.7.4.4 7-(8-Methacryloyloxyoctoxy) coumarin (MAOC-C8)

Yield 90%

^{1}H-NMR (300 MHz, $CDCl_3$): δ/ppm = 1.32 - 1.46 (m, 6H), 1.68 (q, 2H, J = 6.9 Hz), 1.68 (q, 2H, J = 6.9 Hz), 1.81 (q, 2H, J = 6.6 Hz), 1.94 (m, 3H), 4.00 (t, 2H, J = 6.6 Hz), 4.14 (t, 2H, J = 6.6 Hz), 5.54 (m, 1H), 6.09 (m, 1H), 6.24 (d, 1H, J = 9.6 Hz), 6.79 - 6.84 (m, 2H), 7.35 (d, 1H, J = 8.4 Hz), 7.63 (d, 1H, J = 9.6 Hz).

^{13}C-NMR (75 MHz, $CDCl_3$): δ/ppm = 18.0, 25.8, 25.9, 28.6, 29.1, 29.2, 29.6, 64.7, 68.6, 76.4, 98.3, 101.4, 111.0, 113.0, 125.1, 128.2, 143.6, 154.4, 156.1, 162.3, 165.7.

MS (ESI): m/z (%): 457 (19), 441 (21), 381 (4) [M + Na^+], 360 (3) [M + H^+], 313 (100), 291 (4).

HRMS (ESI): calcd. for $C_{22}H_{29}O_5$ (M^+), 358.4281; found 358.4278.

2.7.4.5 7-(9-Methacryloyloxynonoxy) coumarin (MAOC-C9)

Yield 82%

^{1}H-NMR (300 MHz, $CDCl_3$): δ/ppm = 1.33 - 1.47 (m, 10H), 1.66 (q, 2H, J = 6.9 Hz), 1.79 (q, 2H, J = 6.9 Hz), 1.92 (m, 3H), 3.99 (t, 2H, J = 6.3 Hz), 4.12 (t, 2H, J = 6.6 Hz), 5.53 (m, 1H), 6.08 (m, 1H), 6.24 (d, 1H, J = 9.6 Hz), 6.77 - 6.83 (m, 2H), 7.34 (d, 1H, J = 8.4 Hz), 7.62 (d, 1H, J = 9.6 Hz).

^{13}C-NMR (75 MHz, $CDCl_3$): δ/ppm = 18.5, 26.1, 28.8, 29.1, 29.4, 29.5, 29.6, 29.7 64.9, 68.8, 101.5, 112.6, 113.1, 113.2, 125.3, 128.9, 136.7, 143.6, 156.1, 161.4, 162.6, 167.7.

MS (ESI): m/z (%): 537 (4), 499 (3), 432 (4), 395 (100) [M + Na^+], 373 (2) [M + H^+], 335 (25).

HRMS (ESI): calcd. for $C_{22}H_{29}O_5$ (M + H^+), 373.2015; found 373.2010.

2.7.4.6 7-(10-Methacryloyloxydecoxy) coumarin (MAOC-C10)

Yield 89%

^{1}H-NMR (300 MHz, $CDCl_3$): δ/ppm = 1.32 - 1.56 (m, 12H), 1.67 (q, 2H, J = 7.2 Hz), 1.81 (q, 2H, J = 6.9 Hz), 1.94 (m, 3H), 4.01 (t, 2H, J = 6.3 Hz), 4.14 (t, 2H, J = 6.9 Hz), 5.54 (m, 1H), 6.09 (m, 1H), 6.24 (d, 1H, J = 9.3 Hz), 6.80 - 6.85 (m, 2H), 7.36 (d, 1H, J = 8.7 Hz), 7.63 (d, 1H, J = 9.6 Hz).

^{13}C-NMR (75 MHz, $CDCl_3$): δ/ppm = 18.3, 25.9, 28.6, 28.9, 29.2, 29.3, 29.4, 29.6, 29.8, 64.8, 68.7, 98.1, 101.3, 112.4, 112.9, 125.1, 125.2, 128.7, 143.4, 154.4, 156.0, 162.4, 165.5.

MS (ESI): m/z (%): 798 (6) [2 M + Na^+], 680 (6), 514 (100), 410 (94) [M + Na^+], 321 (26), 303 (27).

HRMS (ESI): calcd. for $C_{23}H_{30}O_5$ (M^+), 386.2093; found 386.2082.

2.7.4.7 7-(11-Methacryloyloxyundecoxy) coumarin (MAOC-C11)

Yield 80%

^{1}H-NMR (300 MHz, $CDCl_3$): δ/ppm = 1.32 - 1.54 (m, 14H), 1.67 (q, 2H, J = 7.1 Hz), 1.80 (q, 2H, J = 6.9 Hz), 1.93 (m, 3H), 4.01 (t, 2H, J = 6.3 Hz), 4.14 (t, 2H, J = 6.9 Hz), 5.54 (m, 1H), 6.09 (m, 1H), 6.24 (d, 1H, J = 9.3 Hz), 6.80 - 6.85 (m, 2H), 7.36 (d, 1H, J = 8.7 Hz), 7.63 (d, 1H, J = 9.6 Hz).

^{13}C-NMR (75 MHz, $CDCl_3$): δ/ppm = 18.2, 25.8, 28.6, 28.9, 29.3, 29.4, 29.5, 29.6, 29.8, 64.8, 68.8, 98.4, 101.3, 112.7, 112.9, 125.1, 125.1, 128.6, 143.4, 154.3, 156.1, 162.4, 165.6.

MS (EI, 70 eV): m/z (%): 400 (30) [M^+], 331 (9), 315 (8), 279 (5), 230 (6), 202 (2), 198 (8), 175 (7), 162 (100), 145 (4), 134 (18), 111 (4), 97 (12), 83 (10), 69 (12), 55 (14), 41 (17).

HRMS (EI): calcd. for $C_{24}H_{32}O_5$ (M^+), 400.2250; found 400.2243.

2.7.4.8 7-(12-Methacryloyloxydodecoxy) coumarin (MAOC-C12)

Yield 81%

^{1}H-NMR (300 MHz, $CDCl_3$): δ/ppm = 1.32 - 1.55 (m, 16H), 1.68 (q, 2H, J = 7.0 Hz), 1.81 (q, 2H, J = 6.9 Hz), 1.94 (m, 3H), 4.01 (t, 2H, J = 6.3 Hz), 4.14 (t, 2H, J = 6.9 Hz), 5.54 (m, 1H), 6.09 (m, 1H), 6.24 (d, 1H, J = 9.3 Hz), 6.80 - 6.85 (m, 2H), 7.36 (d, 1H, J = 8.6 Hz), 7.63 (d, 1H, J = 9.6 Hz).

^{13}C-NMR (75 MHz, $CDCl_3$): δ/ppm = 17.9, 25.7, 28.6, 28.9, 29.1, 29.2, 29.4, 29.5, 29.8, 64.8, 68.7, 98.1, 101.3, 112.1, 112.5, 125.1, 125.6, 128.7, 143.4, 154.2, 156.0, 162.6, 165.7.

MS (ESI): m/z (%): 439 (24), 438 (100) [M + Na^+], 432 (3), 416 (8), 355 (4), 330 (3), 310 (2).

HRMS (ESI): calcd. for $C_{25}H_{34}O_5Na$ (M + Na^+), 437.2304; found 437.2298.

2.7.5 4'-Methacryloyloxychalcone (MAOChalc)

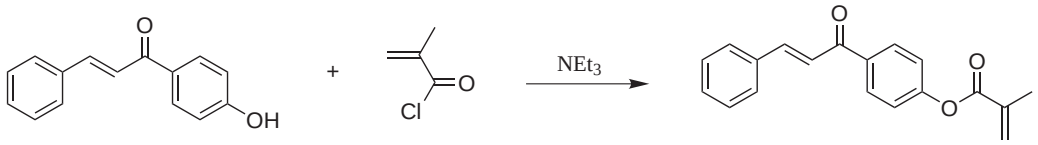

4'-Methacryloyloxychalcone (MAOChalc) was synthesized by esterification of 4'-hydroxychalcone with methacryloyl chloride in the presence of triethylamine. 4'-Hydroxychalcone (8 g, 35.9 mmol) was suspended in dry tetrahydrofuran. After adding triethylamine (1.5 eq., 7.4 mL, 53.4 mmol) the mixture was stirred until a clear solution had formed. Methacryloyl chloride (1.5 eq., 5.2 mL, 53.5 mmol) was added dropwise while stirring vigorously. The reaction mixture was stirred for 24 h at room temperature. The precipitated ammonia salts were filtered off and the solvent was removed under reduced pressure. The residual oil was poured into 1.7 L *n*-pentane. The product crystallized while cooling to 5 °C for 2 d. The yellowish crystals were filtered off and dried under high vacuum.

Yield 69%

^{1}H-NMR (300 MHz, DMSO-d$_6$): δ/ppm = 2.92 (s, 3H), 5.95 (s, 1H), 6.33 (s, 1H), 7.40 (d, 2H, J = 8.7 Hz), 7.46 - 7.48 (m, 3H), 7.60 (d, 1H, J = 15.6 Hz), 7.91 (m, 2H), 7.98 (d, 1H, J = 15.6 Hz), 8.25 (d, 2H, J = 8.7 Hz).

^{13}C-NMR (75 MHz, DMSO-d$_6$): δ/ppm = 17.8, 121.8, 122.1, 128.1, 128.8, 130.1, 130.5, 134.9, 144.0, 154.2, 154.5, 164.3, 188.0.

2.7.6 4-Methacryloyloxystilbene (MAOS)

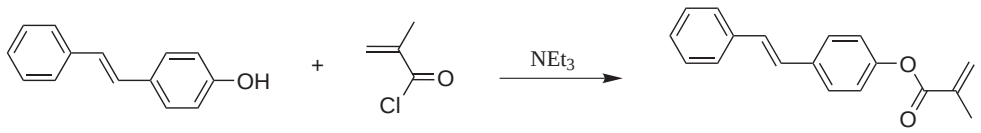

4-Methacryloylstilbene was synthesized accordingly as described in section 2.7.1.

Yield 91%

^{1}H-NMR (300 MHz, DMSO-d$_6$): δ/ppm = 2.94 (s, 3H), 5.91 (br s, 1H), 6.29 (br s, 1H), 7.19 (d, 2H, J = 8.3 Hz), 7.26 (s, 2H), 7.30 (s, 1H), 7.39 (t, 2H, J = 7.7 Hz), 7.61 (d, 2H, J = 7.7 Hz), 7.66 (d, 2H, J = 8.3 Hz).

^{13}C-NMR (75 MHz, DMSO-d$_6$): δ/ppm = 18.0, 121.4, 127.3, 127.8, 128.0, 128.6, 128.7, 129.6, 134.4, 135.3, 137.7, 150.1, 166.0.

MS (EI): m/z (%): 264 (17) [M$^+$], 196 (2), 166 (1), 165 (4), 152 (2), 70 (5), 69 (100), 65 (1), 42 (2), 41 (92), 39 (9), 32 (1), 28 (15).

2.7.7 Polymerizable Coumarin Dimer

In order to obtain a coumarin dimer with a methacrylic functionality at each side for polymerization, 7-hydroxycoumarin dimer was synthesized first in a three step synthesis according to the procedure described by *Chen* and *Chen*.[413] 7-Hydroxycoumarin cannot be dimerized directly in a photochemical reaction because of the ready generation of O$^{\cdot}$ radicals from the phenolic OH-group.[414] This leads to the formation of undesired side products rather than to the desired dimer. A direct dimerization of MAOC

is also not possible because photoinduced polymerization of the methacrylic double bond would lead to an uncontrolled polymerization. Therefore, the synthetic route to 7,7′-(dimethacryloyloxy)dicoumarin necessitates the protection of 7-hydroxycoumarin with an adequate protecting group.[415] In this case an acetic ester is used. After the photochemical dimerization step the acetate ester is cleaved and subsequently esterified with methacryloyl chloride to afford the 7,7′-(dimethacryloyloxy)dicoumarin.

2.7.7.1 7-Acetoxycoumarin

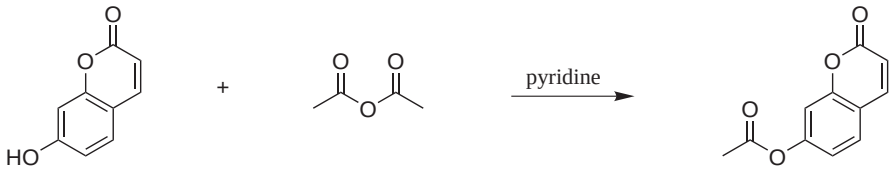

7-Hydroxycoumarin (30 g, 185 mmol), sodium acetate (23 g, 280 mmol), acetic anhydride (150 mL, 1.59 mol) and a few drops of pyridine were slowly heated to 145 °C while beeing stirred. The reaction mixture was then heated at reflux for 16 h. After cooling to room temperature a brown solid was obtained by filtration. The solid was washed with ice cold water and ethanol. Recrystallization from ethanol afforded the product as yellowish crystals.

Yield 58%

^{1}H-NMR (300 MHz, $CDCl_3$): δ/ppm = 2.34 (s, 3H), 7.06 (dd, 1H, J_1 = 9.6 Hz, J_2 = 2.2 Hz), 7.12 (d, 1H, J = 2.2 Hz), 7.41 (d, 1H, J = 8.8 Hz), 7.49 (d, 1H, J = 9.6 Hz), 7.69 (d, 1H, J = 8.8 Hz).

2.7.7.2 7,7'-(Diacetoxy)dicoumarin

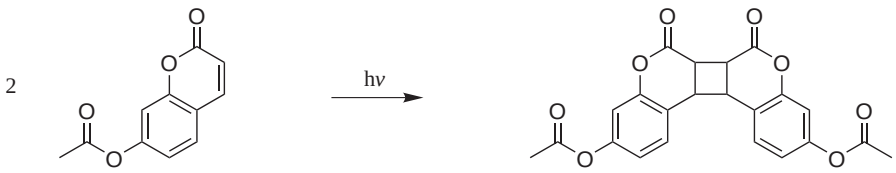

7-Acetoxycoumarin (22 g, 108 mmol) and benzophenone (3.7 g, 20 mmol) were dissolved in degassed dichloromethane. The mixture was irradiated for 4d in a rayonet type

photoreactor. The pyrex glass of the reaction vessels serves as a filter for UV-wavelengths shorter than 300 nm, pushing the equilibrium reaction towards the product side. After evaporation of the solvents the solids obtained were washed with diethylether and recrystallized from acetic acid to give pure *anti* head-to-head 7-acetoxycoumarin dimer as pale yellow crystals.

Yield 52%

^{1}H-NMR (300 MHz, DMSO-d$_6$): δ/ppm = 2.27 (s, 6H), 3.86 - 3.98 (m, 4H), 6.96 (d, 2H, J = 2.1 Hz), 6.99 (dd, 2H, J_1 = 8.3 Hz, J_2 = 2.1 Hz), 7.42 (d, 1H, J = 8.3 Hz).

2.7.7.3 7,7'-(Dihydroxy)dicoumarin

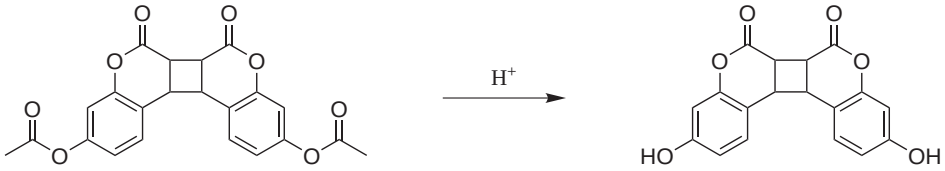

7,7'-(Diacetoxy)dicoumarin (6.6 g, 16.3 mmol) was dissolved in a mixture consisting of equal volumes (124 mL) ethanol and 4 M hydrochloric acid. The clear solution was heated at reflux under argon atmosphere for 4 h. After cooling to ambient temperature and adding deionized water, the reaction mixture was extracted four times with ethyl acetate. The solvent was evaporated from the unified organic phases and the residues were refluxed in acetic acid for 12 h to give 7,7'-(dihydroxy)dicoumarin as a white solid.

Yield 93%

^{1}H-NMR (300 MHz, DMSO-d$_6$): δ/ppm = 3.63 (d, 2H, J = 7.7 Hz), 3.83 (d, 2H, J = 7.7 Hz), 6.46 (d, 2H, J = 2.0 Hz), 6.63 (dd, 2H, J_1 = 8.3 Hz, J_2 = 2.0 Hz), 7.13 (d, 2H, J = 8.3 Hz), 9.82 (br s, 2H).

2.7.7.4 7,7'-(Dimethacryloyloxy)dicoumarin (diMAOC)

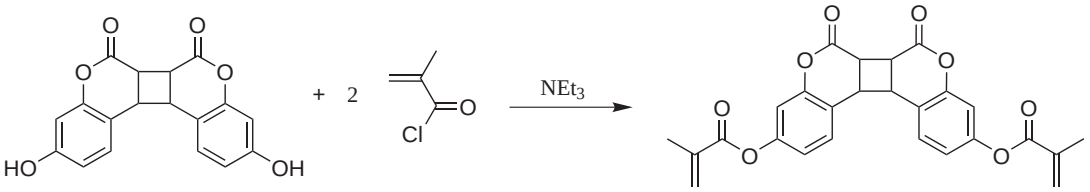

7,7'-(Dihydroxy)dicoumarin (4.8 g, 15 mmol) was dissolved in dry *N*,*N*'-dimethylacetamide and while cooling to 0 °C triethylamine (21 mL, 149 mmol) was added. Methacryloyl chloride (4.4 mL, 45 mmol) was added dropwise while stirring. The reaction mixture was stirred for another 2 h while it was allowed to warm to ambient temperature. The reaction was quenched by adding 50 mL methanol. The methanol was subsequently removed under reduced pressure and the precipitated ammonia salts were filtered off. The filtrate was poured into a great excess of deionized water to precipitate the product. The crude product was purified by preparative HPLC using acetonitrile/water (50:50) as eluent.

Yield 82%

^{1}H-NMR (300 MHz, DMSO-d_6): δ/ppm = 2.11 (s, 6H), 3.97 (d, 2H, J = 8.9 Hz), 4.89 (d, 2H, J = 8.9 Hz), 5.70 (m, 2H), 6.28 (m, 2H), 6.52 (dd, 2H, J_1 = 8.3 Hz, J_2 = 2.3 Hz), 6.65 (d, 2H, J = 2.3 Hz), 7.07 (d, 2H, J = 8.3 Hz).

^{13}C-NMR (75 MHz, $CDCl_3$): δ/ppm = 18.4, 43.9, 45.7, 108.9, 112.7, 123.2, 127.3, 128.0, 135.9, 150.6, 155.5, 166.0, 173.7.

MS (ESI): m/z (%): 483 (11) [M + Na^+], 483 (7) [M + Na^+] 458 (5), 443 (8), 427 (6), 399 (7), 356 (9), 271 (7), 261 (10). 242 (8). 229 (9).

HRMS (ESI): calcd. for $C_{26}H_{20}O_8$ (M^+), 460.1158; found 460.1153.

2.8 Polymerization Procedures

2.8.1 Polymerization in Solution

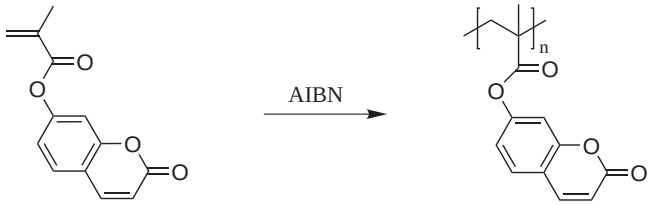

All polymers were prepared by free radical polymerization of the monomers in the presence of 2,2′-azobisisobutyronitrile (AIBN). A solution of 50 mmol monomer and 5.5 mg AIBN was dissolved in 50 mL of dry DMF and degassed by three freeze-thaw-cycles. For the copolymerization of MAOC and BMA both were dissolved in dry DMF in the desired ratio (95 to 50 mol-% MAOC) giving a total amount of 50 mmol monomer and 5.5 mg AIBN were added. The solutions were stirred for 24 h at 60 °C in sealed vessels. The viscous solutions were then precipitated in methanol and filtered off. The polymer was re-dissolved in 80 mL of DMF and re-precipitated. The polymer was then filtered and dried in vacuo at 60 °C for 72 h.

The ratios of MAOC and BMA in the copolymers obtained were derived from ^{1}H-NMR spectra recorded in $CDCl_3$. The signal of the proton attached to C-2 of the coumarin moiety (6.3 ppm) and the signal of the two protons at C-1 of the butyl chain (4.0 ppm) do not overlap with other signals in the spectra. Therefore, these signals have been integrated to calculate the ratio of the two different polymer building blocks.

2.8.2 Bulk Polymerization

Bulk polymerization is a polymerization carried out in the absence of any solvent or dispersant. In case of solid monomers about 10 g of the monomer was melted by heating to 50 - 60 °C while stirring. The appropriate amounts of radical initiator and cross-linker were added and after everything was dissolved the melt was quickly filtered off using 0.45 µm pore size PTFE syringe filters. The melt was immediately filled into the polymerization chamber. The polymerization chamber consisted of a vertical assembly of two glass or PTFE plates of about $10 \times 10\,cm^2$. A 2 mm thick silicone gasket was pla-

ced between the plates. Thereby the volume is formed in which the polymerization was conducted to give a polymer plate of about 2 mm thickness. Loading of the polymerization chamber was carried out in a laminar flow cabinet. After filling the polymerization chamber was placed in a cabinet dryer. The cabinet dryer was flushed with argon and the polymerization assembly was subjected to temperatures between 50 and 110 °C for a time preferably between 72 and 140 h to carry out a free radical polymerization.

2.8.3 Parylene Coating

Parylene, unlike other polymeric materials, is not manufactured or sold as a polymer, but rather is produced by vapor phase deposition and polymerization of *para*-xylylene or its substituted derivatives (Fig 2.4). The parylene process is a relatively simple vacuum application system, that starts with a dimer,[416] which is placed in a vacuum system and converted to a reactive vapor of the monomer. When passed over objects at room temperature, this vapor will rapidly coat them with a polymer film (Fig. 2.5).[417,418] It is neither practical to melt, extrude, or mold as it is possible with thermoplastics, nor can it be applied from solution. Many of the advantages found in parylene coatings are a direct result of the coating deposition process.

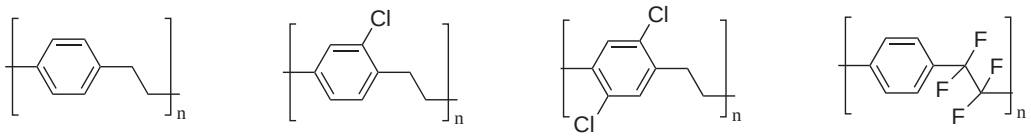

Parylene N Parylene C Parylene D Parylene HT

Figure 2.4: Poly(*para*-xylylene) (Parylene N) and its commercially used derivatives.

Parylene can simultaneously coat many small parts of varying configurations and is extremely resistant to chemical attack. The coating can be applied to virtually any surface material including plastic, elastomer, metal, glass, ceramic and paper. In commercial applications, parylene is deposited in thicknesses ranging from a few hundred nanometers to about 75 µm depending on the function the parylene film has to perform. Parts can be conformaly coated to thicknesses that can be controlled generally to $\pm 10\%$. Because Parylene is not a liquid, the coating does not suffer from the meniscus and edge effects of conventional liquid coatings. As a result of its ultra-thin application, Parylene adds little dimension or mass to critical, weight-sensitive components. Parylene

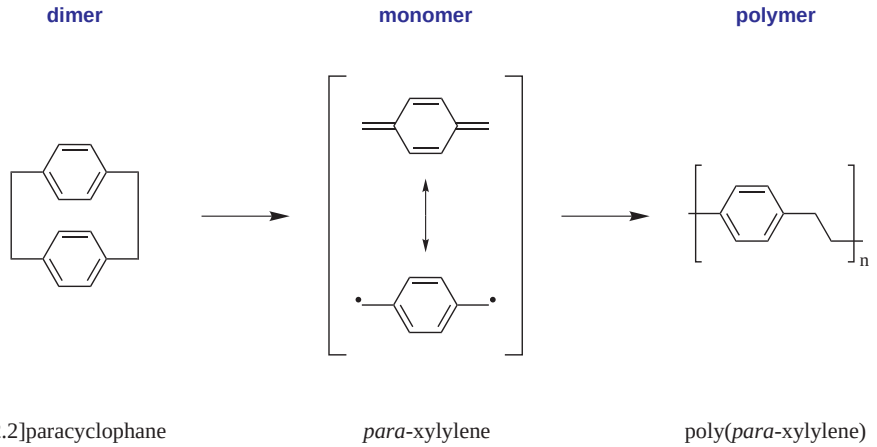

Figure 2.5: Parylene vapor deposition and polymerization process illustrated for Parylene N.

coatings are pinhole-free and have excellent moisture, chemical and dielectric barrier properties. Parylene coatings are biocompatible and biostable. Therefore, they offer exceptional properties for medical device protection. Parylenes N, C, and Parylene HT® comply with biological testing requirements for ISO-10993. Testing included cytotoxicity, sensitization, intracutaneous reactivity, acute systemic toxicity, implantation, hemocompatibility, and pyrogenicity.[419–421] Parylenes N, C, and HT are certified to comply with the biological testing requirements for USP Class VI Plastics.[422] Parylene has proofed to be an ideal surface modification for implantable medical devices such as coronary stents or pacemakers. Medical grade silicone rubber products such as catheters and medical seals require a coating with a high degree of flexibility, which Parylene can also provide. Medical electronic components can be protected from moisture, biofluids and biogasses that can cause such assemblies to fail prematurely.[423–427]

In this work IOLs were coated with Parylene C due to its excellent barrier properties. Parylene C offers significantly lower permeability to moisture and gases compared to Parylene N. A Parylene Deposition Unit Model PDS 2010 (Specialty Coating Systems) was used to carry out the coating process. The thickness of the coating is determined by the amount of paracyclophane that is evaporated and cracked in the coater. Here 1.5 g of DPX C (the precursor of Parylene C) obtained from Specialty Coating Systems was used. To check the coating thickness a microscope slide was always coated together with the IOLs. The polymer layer thickness on the glass slide was determined by profilometry after making a scratch down to the substrate. Parylene layer thicknesses were around 1 µm with very small variations between different coating procedures.

3 Results and Discussion

A typical postoperative complication in cataract surgery is that the refractive power of the implanted IOL is often not sufficient for optimal vision, requiring the patient to use prescription eye wear. The aim of this work is to overcome one major drawback of IOLs. The following chapter explains the numerous experiments that have been conducted to obtain polymers which are tunable in refractive index and suitable for IOL manufacturing. Most profitably the focal length of an IOL is to be tuned postoperatively in a non-invasive manner by changing the refractive index of the implanted lens through a photochemical process. The polymers these IOLs are made of, have a specific photo-active linker group attached to the polymer backbone. As a first step in this work, various linker groups suitable for this application were compared to identify the best of the potentially useful materials.

Once the best photoactive linker system was identified, further important steps in the fabrication of polymers actually suitable for IOL manufacturing were successfully developed. For this purpose, the material properties had to be improved so that a transparent material of good optical and mechanical quality could be obtained. However, through this improvement process, the magnitude of the photoinduced change in refractive index must not be decreased. Developing a material that combines good material and optical properties in terms of refractive index change was a very challenging task. But this problem was solved by the insertion of an alkyl spacer molecule between the photo-active coumarin and the methacrylate moiety used to build up the polymer backbone. Novel polymers were obtained showing all required properties.

In the following step novel monomers were polymerized in a free radical bulk polymerization with an acrylic crosslinker to attain flexible materials. Though bulk polymerization is an established method, problems arising from the newly developed monomers had to be solved. Because the new monomers are all solid at room temperature, they had to be molten, filtered, and polymerized at elevated temperatures. As far as the exact

parameters of the bulk polymerization process such as reaction temperatures, initiator and crosslinker content are concerned, recipes known from standard acrylates could not directly be transferred to the new monomers. In fact, a great number of polymerization experiments were needed here to determine the optimal process parameters. By alteration of the alkyl spacer length, flexibility of the final material may be tuned. A flexible material for IOL production that can be rolled or folded is very important because this allows the insertion of the IOL through a relatively small cut in the eye. This technique does not require any stitching resulting in an accelerated healing process, while reducing the risk of infections. Inside the capsular bag the IOL then needs to relax back to its initial shape.

From the novel polymers with alkyl spacer attached coumarin IOL prototypes were made by machining. This demonstrates the material's suitability for IOL manufacturing. The most important result is that a change in focal length due to a change in refractive index of such IOL prototypes was successfully demonstrated. The maximum change in refractive index of the polymers synthesized here is more than 0.03, enabling a fine-tuning on the order of 2.5 D in a standard IOL. With such postoperative treatment nearly all patients do not need viewing aids after cataract surgery.

3.1 Polymer Attached Linker Systems

The considerations made in the introductory chapter (Sec. 1.5.3.1) concerning suitable linker systems for refractive index change in polymers were used as the basis for further investigations in that field. Polymers containing side groups of the most promising photoactive linker molecules were synthesized and characterized with special respect to the photoinduced refractive index change. Polymers with cinnamic acid side groups were not further considered. Plates of commercially available poly(vinyl cinnamate) (Aldrich) with a suitable thickness for IOL manufacturing showed too much of a brownish tone to be acceptable. Purification of the polymer by dialysis with a cut off mass of 5000 u did not lead to an improvement in terms of chromaticity.

3.1.1 Poly(7-methacryloyloxycoumarin) (PMAOC)

Poly(7-methacryloyloxycoumarin) (PMAOC) as a polymer which can be photochemically cross-linked was synthesized. This polymer employs the described principle of refractive index change due to a change in polarizability (Sec. 1.5.1). Direct irradiation ($\lambda > 300\,\text{nm}$) of coumarins leads exclusively to photochemical dimerization resulting in cyclobutane-type dimers. The polymer bound coumarin has two strong absorption bands at 280 nm and 310 nm which are assigned to $\pi - \pi^*$- and n $- \pi^*$-transitions.[428] The dimerization of polymer bound coumarin molecules was studied in PMAOC films on quartz plates with thickness ranging from 100 nm to 200 nm. The films were irradiated with 313 nm UV light from a mercury lamp. UV/Vis spectra were taken consecutively during the course of irradiation. Measuring the decrease of absorbance at $\lambda_{\text{max}} = 310\,\text{nm}$ is a convenient and accurate way to monitor the dimerization reaction of the coumarin side groups. This is because the decrease of optical density at that wavelength is directly related to the vanishing of the double bond that undergoes the cycloaddition reaction (Fig. 3.1). The presence of an isosbestic point, which may be more easily seen from the difference spectra, indicates that there is a photochemical reaction with one product only (Fig. 3.2).

To assess the refractive index change of PMAOC resulting from the photoinduced dimerization, films with a thickness between 500 nm and 1.5 µm were prepared on silicon wafers. The refractive index of these films was measured with a prism coupler. The exact thickness of the polymer film is not important, as the method for refractive index determination utilizing the prism coupler is independent of layer thickness. The film thickness only needs to be within the measurement range of the prism coupler. Refractive indices were measured also after increasing photon energy doses at a wavelength of 313 nm. For PMAOC an initial refractive index of 1.6226 and a maximum refractive index change of 0.0218 were determined. The change in refractive index, as well as the change in optical density at the maximum of the band that corresponds to the coumarin double bond (310 nm) is plotted versus the irradiated light energy. From this diagram the direct relation between the dimerization reaction and the refractive index is clearly seen (Fig. 3.3). Both the refractive index and the optical density show an exponential decay with increasing photon energy doses. The exponential relationship implies that about 80% of the total conversion is accomplished with roughly 10% of the total energy applied.

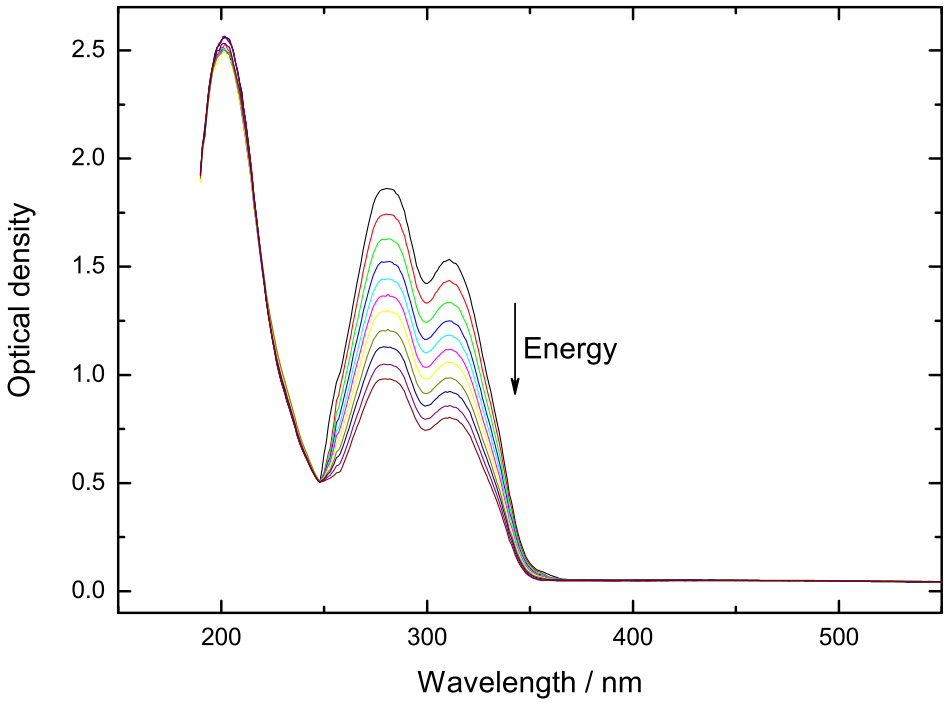

Figure 3.1: Photochemical $[2\pi + 2\pi]$ dimerization of polymer-bound coumarin moieties in a PMAOC film. The dimerization reaction leads to a decrease of optical density at $\lambda_{max} = 310\,\text{nm}$.

The PMAOC sample synthesized in this work had a number average molar mass $\bar{M}_n$ of 52460 g mol^{-1} and a weight average molar mass $\bar{M}_w$ of 122300 g mol^{-1}. These values lead to a polydispersity index $PDI = \bar{M}_w / \bar{M}_n$ of 2.3 which is a typical value for a free radical polymerization. The temperature of five percent decomposition ($T_{5\%}$) was 307 °C and the glass transition temperature (T_g) 119 °C. There is a sufficient "window" between the glass transition point and the onset of thermal decomposition. Therefore there are good reasons to believe that melt processing of the polymer should be possible. Of course, a polymer that is intended for the use in intraocular lenses must have no mentionable absorption in the visible range of the electromagnetic spectrum. The VIS spectrum of a PMAOC film on quartz shows virtually no absorption between 400 and 800 nm.

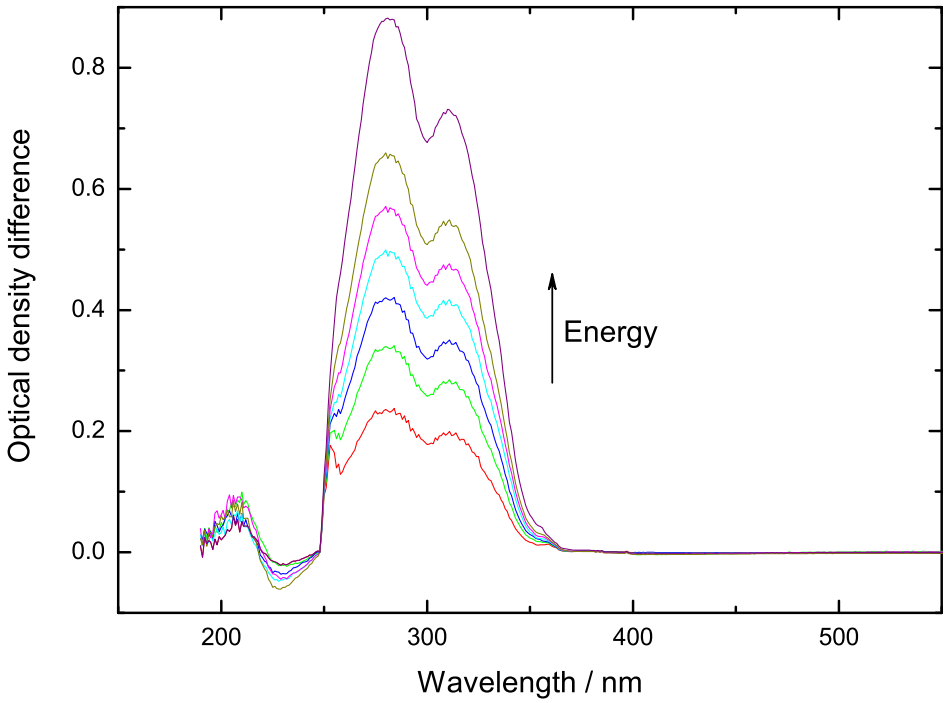

Figure 3.2: Energy-dependent UV difference spectra during the course of dimerization of the coumarin moieties in a PMAOC film.

3.1.2 Polymer with Coumarin Crosslinker

As mentioned above coumarin dimers can be photochemically cleaved when the irradiation wavelength is shorter than 300 nm. The cycloreversion reaction of the cyclobutane ring leads exclusively to the monomeric coumarin.[392] Therefore, 7,7′-(Dimethacryloyloxy)dicoumarin (diMAOC) has been synthesized. It is a coumarin dimer which bears a polymerizable methacryloyl moiety at each of the two coumarin molecules comprising the dimer. This makes the substance practically the dimer of MAOC. However, diMAOC cannot be synthesized by a simple photoinduced dimerization of MAOC because the UV light would cause an undesired polymerization of the methacryloyl groups. DiMAOC needs to be synthesized in a four step procedure involving protection of the OH-group of the coumarin, photodimerization, and deprotection (Sec. 2.7.7). It is important that both coumarins forming the dimer bear a polymerizable moiety. Otherwise the release of monomeric coumarin from the polymer upon dimer cleavage could not be excluded. In order to realize the described concept of a polymer contai-

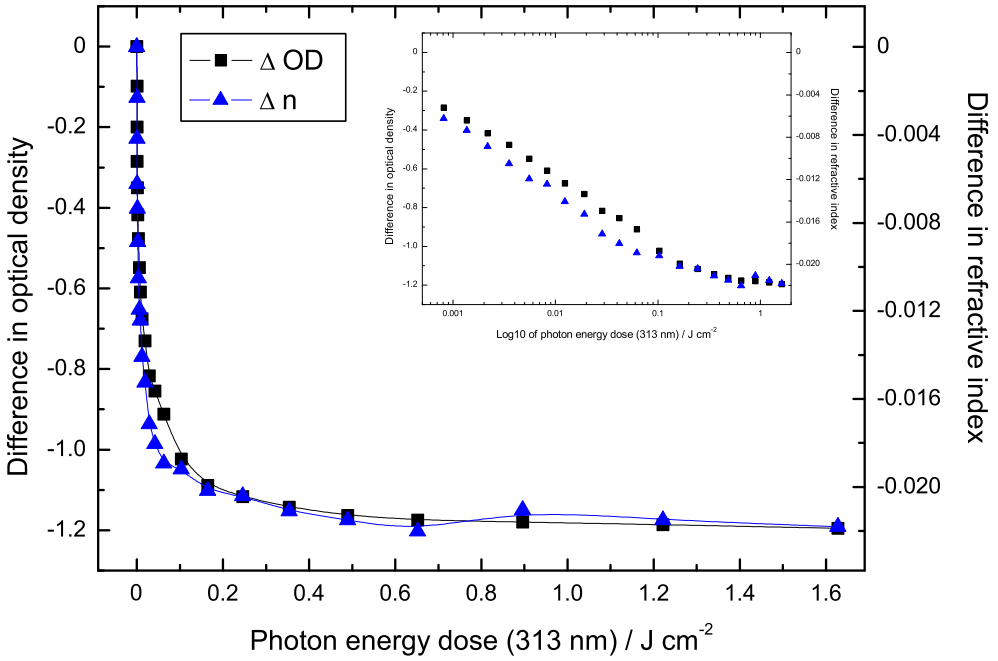

Figure 3.3: Change of refractive index and optical density at 310 nm of a PMAOC film prepared on a silicon wafer as a function of the applied light energy at 313 nm (insert: same set of data shown on a logarithmic energy scale).

ning coumarin dimer groups as a photocleavable cross-linker, diMAOC was dissolved in *n*BMA (50%, w/w) and 1‰ of AIBN was added. A wafer and a quartz plate were coated with the solution and subsequently polymerization and evaporation of excess *n*BMA was carried out at 60 °C for 72 h. The films were irradiated with 254 nm light from a mercury lamp to cleave the dimer and UV/Vis spectra were consecutively taken in a similar way as described for the PMAOC films (Fig. 3.4). The increase of optical density around 310 nm is caused by the formation of monomeric coumarin and shows the dimer cleavage. The difference spectra also show an isosbestic point owing to the fact that, at least in the initial stage of the irradiation process, a single defined reaction is observed ((Fig. 3.5)).

However, the change in optical density is quite low. This result is consistent with a low change in refractive index. The initial refractive index of the film was 1.5482 and could be lowered by only 0.0089. This is because the coumarin dimer content of the polymeric material is only about 50%. It is not possible to increase the diMAOC content because the solubility of the coumarin dimer, which is an unmeltable solid in the acrylic como-

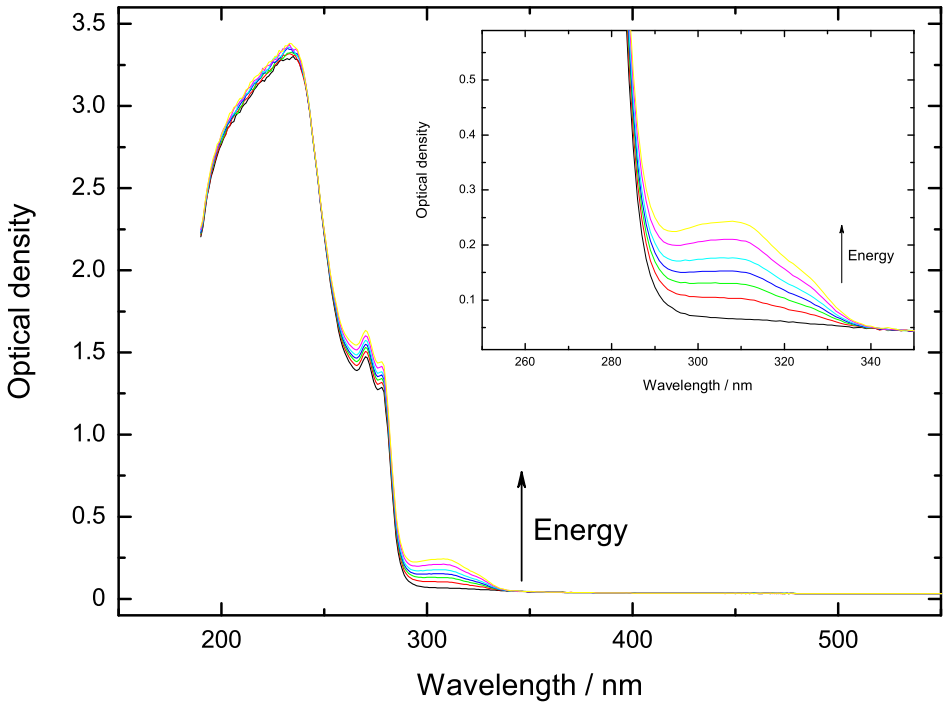

Figure 3.4: Energy-dependent UV/Vis spectra during the single-photon-induced cycloreversion reaction of polymer attached coumarin dimers. The film was irradiated with 254 nm UV light.

nomer, is the limiting factor. The maximum photon energy dose at 254 nm is another limitation. When proceeding to higher total energies, the characteristic band structure of the coumarin spectrum disappears and no isosbestic point is observed anymore. This can be contributed to a main chain degradation of the polymer at that wavelength region due to *Norrish* type degradation reactions. Given the discussed disadvantages and the fact that the polymer would be very hard and brittle due to the extremely high initial crosslinker content this approach is unfavorable for IOL manufacturing. Therefore, only systems that contain the photodimerizable molecule initially in its monomeric form will be considered. The dimerization reaction will then take place in the implanted IOL inside the eye. The hardening of the material once it is inserted into the capsular bag will not pose a problem. In contrast, it is undesired during implantation of the IOL.

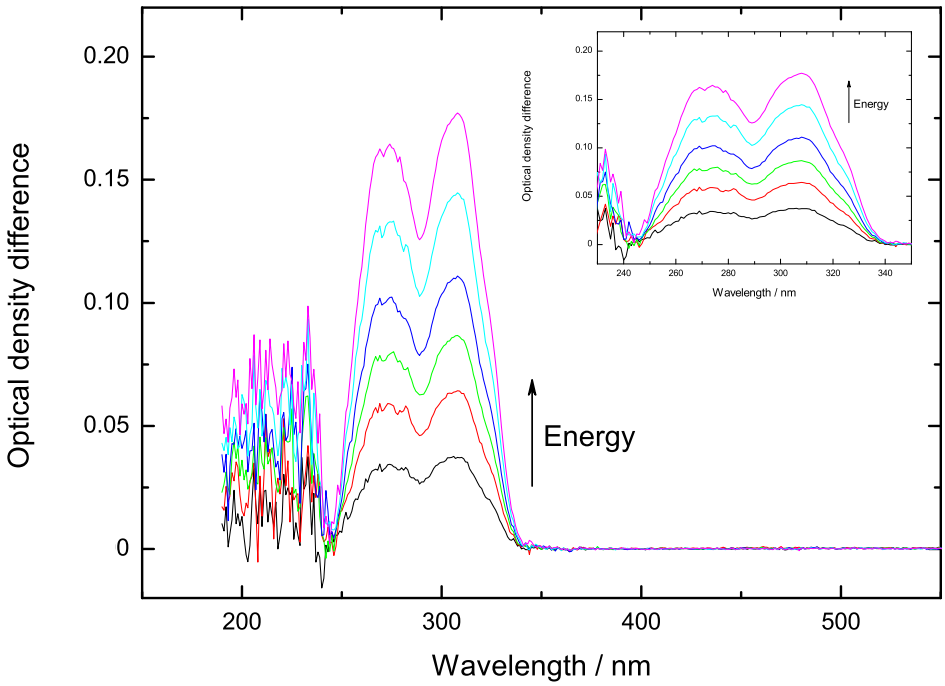

Figure 3.5: Energy-dependent UV difference spectra of diMAOC in a polymer matrix during the course of dimer cleavage.

3.1.3 Poly(4'-methacryloyloxychalcone) (PMAOChalc)

Investigating alternatives to PMAOC, a polymer with chalcone side groups was synthesized. This polymer, poly(4'-methacryloyloxychalcone) (PMAOChalc), can be photochemically cross-linked in a similar fashion as PMAOC. Irradiation with UV light of wavelengths shorter than 300 nm leads to photochemical dimerization of the chalcone moieties resulting in cyclobutane-type dimers. However, in contrast to coumarin, the double bond is not affixed in a ring and can therefore *cis-trans* isomerize as a second possible reaction pathway beside the dimerization reaction. The dimerization of the polymer bound chalcone in PMAOChalc was also studied in films coated on quartz plates ranging from 100 nm to 200 nm in thickness. The films were irradiated with 313 nm UV light from a mercury lamp. UV/Vis spectra were taken consecutively during the course of irradiation. It was found that PMAOChalc initially shows a strong absorption band at 310 nm, whereas the dimerized polymer shows a strong absorption band at 253 nm (Fig. 3.6). Similar to PMAOC the band at 310 nm is the perfect indicator of the pho-

tochemical conversion process. This is because the decrease in optical density at that wavelength is directly related to the vanishing of the double bond that undergoes the cycloaddition reaction. The presence of an isosbestic point, which may more easily be seen from the difference spectra, indicates that there is a photochemical reaction with one product only (Fig. 3.7).

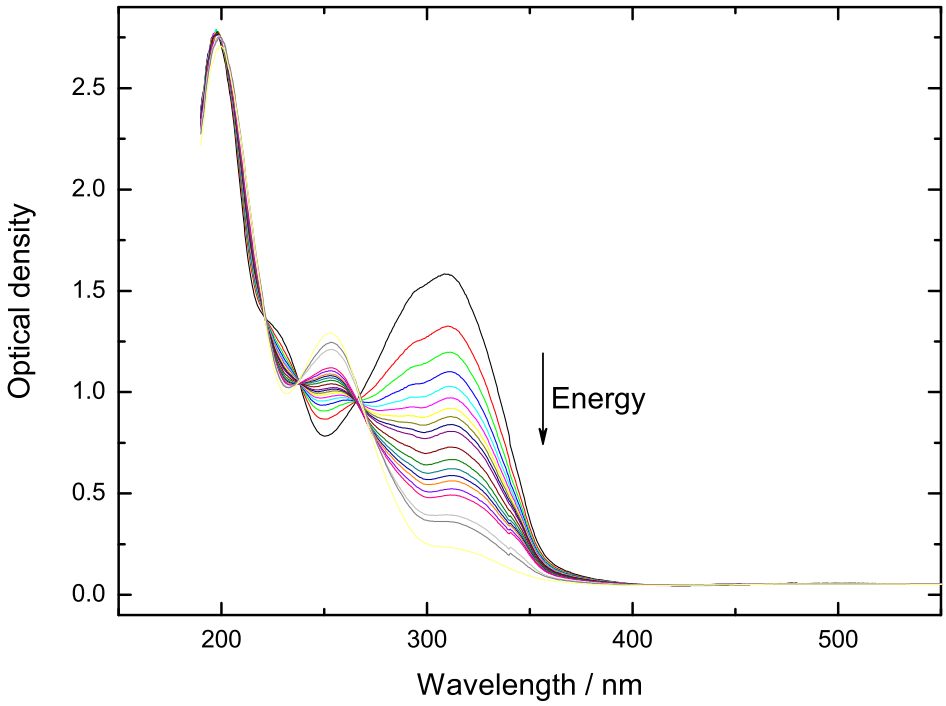

Figure 3.6: Photochemical $[2\pi + 2\pi]$ dimerization of polymer-bound chalcone moieties in a PMAOChalc film. The dimerization reaction leads to a decrease in optical density at $\lambda_{max} = 310\,nm$.

The refractive index change in PMAOChalc films caused by UV irradiation was also measured with a prism coupler. The films had a thickness between 800 nm and 1.5 µm and were prepared on silicon wafers. Refractive indices were also taken after increasing photon energy doses at a wavelength of 313 nm. For PMAOChalc, the initial refractive index is 1.6252 and the maximum refractive index change is 0.0331. The change in refractive index, as well as the change in optical density at the maximum of the band that corresponds to the chalcone double bond (310 nm) was plotted versus the energy of irradiated irradiated light. A good relation between the dimerization reaction and

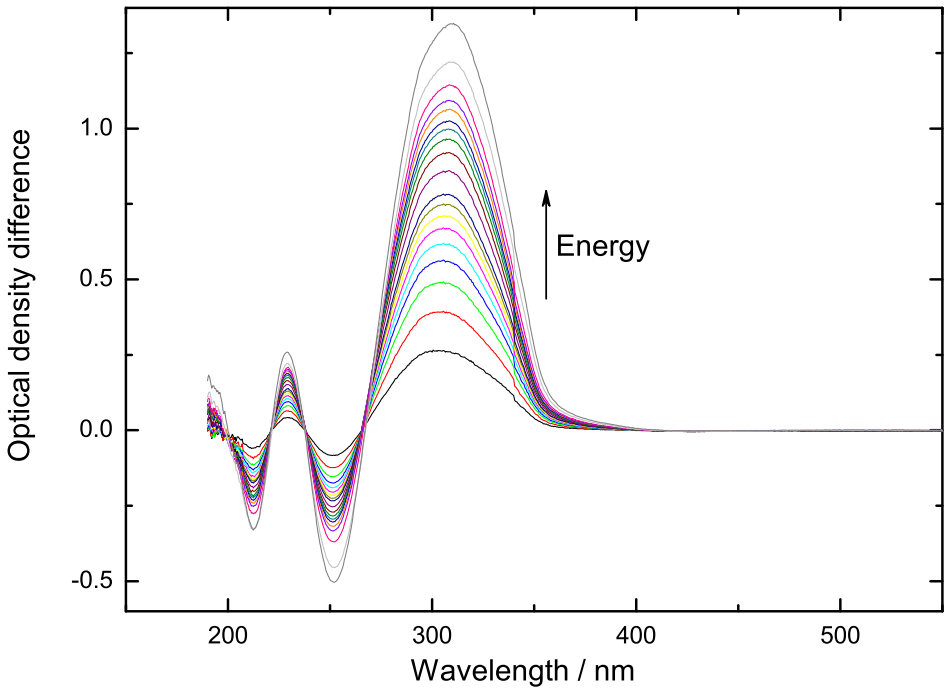

Figure 3.7: Energy-dependent UV difference spectra during the course of dimerization of the chalcone moieties in a PMAOChalc film.

the refractive index can be seen from that diagram (Fig. 3.8). Both refractive index and optical density show an exponential decay with increasing photon energy doses.

The PMAOChalc synthesized had a number average molar mass $\bar{M}_n$ of 52300 g mol^{-1} and a weight average molar mass $\bar{M}_w$ of 90979 g mol^{-1}. These values result in a polydispersity index $PDI = \bar{M}_w/\bar{M}_n$ of 1.7. The values are in the same range as those of PMAOC but the molar mass distribution is more narrow as indicated by the lower PDI. The temperature of five percent decomposition ($T_{5\%}$) was 257 °C and the glass transition temperature (T_g) 168 °C. The T_g value is nearly 50 °C higher than that of PMAOC whereas the $T_{5\%}$ is about 50 °C lower making the material less favorable for melt processing. The Vis spectrum of a PMAOChalc shows no absorption between 400 and 800 nm.

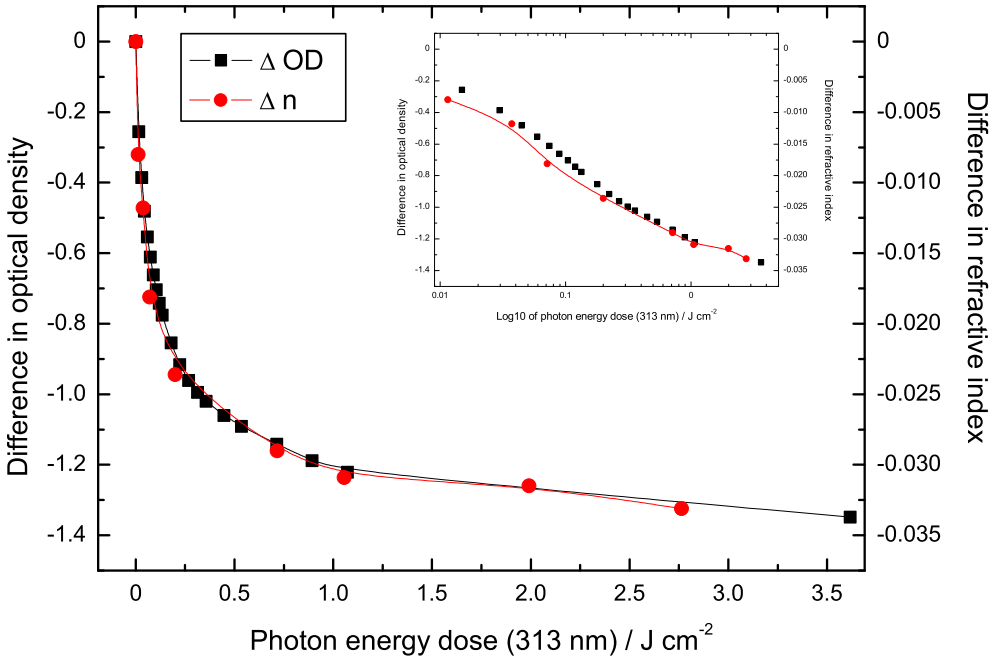

Figure 3.8: Change in refractive index and optical density at 310 nm of a PMAOChalc film prepared on a silicon wafer as a function of the applied light energy at 313 nm (insert: same set of data shown on a logarithmic energy scale).

3.1.4 Poly(4-methacryloyloxystilbene) (PMAOS)

As a further example for a polymer that could show refractive index changes due to a polarizability change poly(4-methacryloyloxystilbene) (PMAOS) was synthesized. The stilbene molecule is very similar to the chalcone molecule. The only difference is the missing of the keto group (C=O) next to the double bond in the stilbene. Therefore, it is not unexpected that stilbene can also be dimerized with 313 nm UV light. The strong absorption band at 288 nm is used to monitor the photoinduced dimerization reaction (Fig. 3.9). UV/Vis difference spectra taken during the course of irradiation of films on quartz plates with a thickness equal to the PMAOC and PMAOChalc films were recorded. Assessing these spectra does not show a clearly defined isosbestic point (Fig. 3.10). The blurred out isosbestic point leads to the conclusion that *cis-trans* isomerization of the stilbene or other side reactions occur to a considerable extent next to the desired dimerization reaction.

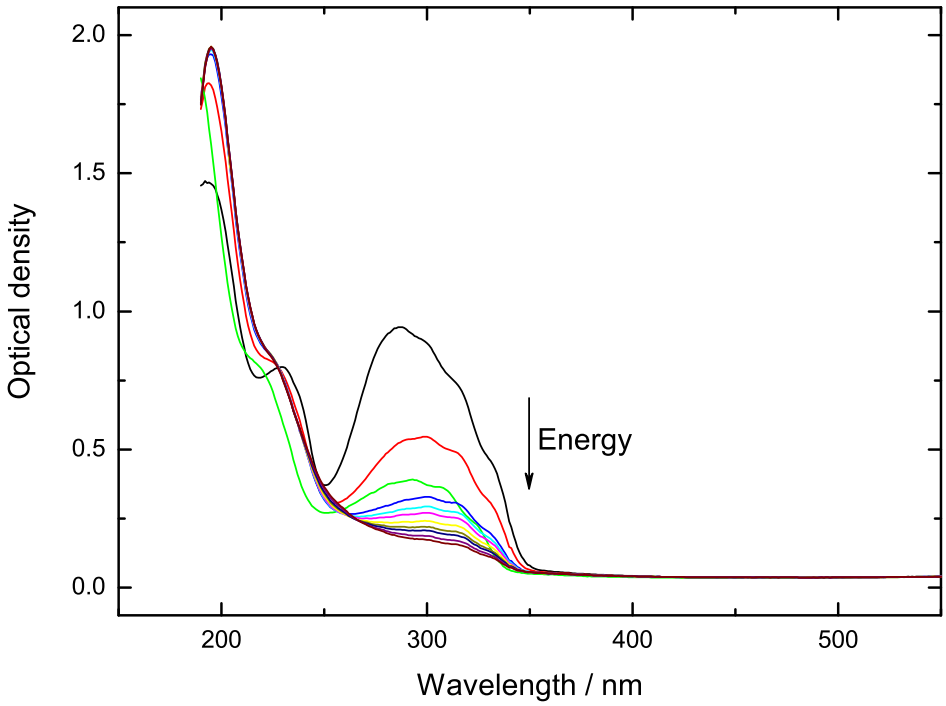

Figure 3.9: Photochemical $[2\pi + 2\pi]$ dimerization of polymer-bound stilbene side groups in a PMAOS film. The dimerization reaction leads to a decrease of optical density at $\lambda_{max} = 288\,nm$.

The initial refractive index of the PMAOS films, also measured with a prism coupler, was 1.5958. The change in refractive index due to the UV light irradiation was comparatively low and amounted to 0.0178. The film had a thickness of 1.2 µm and was prepared on a silicon wafer. The number average molar mass of the polymer was $\bar{M}_n$ 39658 g mol^{-1} and the weight average molar mass $\bar{M}_w$ was 83949 g mol^{-1} giving a PDI of 2.1. These values are slightly lower as those of the PMAOC and PMAOChalc. The temperature of five percent decomposition ($T_{5\%}$) was 263 °C and the glass transition temperature (T_g) 132 °C. The T_g and $T_{5\%}$ values are in the range of those measured for PMAOC and PMAChalc. The VIS spectrum of a PMAOS does not show any absorption between 400 and 800 nm.

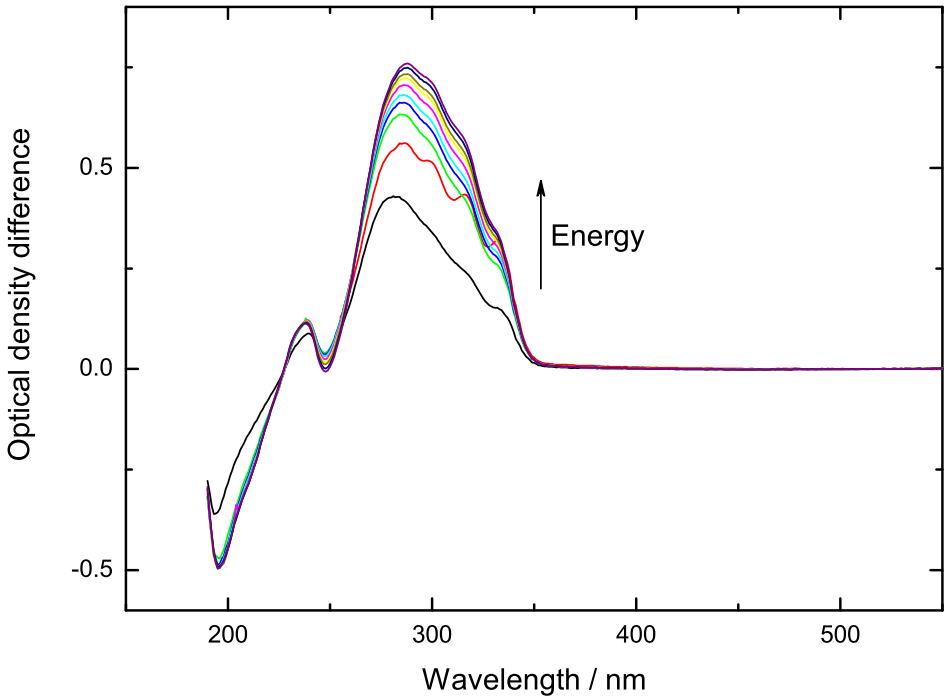

Figure 3.10: Energy-dependent UV difference spectra during the course of dimerization of the stilbene moieties in a PMAOS film. The smudged isosbestic point is indicative for the occurrence of side reactions.

3.1.5 Evaluation of the Examined Polymer Attached Linker Systems

Taking all the results mentioned above into account, we have to decide which material shall primarily be used for the further development towards an IOL prototype. Considering the outcome of the diMAOC experiment it seems quite favorable to use a polymer with the crosslinker in its undimerized monomeric form as a starting material. This linker will not be dimerized to induce the refractive index change in the IOL until the IOL is implanted. At this point the hardening of the material due to the high degree of cross linked sites is not an issue anymore. The three polymers PMAOC, PMAOChalc, and PMAOS are compared to decide which of the polymers is the most promising one for further research. One of the most important properties is of course the change in refractive index. Considering this property, PMAOChalc is the best with a Δn value of 0.0331 followed by PMAOC with 0.0218. For making lenses, especially IOLs, a high initial refractive index of the material is always favorable because the lens

will get thinner and lighter for a given refractive power. Looking at the initial refractive index, PMAOChalc and PMAOC have quite similar values. PMAOS is less favorable both because of its lower initial refractive index and, in particular, its lower maximum change in refractive index. Very important also, is the amount of light energy needed to induce a certain change in the refractive properties. Because several structures of the eye, especially the retina, may be damaged by electromagnetic radiation, the amount of light energy needed to induce the refractive index change should be as low as possible. The optical density change, which indicates the degree of dimerization, was plotted as a function of the photon energy dose for all three polymers. Characteristic differences were observed (Fig. 3.11). The films used for this comparison had equal thickness and comparable molecular weight distributions. Therefore, the obtained curves can be compared directly. The exponential decay is steepest for PMAOC meaning that most of the overall refractive index change can be induced with fewer photons compared to PMAOChalc and PMAOS.

Table 3.1: Important material properties of the three synthesized polymers. PMAOC was chosen as the most suitable polymer for further research and development.

Polymer	$\mathbf{T_g}$/°C	$\mathbf{T_{5\%}}$/°C	**n**	**Δn**	**ΔD** ‡
PMAOC	119	307	1.6226	0.0218	1.7
PMAOChalc	168	257	1.6252	0.0331	2.6
PMAOS	132	263	1.5958	0.0178	1.6

The T_g and $T_{5\%}$ are first means to decide how easy the polymer can be processed. Here PMAOC is in favor because of its lower T_g value and larger difference between T_g and $T_{5\%}$ compared to PMAOChalc. Despite the fact that the refractive index change measured for PMAOChalc is about 35% higher than that of PMAOC, PMAOC is considered to be the most promising material for further research and development taking all properties into account. The refractive index change of PMAOC is still high enough to achieve a focal length change of more than 1.5 D ‡ in a standard IOL (Tab. 3.1). Further investigation will therefore focus on polymers with coumarin side groups.

‡The change in diopters for a given refractive index change is dependent on the initial diopter value of the lens. Typical IOL data were used and the focal length was calculated with paraxial formulas for lenses in arbitrary media to account for the effect when the lens is in contact with the aqueous humor and the vitreous body. The initial focal length of the treated IOL was 23 D and the change in diopters was calculated assuming that only the refractive index of the IOL changed. This calculation method is used for calculating all ΔD values throughout the work.

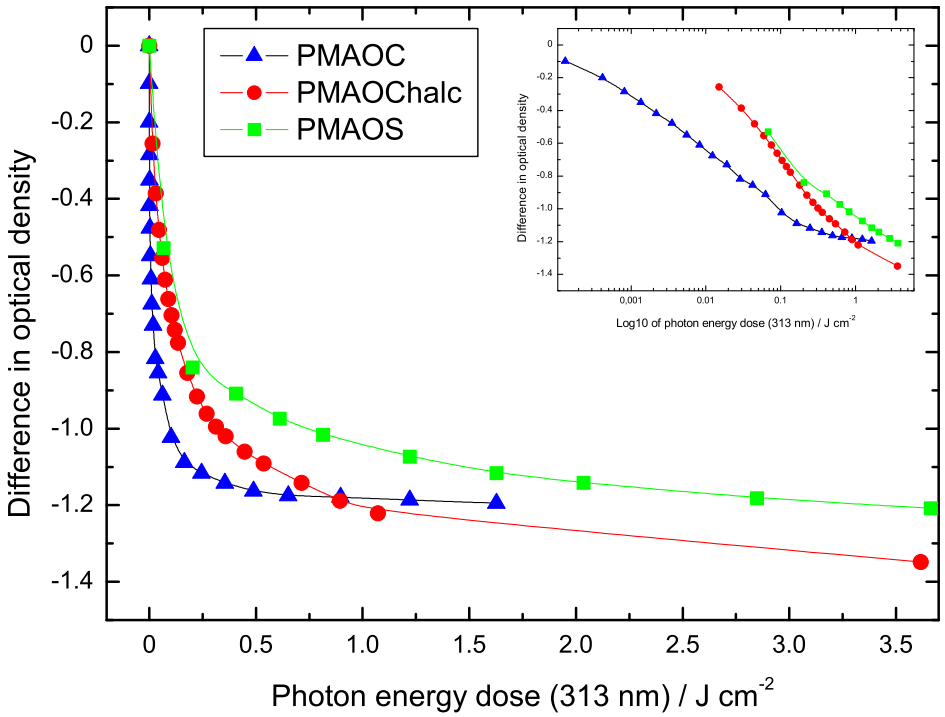

Figure 3.11: Change in optical density of PMAOC, PMAOChalc, and PMAOS at the respective band maximum characteristic for the double bond as a function of the UV light energy at 313 nm. The films measured were of similar thickness allowing a comparison of the energies needed to induce a certain change in the different polymers (insert: same set of data shown on a logarithmic energy scale).

3.2 Developing Photoactive Polymers for IOL Manufacturing

Having chosen PMAOC as the most ideal polymer to proceed with the development of a refractive power tunable IOL the processability needed to be studied. The optics of a typical IOL have a diameter of about 7 mm and a maximum thickness between 0.7 mm and 2 mm. This means that disk shaped cylindrical pieces of the polymer with at least the given dimension have to be made. This intermediate polymer piece will then be used to mill and turn the IOL. The finished IOL must be of very good optical quality, requiring the polymer precursor disk or plate to be of excellent quality, too. The polymer pieces need to be of uniform constitution not containing any sort of streak, cracks, bubbles, or inclusions like dust or lint. Hence, a polymer that shows the required refractive index change capability in form of a thin film is an important step. Further, there

are also important requirements in terms of polymer processing to manufacture an IOL of satisfying quality. This section deals with the development of a bulk polymeric material in disc or plate like shape of sufficient dimension that can actually be used for IOL manufacturing.

The most obvious attempt was to try to make such polymer pieces out of PMAOC by compression molding. For compression molding a conventional hydraulic heating press was used. As press molds either a PTFE mask or an evacuable stainless steel pressing mold with a diameter of 13 mm were used. A great number of molding experiments at varying temperatures up to 160 °C and pressures of 200 bar were conducted. Unfortunately, compression molding did not lead to the desired outcome of a transparent and homogeneous workpiece (Fig. 3.12). At lower temperatures the polymer powder only sinters without forming a transparent uniform piece. Elevating the temperature leads to the onset of thermal degradation. As can be seen by the color of the polymer turning more and more towards brown. Using the evacuable stainless steel mold the polymer discs got slightly better but are still suboptimal. It seems that even at high pressures the polymer cannot be heated to temperatures high enough, to get a low enough melt viscosity that allows the formation of a uniform transparent piece. Furthermore, it was investigated whether rapid cooling of the hot mold with dry ice or slow cooling by just turning off the heat produced better results. The rapid cooling produced slightly better polymer pieces. In addition to the already described melt processing problems, all pieces of PMAOC were so brittle that the formation of further cracks when removing from the mold were practically unavoidable.

Figure 3.12: PMAOC disc produced by compression molding in an evacuated mold. The material is very inhomogeneous, opaque, and brittle.

In summary it can be said, that PMAOC rather degrades thermally, even if high pressures are applied, before the desired raw materials can be prepared. In view of the inap-

propriate results of the polymer compression molding tests, solutions had to be found to overcome the processability problems. Especially a modification of the polymer that leads to a significantly lower glass transition temperature seems to be an appropriate way to overcome the material's drawbacks. Novel materials have to be developed that show both lower glass transition temperatures as well as equal or increased refractive index changes compared to PMAOC. Two routes have been explored to reach the desired properties. First, the copolymerization of MAOC and BMA in various ratios, and second, the introduction of an alkyl spacer between the polymer backbone and coumarin side group.

3.2.1 Copolymers

Since the goal is to lower the glass transistion temperature of the optically active polymer, *n*BMA was chosen as a comonomer because its homopolymer has a glass transition temperature of about 20 °C.[429] Copolymers of MAOC and *n*BMA were synthesized with an *n*BMA content of 5 to 50% in 5% increments. The actual composition of the copolymer was checked by ^{1}H-NMR. The $\bar{M}_n$ values ranged from 123300 to 286600 g mol^{-1} and the $\bar{M}_w$ values were between 278100 and 433200 g mol^{-1}. The respective PDI values for each polymer were between 1.6 and 2.3.

When analyzing the data of the MAOC/*n*BMA copolymers, surprisingly it was found that copoylmers with an *n*BMA content of 5 to 20% show an even higher T_g than pure PMAOC. 50% of *n*BMA content in the copolymer is required to achieve about the same glass transition temperature as pure PMAOC (Tab. 3.2). The temperatures for 5% weight loss ($T_{5\%}$) obtained by TGA measurements are all significantly higher than the T_g values. This indicates that the polymers are suitable for melt processing. The refractive index of the copolymers decreases constantly with increasing *n*BMA content up to about 0.05 at 50% *n*BMA. The maximum change in refractive index is achieved for 10 and 20% *n*BMA contents. The respective values are a few percent higher than for unmodified PMAOC, but then drop off by about 30% for 50% *n*BMA content in the copolymer. For low *n*BMA contents in the copolymer, a slightly higher Δn is observed compared to PMAOC. The reason could be that the *n*-butyl side groups provide for greater free volume allowing more coumarin molecules to properly arrange themselves towards each other and dimerize.

Table 3.2: Material properties of MAOC/*n*BMA copoylmers

Copolymer		$\mathbf{T_g}$/°C	$\mathbf{T_{5\%}}$/°C	**n**	**Δn**	**ΔD**	**Appearance**
PMAOC		119	307	1.6226	0.0218	1.7	Opaque
P(MAOC/*n*BMA)	95:5	153	310	1.6210	0.0179	1.4	Opaque
P(MAOC/*n*BMA)	90:10	141	261	1.6152	0.0233	1.8	Opaque
P(MAOC/*n*BMA)	80:20	145	308	1.6045	0.0222	1.7	Opaque
⋮	⋮	⋮	⋮	⋮	⋮	⋮	⋮
P(MAOC/*n*BMA)	50:50	120	291	1.5714	0.0134	1.1	Opaque
⋮	⋮	⋮	⋮	⋮	⋮	⋮	⋮
P(MAOC/*n*BMA)	40:60	98	276	1.5611	0.0093	0.7	Opaque

In summary, it can be said that the desired improvements of the material properties compared to the PMAOC reference cannot be achieved by making copolymers with *n*BMA. The desired decrease of the glass transition could not be achieved. The maximum change in refractive index (Δn) that can be achieved is significantly lowered for higer *n*BMA contents in the copolymer. The copolymer with an *n*BMA content of 60% shows a refractive index or diopter change, respectively, that is too low to achieve the required change in an IOL. Therefore, it does not make sense to go on to even higher BMA contents. Even worse is that the opacity problem was not solved with the copolymer approach.

Despite the disappointing results from the MOAC/*n*BMA copolymer a few copoylmers with up to 20% *t*BMA content were synthesized to determine whether the branched *tert.*-butyl side chain has an advantage over the linear chain in the *n*-butyl methacrylate. However, the outcome in terms of glass transition temperatures and opacity was even worse than for the *n*BMA copoylmers. Therefore, the copoylmer approach was not pursued any further.

3.2.2 Polymers with Alkyl Spacers

3.2.2.1 Monomers with Spacer Attached Coumarin

To synthesize the monomers with coumarin attached to the methacrylic acid via a linear alkyl chain spacer a two step procedure is required. As a fist step an etherification

of 7-hydroxycoumarin with the corresponding linear ω-bromoalkanol was conducted. The residual free OH-group at the end of the alkyl spacer was then esterified with methacryloyl chloride to give the desired monomer. The finished product was purified by either recrystallizing for spacer lengths of up to seven carbon atoms. Monomers with longer alkyl chains of eight and more carbon atoms were purified by column chromatography. Recrystallization was not feasible due to their relatively low melting points. Careful purification of the monomer is crucial to remove any impurities or side products. They would negatively affect the outcome of the subsequent polymerization. Altogether various monomers with linear alkyl spacers having a length from three to twelve carbon atoms were synthesized.

The identity of the new substances at the monomeric stage was verified spectroscopically and the purity was checked by HPLC. The melting points were determined by DSC. The melting points of the monomers monotonically decrease with greater length of the spacer (Fig. 3.13). From a spacer length of eight carbon atoms onward the melting point drops below 50 °C. These relatively low melting points are a very important property of the monomers because they allow to form a melt at convenient temperatures. The comparatively low temperatures help to avoid oxidative degeneration that would occur at higher temperatures. This makes a bulk polymerization of a monomer melt with commercially availabe thermal radical initiators feasible. A bulk polymerization would be impossible with MAOC or its alkyl spacer derivatives with low spacer lengths because the melting points are far too high. This would render it impossible to get a melt of low viscosity at temperatures that are compatible with the temperature needed for common radical initiators. Free radical poylmerizations are normally conducted at temperatures ranging from below room temperature to about 90 °C. However, some high temperature initiators that can be used at tempertures up to about 150 °C are availabe.[429] Furthermore, the thermal stability of the monomers with C8 and longer alkyl chains was evaluated by TGA. The onset of the thermally induced weight loss takes place between 240 and 260 °C. Thermal degradation of the monomers does not constitute a problem for the bulk polymerization of the monomer melt.

3.2.2.2 Material Properties of the Spacer Polymers

First of all, the monomers with coumarins attached via a linear alkyl spacer were polymerized in solution with AIBN as a radical initiator. The polymers were, after being re-

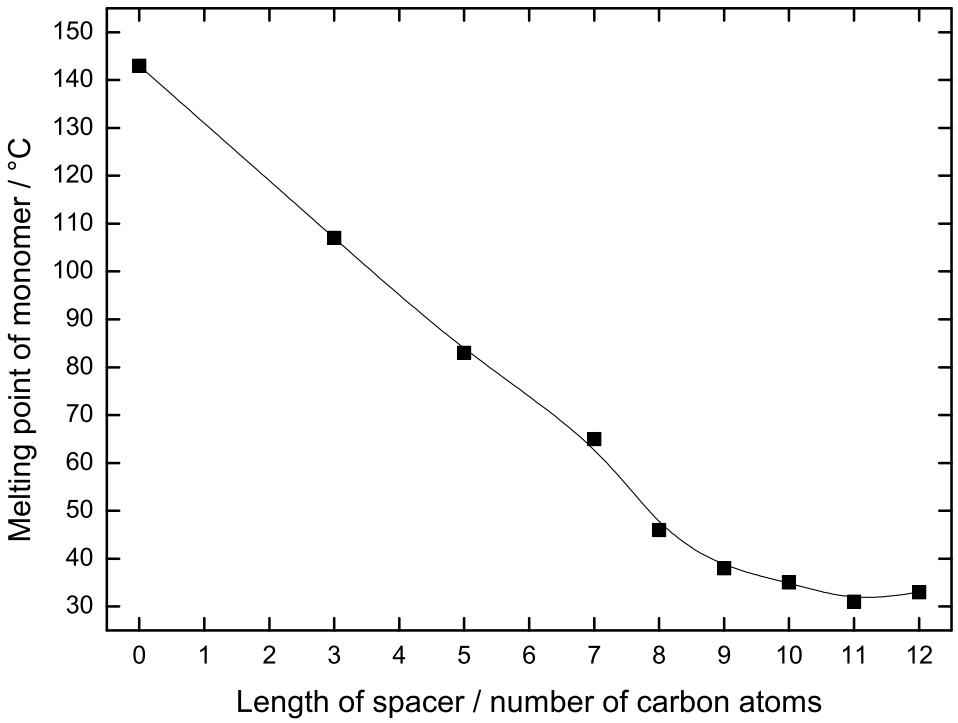

Figure 3.13: Melting points of the monomers with spacer attached coumarin as a function of the spacer length. The melting points were determined by DSC at a heating rate of 1 K min^{-1}.

precipitated twice in methanol, scrutinized in the same way as it was done for PMAOC. The $\bar{M}_n$ values ranged from 90130 to 131200 g mol^{-1} and the $\bar{M}_w$ values were between 138500 and 231300 g mol^{-1}. The respective PDI values for each polymer were between 1.5 and 1.8.

Films were also prepared on quartz plates and silicon wafers to investigate the optical density and refractive index changes under UV irradiation, respectively. However, in contrast to the former experiments, a pulsed, frequency-trippled Nd:YAG laser operating at 355 nm was used to irradiate the films. The laser's wavelength of 355 nm is shifted to the right of the coumarin absorption band. There the absorbance is lower compared to the 313 nm wavelength of the UV lamp which is quite close to the center of the absorption band. The adverse effect due to the less favorable wavelength of 355 nm is, however, overcompensated due to the high photon flux of the laser by several orders of magnitude. Therefore, the laser offers a much quicker way to induce dimerization in the polymer films. The UV/Vis spectroscopic monitoring of the dimerization reaction

was done the same way as it had been for PMAOC. From the spectra it can be seen that the dimerization reaction proceeds in the same way as it has been observed when using the UV lamp. The spectra obtained from a PMAOC-C5 film are shown here as a typical example (Fig. 3.14). The noticeable difference between the polymers with spacer and the spacerless PMAOC is that the absorption maximum of the band associated with the dimerizable double bond is shifted by about 10 nm towards longer wavelengths. It is now located around 320 nm. Isosbestic points are also present in the spectra, which may more easily be seen from the difference spectra. These findings indicate that there is a photochemical reaction with one product only for the spacer polymers as it has been found for plain PMAOC (Fig. 3.15). All the polymers reported here have virtually no absorption between 400 and 800 nm making them potentially suitable for IOL manufacturing.

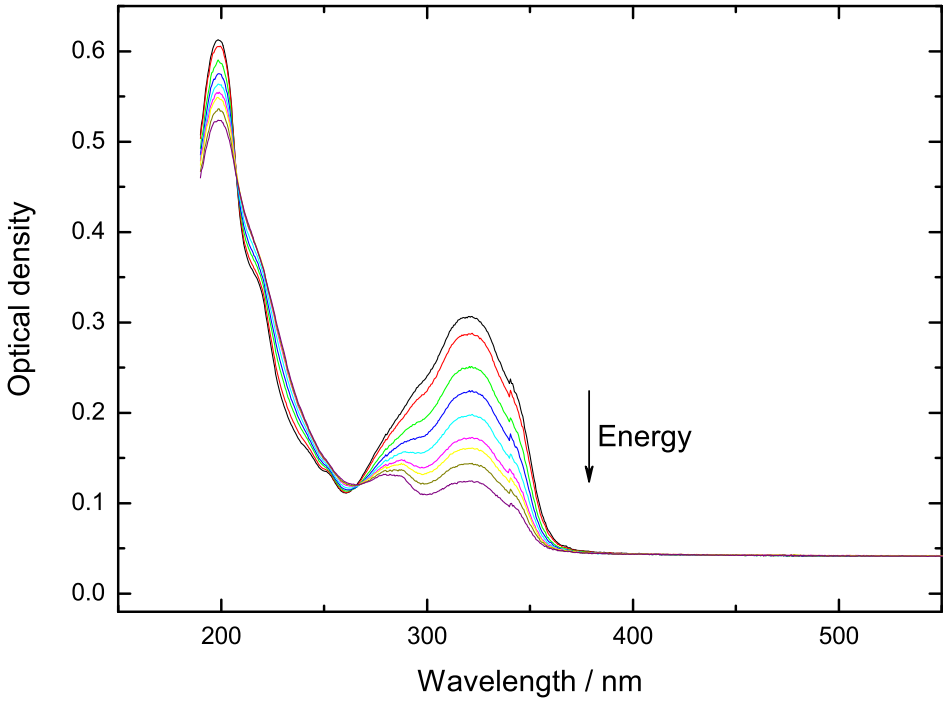

Figure 3.14: Photochemical $[2\pi + 2\pi]$ dimerization of polymer-bound coumarin moieties in a PMAOC-C5 film with 355 nm UV light. The dimerization reaction leads to a decrease in optical density at $\lambda_{max} = 322$ nm.

Naturally, the refractive index change of the polymers with spacer was also examined. The refractive index change is well correlated to the change in optical density of the

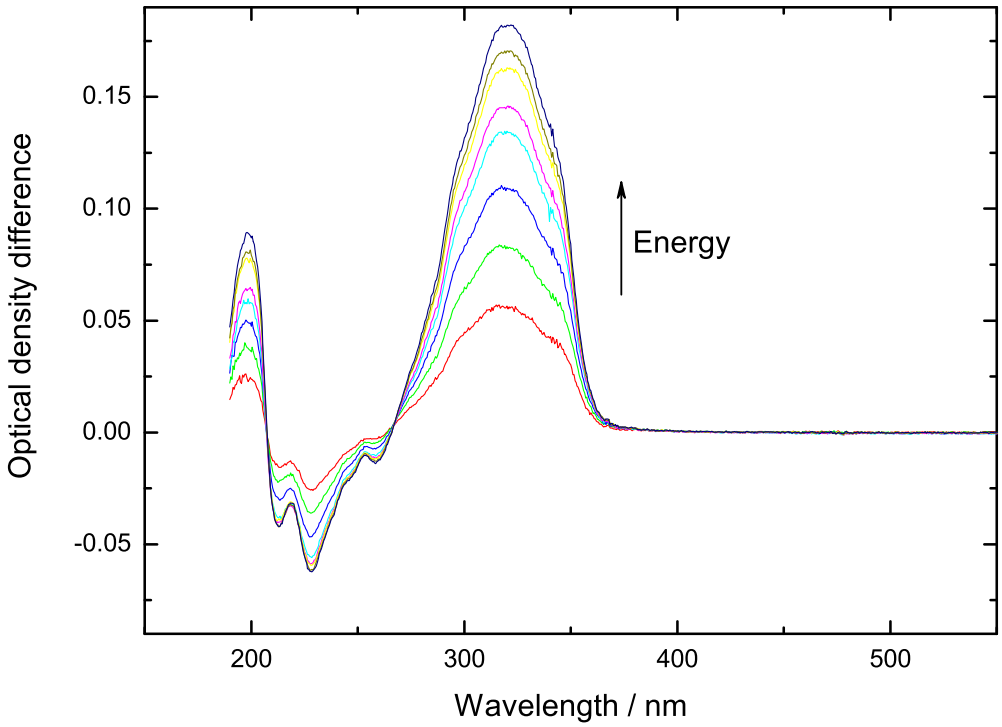

Figure 3.15: Energy-dependent UV difference spectra during the course of dimerization of the coumarin moieties in a PMAOC-C5 film.

film. In an analogous manner as for the PMAOC films it has to be concluded that the refractive index change is caused by the vanishing of the double bond in the coumarin's lactone ring during the photochemical dimerization. Both refractive index and optical density show a practically exponential decay, which is shown here for PMAOC-C5 and PMAOC-C8 films as representative examples (Fig. 3.16, 3.17). It is unlikely that a refractive index change results from photoreactions on the methacrylic backbone rather than from the coumarin itself. It was experimentally proven that the backbone remains unaffected under the experimental conditions used here. A 3 µm thick PMMA film was irradiated in the same fashion with a ten times higher photon energy dose than any of the coumarin containing polymer films were subjected to. No change in refractive index of that PMMA film was observed within the error margins of the equipment used for measurement. At worst the refractive index uncertainty is 0.0015 which is only about 4% of the total refractive index change measured. Therefore, it can be definitly concluded that the refractive index change is attributed to the dimerization reaction of the two coumarins.

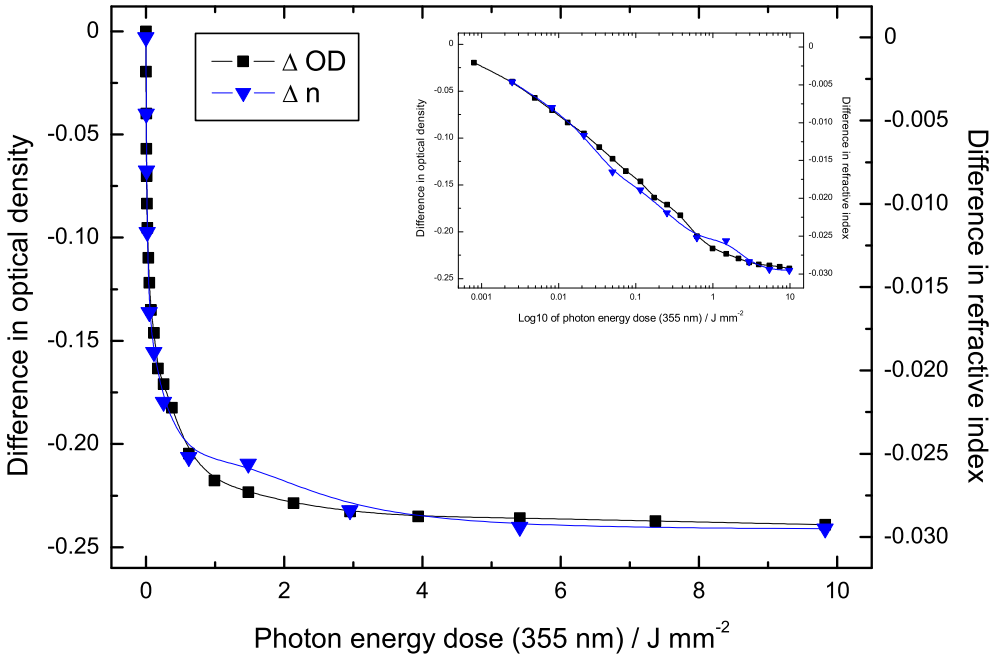

Figure 3.16: Change in refractive index and optical density at 322 nm of a PMAOC-C5 film prepared on a silicon wafer as a function of the applied light energy at 355 nm (insert: same set of data shown on a logarithmic energy scale).

Employing a spacer between the polymer backbone and the coumarin moieties leads to two main advantages. First, the glass transition temperature is significantly lowered with increasing length of the aliphatic spacer (Tab. 3.3, Fig. 3.19). This can be explained by the higher internal flexibility of the polymer chains compared to the very rigid PMAOC, increasing inter chain moveability in the polymer. The relatively low T_g values for polymers with spacer lengths of seven and more carbon atoms which are below 45 °C not only make compression molding much easier but allow for the manufacturing of transparent workpieces for the first time. The $T_{5\%}$ values are also slightly higher compared to pure PMAOC and the MAOC/BMA copolymers. A compression molding test with PMAOC-C7 prodcued good results in terms of melting the polymer and transparency of the finished workpiece. However, the material is still somewhat brittle at room temperature which can be seen from the unavoidable cracks that formed in the disc when removed from the mold (Fig. 3.18).

The most important advantage is that the change in refractive index of the polymers with spacer always exceeds the value of PMAOC (Tab. 3.3, Fig. 3.20). When plotting the

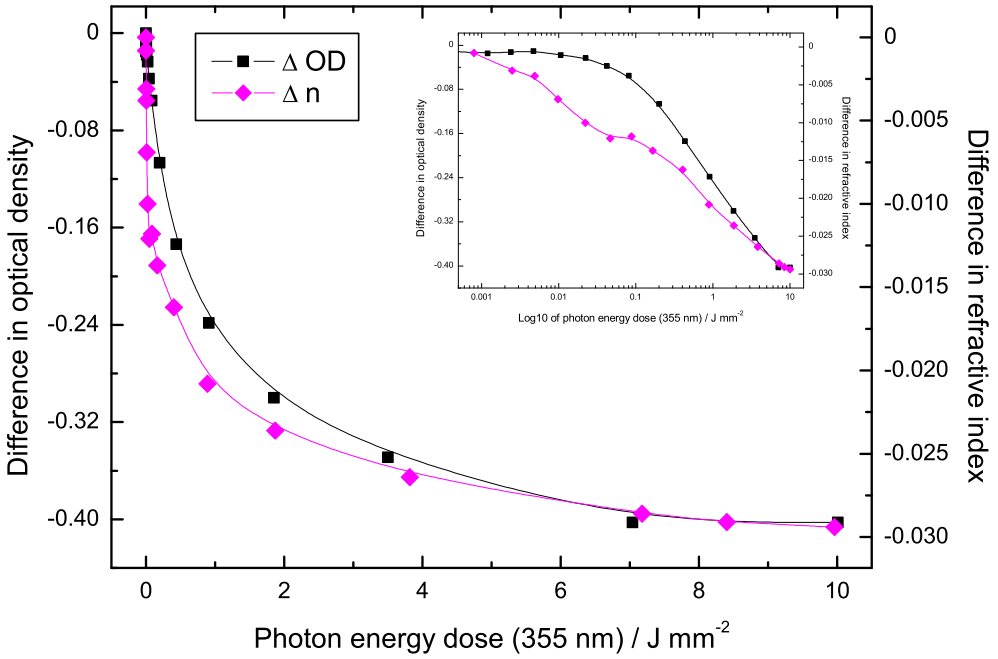

Figure 3.17: Change in refractive index and optical density at 320 nm of a PMAOC-C8 film prepared on a silicon wafer as a function of the applied light energy at 355 nm (insert: same set of data shown on a logarithmic energy scale).

maximum refractive index change as a function of the spacer length, it can be seen that the refractive index change at first increases with increasing spacer length. It reaches a maximum for a spacer length of seven carbon atoms and then decreases for longer spacers. However, the Δn value for the polymer with the longest spacer length that was investigated, i.e. PMAOC-C12, is still greater than that of plain PMAOC. The trend governing the maximum refractive index change values may be explained as follows. In PMAOC the coumarin molecules are attached without any spacer to the main chain. The relatively large coumarin groups tend to adopt a staggered configuration. This leaves very little flexibilty for the main chain resulting in a great persistence length. The result is a stiff backbone and the polymer becomes quite hard, brittle, and shows a high T_g. The coumarins are relatively limited in their movability. Therefore, only a fraction of them can dimerize for steric reasons, i.e. two polymer bound coumarin molecules must have an appropriate distance and angle relative to each other. From spectroscopic measurements it can be concluded that in PMAOC only approximately 50% of the coumarin moieties are dimerized when the refractive index change saturates towards its final value. By employing the alkyl spacer, the polymer becomes more flexible and the

Figure 3.18: Disc of PMAOC-C7 produced by compression molding in an evacuated mold. The disc has a diameter of 13 mm and a thickness of about 5 mm. The material is transparent though brittle.

T_g is lowered because the coumarins are at a certain distance from the backbone. Also, the coumarin molecules at the end of the alkyl spacer can rotate and move to a certain extend which is, though limited, more pronounced than in the case of PMAOC. For statistic reasons it is not possible to dimerize all sidegroups of the polymer.[430] However, the increased flexibility increases the probability that two coumarins can approach each other with the right orientation for the dimerization reaction. In the spacer containing polymers most of the coumarin moieties can be dimerized. Past a maximum peak value for PMAOC-C7 the Δn values begin to decrease for longer spacers. This is because the spacer itself occupies a certain volume within the polymer network. Therefore, the presence of the spacer reduces the number of coumarin molecules per unit volume. Since the dimerization of the coumarin molecules is responsible for the refractive index change, fewer coumarins per unit volume mean less refractive index change.

In summary, we observe here two competing effects: first, the increase of the number of molecules that will dimerize due to the increased internal flexibility of the polymer; second, an internal depletion of the dimerizable coumarin molecules caused by the presence of the spacer. The concurrence of these two effects is responsible for the observed refractive index change curve that increases, goes through a maximum value, and decreases as a function of increasing spacer length.

A high initial refractive index of the materials for IOL manufacturing is, beside good thermal processing properties, advantageous. The higher the refractive index, the thinner a lens needs to be for a given focal length. In this respect PMAOC is still the best material among those investigated here. The refractive indices of the novel polymers with alkyl spacer attached coumarin presented here are in the range of 1.56 to 1.60.

These values are remarkably higher than the refractive indices of most acrylates used in IOL manufacturing (Tab. 3.3, Fig. 3.20). For instance, the refractive index for poly(methyl methacrylate) is 1.49, and for poly(2-hydroxyethyl methacrylate) it is 1.51. However, there are acrylates with very high refractive indices up to about 1.71 like poly(pentabromophenyl methacrylate), but they are not used in commercially availabe IOLs anyway.[429]

Table 3.3: Material properties of PMAOC derived polymers with alkyl spacers.

Polymer	T_g/°C	$T_{5\%}$/°C	n	Δn	ΔD	Appearance
PMAOC	119	307	1.6226	0.0218	1.7	Opaque
PMAOC-C3	76	342	1.6006	0.0297	2.4	Slightly opaque
PMAOC-C5	52	343	1.5919	0.0295	2.3	Transparent
PMAOC-C7	45	317	1.5723	0.0331	2.6	Transparent
PMAOC-C8	30	339	1.5836	0.0294	2.4	Transparent
PMAOC-C9	13	356	1.5749	0.0297	2.4	Transparent
PMAOC-C10	20	322	1.5656	0.0289	2.3	Transparent
PMAOC-C11	14	325	1.5650	0.0264	2.1	Transparent
PMAOC-C12	19	343	1.5599	0.0236	1.9	Transparent

The approach to overcome the drawbacks of PMAOC by the introduction of alkyl spacers into the polymer is clearly the method of choice. One shortcomming is present so far. During IOL test manufacturing of discs produced out of the alkyl spacer polymers, it became evident that these materials show too much compression set to be easily introduced to a commercial IOL manufacturing process. This means, that the polymer workpieces show a plastic rather than the desired elastic behavior at elevated temperatures and mechanical stress present during the manufacturing process. To overcome this problem, a crosslinker needs to be introduced to prevent the plastic deformation and to obtain a material with elastomeric properties. Cross linked polymers were synthesized and examined (Fig. 3.19, 3.20).

3.2.2.3 Chamber Polymerization of Polymer Plates

To provide a polymer with ideal material properties for IOL manufacturing a crosslinker is needed. A crosslinked polymer, however, is insoluble because of the chaines that are linked together at numerous points. In other words, the whole workpiece is basical-

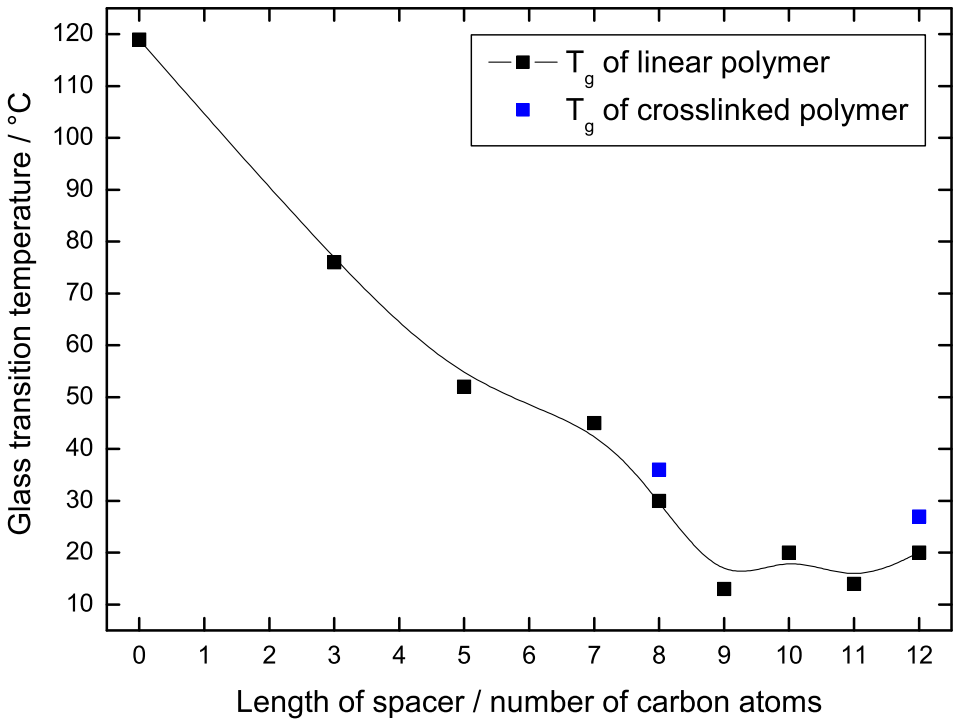

Figure 3.19: Glass transition temperatures of the polymers with alkyl spacer attached coumarin as a function of the spacer length. Values for cross linked polymers are also shown for comparison.

ly one molecule. Therefore, bulk poylmerization is the method of choice. The monomers are polymerized without any solvent and in a mould of the form of the desired plate. This process is called chamber polymerization and is widely used to make polymer plates for IOL manufacturing. It is of great advantage that the novel monomers developed in this work are compatible with the chamber polymerization process allowing the use of equipment already available from the chamber polymerization of other acrylates. The monomer is melted at 50 °C and degassed in vacuum while stirring. Then the desired amount of crosslinker and initiator is added. When the initiator granules are dissolved the melt is filtered through a 0.45 µm pore size PTFE filter membrane and rapidly transferred into the polymerization chamber. The filtering step is crucial for a contamination free material suitable for optical applications. The polymerization chamber consists of two glass or PTFE plates arranged in parallel and sealed with a flexible silicone gasket to form the volume in which the polymerization takes place. The whole chamber is held together by retaining clips and put in a holder to keep it vertical. After

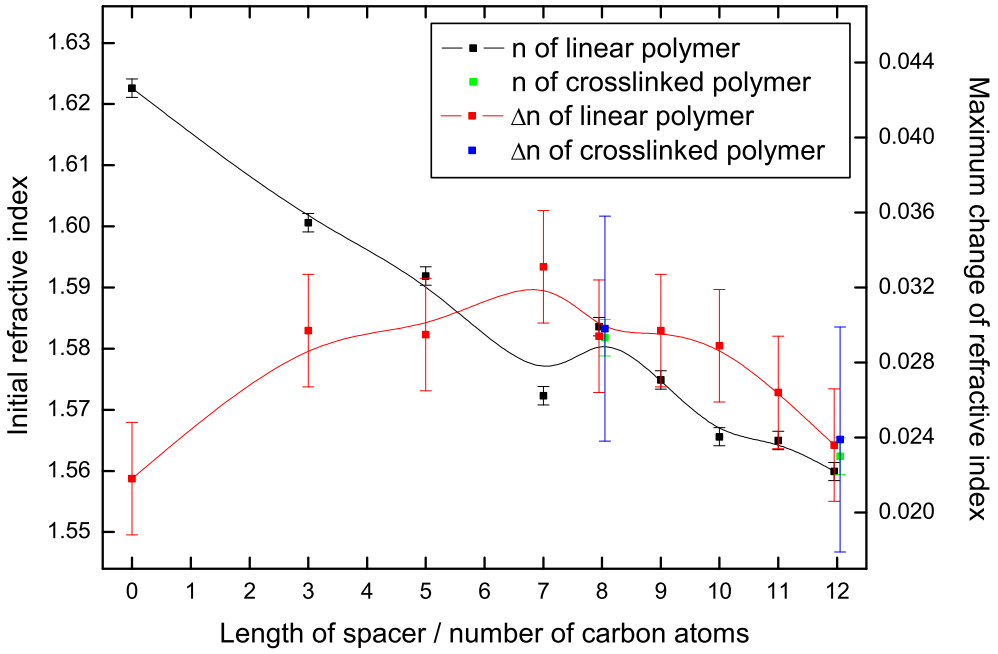

Figure 3.20: Refractive inidices and their maximum inducable change for the polymers with alkyl spacer attached coumarin. The values are plotted against the spacer length. Values for cross linked polymers are also shown for comparison.

a heat treatment of 50 °C for three days and of 80 °C for another three days the plate can be removed from the chamber. The plate is then extracted with methanol for three days to remove residual monomers. The plates obtained are homogenious and show a good transparency (Fig. 3.21).

PMAOC-C8 was chosen as an example for a rather rigid material having a T_g that is above room temperature. As a further model substance PMAOC-C12 represents a flexible and foldable material because its T_g is below room temperature. The corresponding monomers were mixed with 5% (w/w) ethylene glycol dimethacrylate (EGDMA) which is a bifunctional methacrylic monomer and acts as a crosslinker. Evaluation of the material properties reveals, that the glass transition temperature is increased by 6 °C compared to the corresponding polymer without crosslinker (Fig. 3.19). The initial refractive index and the change in refractive index are practically unaffected by the 5% crosslinker content (Fig. 3.20). Thus, it has been demonstrated that additives up to a content of 5% are well tolerated by the system and leave the optical properties unaffected while greatly improving the rheologic properties of the material. The improvement

Figure 3.21: Plate of PMAOC-C8 produced by chamber polymerization. The plate is about $7 \times 7\,cm^2$ in dimension and has a thickness of about 2 mm. The material is very homogenious and clear, making it suitable for IOL manufacturing.

caused by the crosslinker becomes obvious when looking at the stress-strain curves of the same polymer with and without crosslinker (Fig. 3.22). The polymer without crosslinker shows a viscoelastic behaviour. Viscoelasticity is the property of materials that exhibit both viscous and elastic characteristics when undergoing deformation. A high strain is observed with relatively low stress applied but the material does not relax to its initial shape once the stress is released. This material behaviour is very unfavorable for IOLs. The IOL must relax to its original shape in the eye after mechanical stress applied during the surgical insertion is released. The stress-strain curve for the same polymer containing a crosslinker shows a strongly linear progression. This means that the material shows an elastic response only under the same conditions as the polymer without crosslinker showed some plastic deformation. In comparison, a sample of the crosslinked polymer was completly dimerized by UV irradiation and a stress-strain measurement was conducted under the same conditions. The increased slope of the stress strain curve compared to the same material before UV irradition shows that the polymer becomes much harder due to the greatly increased number of crosslinks after dimerizing the coumarin moieties. This result is no surprise but an obvious consequence of the photoinduced dimerization. In addition to the considerations made in the preceeding paragraphs this is another reason why the IOL should contain the cou-

marin in undimerized form at the time of implantation. The refractive index change is then induced after implanting the IOL by dimerization of the polymer's coumarin side groups. The hardening of the material caused by the dimerization reaction will not pose a problem once the lens is inside the eye. A material containing a great number of polymer bound coumarin dimers to be cleaved later for tuning of the refractive power would have very poor mechanical properties at the time of surgery.

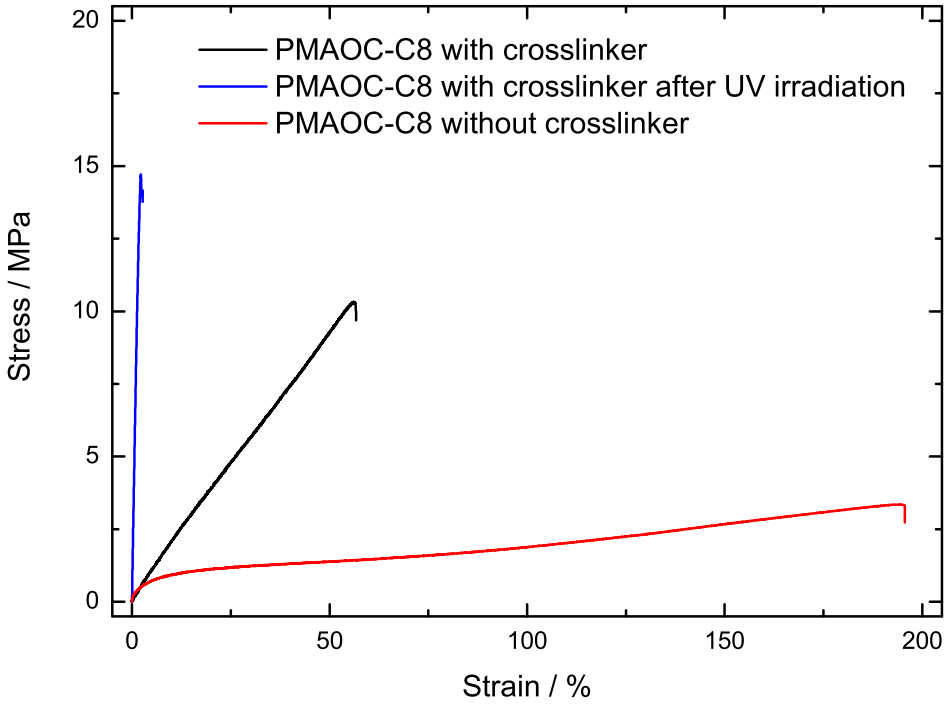

Figure 3.22: Stress strain curves from PMAOC-C8 samples with and without 5% EGDMA as a crosslinker. All samples were linearly extended at a speed of 10 mm min^{-1}.

State of the art IOLs are foldable and can therefore be implanted through smaller incisions as would be necessary for a rigid lens. Crosslinked PMAOC-C12 is a material that offers a refractive index change plus foldability. The polymer shows elastomeric properties and readily relaxes completely to its initial shape once the folding stress is released (Fig. 3.23).

When conducting a bulk polymerization, there will always be more or less residual monomers present at the end because a polymerization reaction does not proceed to

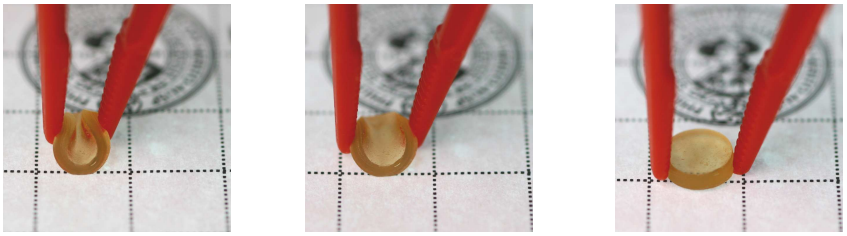

Figure 3.23: Subsequently taken images of polymer disc made of crosslinked PMAOC-C12 to demonstrate its foldability and elastic properties. The disc has a diameter of 8 mm and a thickness of about 2 mm.

the point where exactly 100% of the monomer is converted. Residual monomers in the polymer plate are a problem for two reasons. First, any low molecular mass substance present in the polymer network, in this case the residual monomer acts as a plasticizer. The rheological properties of the material will thus be different if compared to the same material without any residual monomers. Second, for medical applications like an IOL, a residual content of low molecular mass substances is potentially harmful because it will be released from the implated IOL by diffusion. The residual monomer content of the crosslinked polymer plates made by chamber polymerization was determined here. To accurately determine the residual monomer content small pieces of a PMAOC-C8 plate with a total mass of about 2 g were extracted in a *Soxhlet* extractor for 24 h. The methanol used was then replaced with fresh methanol and extraction was continued for another 24 h. The concentration of monomers in each of the methanol portions used for extraction was determined by HPLC. A highly pure sample of the monomer MAOC-C8 dissolved in ACN was used as a standard for the determination of the remaining amount of monomer within the PMAOC-C8 pieces via HPLC. A cumulative residual monomer content of 0.9% based on the initial mass of the PMAOC-C8 pieces before extraction was found. A third extraction with methanol was conducted. Further monomer extraction was not detected ensuring that the previous extractions led to a complete removal of the residual monomer. The residual monomer content found is comparatively low. Furthermore, it was shown that the residual monomer can be easily removed by extraction with methanol to yield a monomer free material for IOL manufacturing after drying the extracted plate in vacuum.

3.2.2.4 Thickness and Density Changes in the Spacer Polymers

The photoinduced changes of the refractive indices and other properties of the polymers have already been characterized. However, one physical property that might change as a result of the photoinduced dimerization reaction has not been considered yet. One might expect that the density of the polymer could also change as a result of the coumarin dimerization. Further, it can be expected that the density of the dimerized form would be greater than that for the undimerized polymer because one coumarin dimer might occupy less volume than two monomeric coumarin molecules.

In the first instance, film thickness measurements by profilometry as well as by the prism coupler technique have been performed. Upon intermolecular crosslinking of polymer chains an increase in density and a shrinkage of the volume could be considered as a change in film thickness. However, this has not been observed. For all polymers with alkyl spacer attached coumarin, large data sets of film thickness as a function of the UV light irradiation energy were obtained. The films thickness varies only because the films are not homogeneous in thickness and the location of the measurement cannot be exactly reproduced after each irradiation step. Statistical analysis of the data shows no evident trend of film thickness decrease or increase as a function of the photon energy dose. No significant dependence of the film thickness has been observed (Fig. 3.24). It should be mentioned that because of experimental reasons, the films investigated were only a few microns thick.

Despite the fact that both profilometry and the prism coupler technique can measure the film thickness with an accuracy of 0.5% of the obtained values one might argue that the films examined were too thin to see the effect of a density change. Hence, density measurements using a *Mohr-Westphal* density balance were conducted using undimerized and completely dimerized bulk material of crosslinked PMAOC-C8. The pieces of polymer used were of greater dimensions than an IOL and had a total mass of more than 5 g to keep the uncertainty of the measurement as low as possible. The final results were obtained as the mean value of six different measurements. The density of both unirradiated and irradiated polymer was determined to be $1.183 \pm 0.003\,\mathrm{g\,cm^{-3}}$. Thus, the density measurements of PMAOC-C8 also showed no change in density within error margins as a result of the photochemical dimerization reaction. This provides further evidence, in addition to the film thickness measurements, that no significant density changes result from the crosslinking of the coumarin molecules.

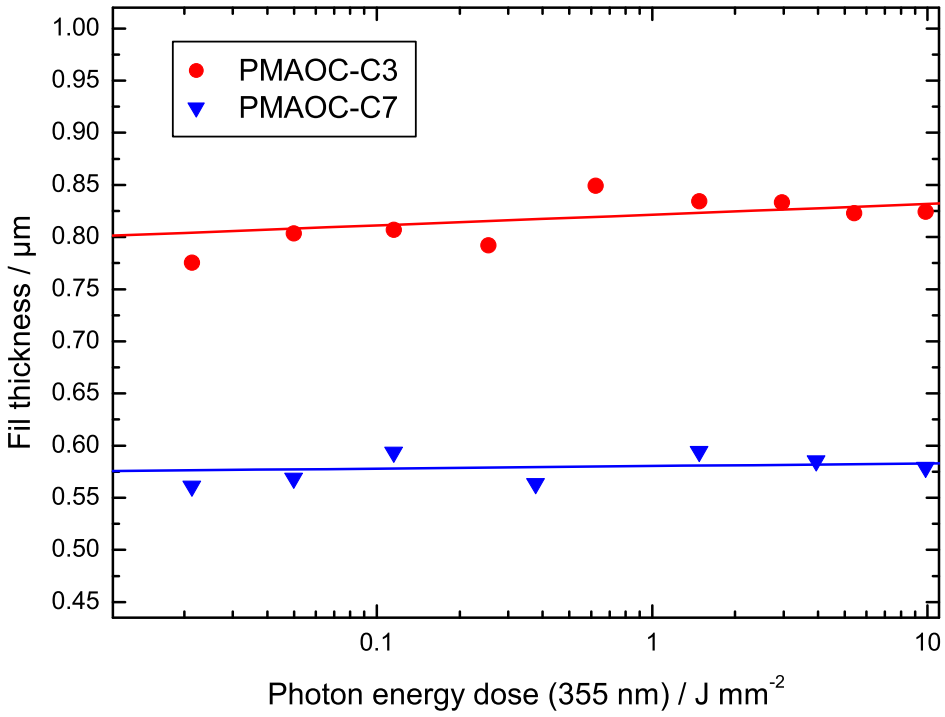

Figure 3.24: Photoinduced thickness changes in films of alkyl spacer polymers. PMAOC-C3 and PMAOC-C7 are shown as typical examples. No significant changes as a result of the coumarin side groups are observed.

3.2.2.5 Molar Refraction Calculations for the Polymers with Alkyl Spacer

Molar refraction is a concept to correlate the refractive index with the chemical structure of electrically insulating materials like polymers. Several different approaches to do so exist (Sec. 1.5.1). Here, the most common models according to *Lorentz–Lorenz*, *Gladstone–Dale*, and *Vogel* are used. For all models the so-called group contributions for different entities comprising a molecule are tabulated in the literature.[267] The group contribution values for the molecule of interest according to the specific model need to be summated. In the case of polymers the values for the monomeric repeat unit as it is found in the polymer have to be used.[267,272] The calculation of the theoretical molar refraction values for PMAOC-C8 according to the three models mentioned has been performed. Because the refractive index before and after dimerization is of interest, the undimerized polymer (Tab. 3.4) as well as the dimerized polymer (Tab. 3.5) were considered. For the completely dimerized polymer the photodimer of two repeat units of the

undimerized form becomes the new repeat unit for which the molar refraction needs to be calculated.

Table 3.4: Calculation of the molar refraction values for undimerized PMAOC-C8 from the group contributions of different models. The calculation is made for four theoretical models: *Lorentz–Lorenz* (R_{LL}), *Gladstone–Dale* (R_{LL}), *Vogel* (R_V) and a modification of the *Lorentz–Lorenz* model ($R_{LL,mod}$)

	Groups	$\mathbf{R_{LL}}$	$\mathbf{R_{GD}}$	$\mathbf{R_V}$	$\mathbf{R_{LL,mod}}$
1	$-CH_3$ (general)	5.644	8.82	17.66	5.644
9	$-CH_2-$ (general)	41.841	70.479	185.76	41.841
1	–COO– (higher esters)	6.206	10.47	64.2	6.206
1	–O– (attached to benzene ring)	1.77	2.84	22.6	2.0
1	o-phenylene	24.72	44.2	129.0	27.934
1	–COO– (attached to benzene ring)	6.71	11.31	64.8	7.582
1	=CH– (general)	3.616	6.8	23.49	4.086
1	=CH– (attached to benzene ring)	3.52	6.34	21.4	3.978
	Constitutional increments				
1	Δ C=C *trans*	1.94	2.09	−6.37	2.192
1	Δ ring structure	−0.13	−0.92	−4.44	−0.147
	Σ	95.84	162.43	518.1	101.32

With the molar refraction calculated as the sum of the group contribution values, one important value for the theoretical calculation of the refractive indices is now available. In addition, the molar volume of the polymer is required for the calculations using the *Lorentz–Lorenz* and the *Gladstone–Dale* model. The molar volume V_m of the polymer is the molecular mass of the repeat unit divided by the experimentally obtained density. For the undimerized form of PMAOC-C8 the molar volume is 302.77 $cm^3\,mol^{-1}$ and for the completely dimerized form it is 605.55 $cm^3\,mol^{-1}$. Obviously, the molar volume of the completely dimerized polymer is twice the value of the undimerized form because the polymer repeat unit has twice the molecular mass and the density has been found to remain constant. For *Vogel's* model only the molecular mass of the repeat unit is needed which is 358.18 $g\,mol^{-1}$ for PMAOC-C8 and 716.36 $g\,mol^{-1}$ for the completely dimerized polymer, respectively. Refractive indices according to the model of *Lorentz–Lorenz* can then be calculated by

$$n_{LL} = \sqrt{\frac{1 + \frac{2 \cdot \sum R_{LL}}{V_m}}{1 - \frac{\sum R_{LL}}{V_m}}} \tag{3.1}$$

Table 3.5: Calculation of the molar refraction values for completely dimerized PMAOC-C8 from the group contributions of different models. The calculation is made for four theoretical models: *Lorentz–Lorenz* (R_{LL}), *Gladstone–Dale* (R_{GD}), *Vogel* (R_V) and a modification of the *Lorentz–Lorenz* model ($R_{LL,mod}$)

	Groups	$\mathbf{R_{LL}}$	$\mathbf{R_{GD}}$	$\mathbf{R_V}$	$\mathbf{R_{LL,mod}}$
2	$-CH_3$ (general)	11.29	17.64	35.32	11.29
18	$-CH_2-$ (general)	83.68	140.96	371.52	83.68
2	–COO– (higher esters)	12.41	20.94	128.4	12.41
2	–O– (attached to benzene ring)	3.54	5.68	45.2	4.0
2	o-phenylene	49.44	88.4	258.0	55.87
2	–COO– (attached to benzene ring)	13.42	22.62	129.6	15.16
2	=CH– (general)	7.23	13.6	46.98	8.17
2	=CH– (attached to benzene ring)	7.04	12.68	42.8	7.96
	Constitutional increments				
2	Δ ring structure	−0.26	−1.84	−8.88	−0.29
	Σ	187.79	320.68	1048.94	198.25

where $\sum R_{LL}$ is the sum over all group contributions according to that model. In a similar fashion the refractive indices using the other models are calculated. For the *Gladstone–Dale* model the refractive index is

$$n_{GD} = 1 + \frac{\sum R_{GD}}{V_m} \tag{3.2}$$

and for the model of *Vogel*

$$n_V = \frac{\sum R_V}{M}. \tag{3.3}$$

The results of the refractive index calculations using the different models together with a comparison to the experimental values are listed in table 3.6. When looking at the calculated values for the undimerized polymer, it is most obvious that the refractive index predicted by the model of *Vogel* greatly differs from the experimental value. In contrast to the other two models the *Vogel* model uses the molecular mass instead of the molar volume for the refractive index calculation (Eqn. 3.3). Since the calculation according to *Vogel* does not contain the polymer density the model is rendered useless to describe the polymers under investigation here. Furthermore, a general trend of *Vogel's* model to underestimate the refractive index can be seen when refractive index values for standard polymers are calculated with that model and compared to the respecti-

ve measured values. Even worse the *Vogel* model predicts an increase in the refractive index as a result of the dimerization reaction whereas the other two models yield a refractive index decrease. A decrease in refractive index is of course the correct result. It is not only in agreement to the experimentally obtained values but also with the trend predicted by the considerations made about the polarizability change. It is suggested that the *Vogel* model should only be used for liquid compounds, the purpose it was actually designed for.[277,278]

The prediction of the refractive index by the *Lorentz–Lorenz* and *Gladstone–Dale* models for the undimerized PMAOC-C8 is better, but still in only poor agreement with the experimental value. All available models suffer from the shortcoming that they do not take cooperative effects in a π-conjugated system into account. There are group contribution values for small conjugated systems, e.g. a benzene ring. However, there is no possibility to accurately describe the effects due to the interaction of two or more adjacent conjugated systems. Therefore there is no existing method to accurately model the conjugated system consisting of a substituted benzene ring and the lactone six membered ring which also contains an ethylenic double bond. The work of *Yang* and *Jenekhe* tries to improve the accuracy of the semiempirical prediction of the refractive index of conjugated polymers.[274,281] The authors have investigated several conjugated polymers and report modifications to the *Lorentz–Lorenz* model in order to predict the refractive index of such conjugated polymers more accurately. Unfortunately *Yang* and *Jenekhe* do not provide values for the coumarin group or polymers, at least similar to the polymers in question here. Hence, their work is only of limited usability for polymers with coumarin side groups. However, the authors have found that the R_{LL} values at 589 nm for functional groups involved in a π-system should be higher by a factor of 1.2 to 1.9 than the previously known values. Based on that finding, a modification of the *Lorentz–Lorenz* approach for the coumarin containing polymers is proposed. It was found that a good agreement with the experimental value is obtained when the group contribution values of the moieties comprising the coumarin are multiplied by a factor of 1.13. The R_{LL} values for the methacrylate backbone and the alkyl spacer are left unmodified because they do not contribute to the conjugated system. With this modified *Lorentz–Lorenz* model the initial refractive index of PMAOC-C8 is described accurately. The modified *Lorentz–Lorenz* model as well as the other models, do not accurately predict the refractive index change after the photochemical dimerization. Even the modified *Lorentz–Lorenz* calculations give a refractive index change that is only about half the measured value. Given the fact that all model calculations assume a complete dime-

rization of all coumarin moieties in the polymer, the calculated refractive index change should be slightly higher than the experimentally found value because it is never possible in the experiment to dimerize all coumarin side groups. In conclusion, it can be said that none of the models is able to completely describe the refractive index change caused by the diminution of the conjugated π-system when the coumarin dimer is formed. From the calculated data it can be roughly estimated that about 50% of the maximum refractive index change has to be attributed to the conversion of a double to a single carbon-carbon bond. The remaining refractive index change must be attributed to cooperative effects in the conjugated system.

Table 3.6: Calculated refractive indices of undimerized and dimerized PMAOC-C8 with various models. For the calculations experimentally determined molar volumes have been used. The experimental values are shown for comparison.

	n (undimerized)	**n (dimerized)**	**Δn**
Lorentz–Lorenz model	1.5458	1.5325	0.013
Gladstone–Dale model	1.5365	1.5296	0.007
Vogel model	1.4465	1.4643	−0.018
modified *Lorentz–Lorenz* model	1.5839	1.5685	0.015
Experimental values	1.5836	1.5542	0.029

3.3 Characterization of IOL Prototypes

From the polymer plates of PMAOC-C8 prototype IOLs were manufactured. [§] First, IOLs with a so called Saturn ring were made which do not have haptics. These IOLs were mainly used for first optical and handling experiments. From a second plate, three piece IOLs were turned which were also of much better optical quality (Fig. 3.25). The glued in haptics were made of PMMA demonstrating that the manufacturing of three piece IOLs with an optical part made of the coumarin functionalized polymers is possible with an established industrial processes. Making the haptics of another polymer not only reduces the amount of coumarin functionalized polymer needed in the manufacturing process but also allows the haptics to be made up of a material best suited for this application. The haptics are only tenths of a millimeter in thickness and need

[§]IOL manufacturing was conducted by Dr. Schmidt Intraocularlinsen GmbH, Sankt Augustin, Germany.

to be designed very ruggedly to avoid breakage at the time of implantation, and later holding the IOL safely in place.

(a) (b)

Figure 3.25: Photographs of prototype IOLs manufactured. (a) IOL with Saturn ring made of crosslinked PMAOC-C8. (b) PMAOC-C8 IOL with glued in PMMA C-type haptics.

The performance of the prototype IOLs was assessed under conditions similar to those when implanted in the eye. Therefore, they were immersed in physiological saline and shook at 36 °C which is about the temperature persistent in the human eye. Unfortunately, after the lens was immersed for more than 48 h an opacification of the IOL became obvious (Fig 3.26). As a solution the other prototype IOLs were coated with about 2 µm of Parylene C. This polyxylylene type polymer is already in industrial use for a wide range of applications. These polymers are especially useful as a coating for medical implantable devices for many reasons. Parylene C is a biostable but biocompatible coating. It fulfills ISO standards for medical implants and a FDA permission is available. It has been used, for example, with great success to coat stents. The thin and transparent coating forms a completely homogeneous surface and is suitable for complexly arranged substrates also on edges and is micropore free starting at 0.2 µm layer thickness. It is resistant to friction, chemically resistant with good barrier properties, highly corrosion resistant and stable up to several hundred degrees. Therefore, the coating would not pose any risk when implanted into the human body nor would handling and sterilization of the IOL be negatively affected by the coating. Another great advantage of Parylene is that during the coating procedure the substrate remains at ambient temperature in vacuum. It could be shown that the Parylene C coating effectively prevented water uptake which seems to be the reason for the opacification of the IOL (Fig 3.26). The absorption spectrum of Parylene C shows no absorption for wavelengths longer

than 300 nm. Therefore, the coating does not interfere with the photoinduced dimerization reaction.[418]

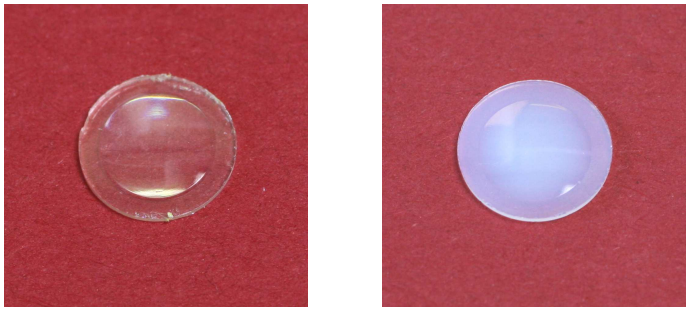

(a) (b)

Figure 3.26: Prototype IOLs of PMAOC directly after being immersed in water for three days at 36 °C. One IOL (a) was coated with PPX while the other (b) is uncoated showing the effectiveness of the coating procedure.

Even though a solution to overcome the opacification of the IOLs when coming in prolonged contact with water has already been provided, the proposed water uptake will be further investigated. First, several prototype IOLs were carefully dried in vacuum and the water uptake was gravimetrically determined. The IOLs were weighted when dry and after they have become opaque in water. Although the error of that measurement is relatively high because the IOLs have a total weight that is only between 30 to 40 mg the gravimetically determined water content was in the range of 1 to 2% (w/w). However, this comparably low water content obviously has a dramatic effect on the optical properties of the polymer. For further investigation an IOL was allowed to soak in a 1% osmium tetroxide solution for staining until it turned completely black.[431] The osmium tetroxide reacts with double bonds present in the polymer making it appear as dark contrast in electron microscope images due to the high mass of the osmium atoms. The lens was then carefully rinsed with fresh water and dried. Unreacted excess osmium salts are washed away when rinsing the polymer pieces. The stained IOL was then embedded in epoxy resin in order to perform microtome cuts (Fig. 3.27). The IOL fragments were put in a cone like mold made of polyethylene specially designed for that purpose and filled with liquid epoxy resin. The epoxy resin was cured at 50 °C for three days and the hardened cone shaped epoxy piece with the embedded lens was removed from the mold. The cone had a diameter of about 7 mm at the base and a height of about 15 mm. From the embedded lens about 5 µm thick microtome cuts were made for

imaging with a conventional optical light microscope. 200 nm thick cuts were collected on cooper grids for transmission electron microscopy (TEM) imaging.

Figure 3.27: Embedding of IOL fragments in epoxy resin for microtome cuts. (a) Embedding in a specially designed mold and hardening. (b) After removal from the mold microtome cuts were made with a diamond knife.

Looking at the microtome cuts under the light optical microscope, the polymer appears to be quite homogeneous. No cavities or bubble like structures can be seen that are sometimes found as so called glistenings in other acrylic polymers (Fig. 3.28).

Figure 3.28: Light optical microscope image at 40× magnification of a microtome cut through a PMAOC-C8 IOL stained with OsO_4.

The TEM images reveal that there are cavities present in the material that are too small to be readily seen under the light microscope. However, they are large enough to scatter light making the polymer appear opaque. These voids are of ellipsoidal shape having a thickness between 100 to 200 nm while being several microns long (Fig. 3.29). Obviously, these voids are filled with water through diffusion after a period of about 24 to 48 h. Since water has a refractive index remarkably different from that of the polymer,

the water filled cavities act as scatter centers whose dimension are on the order of the wavelength of light. Despite the Parylene coating another approach to overcome this problem would be a further optimization of the bulk polymerization process to prevent the formation of such voids in the material.

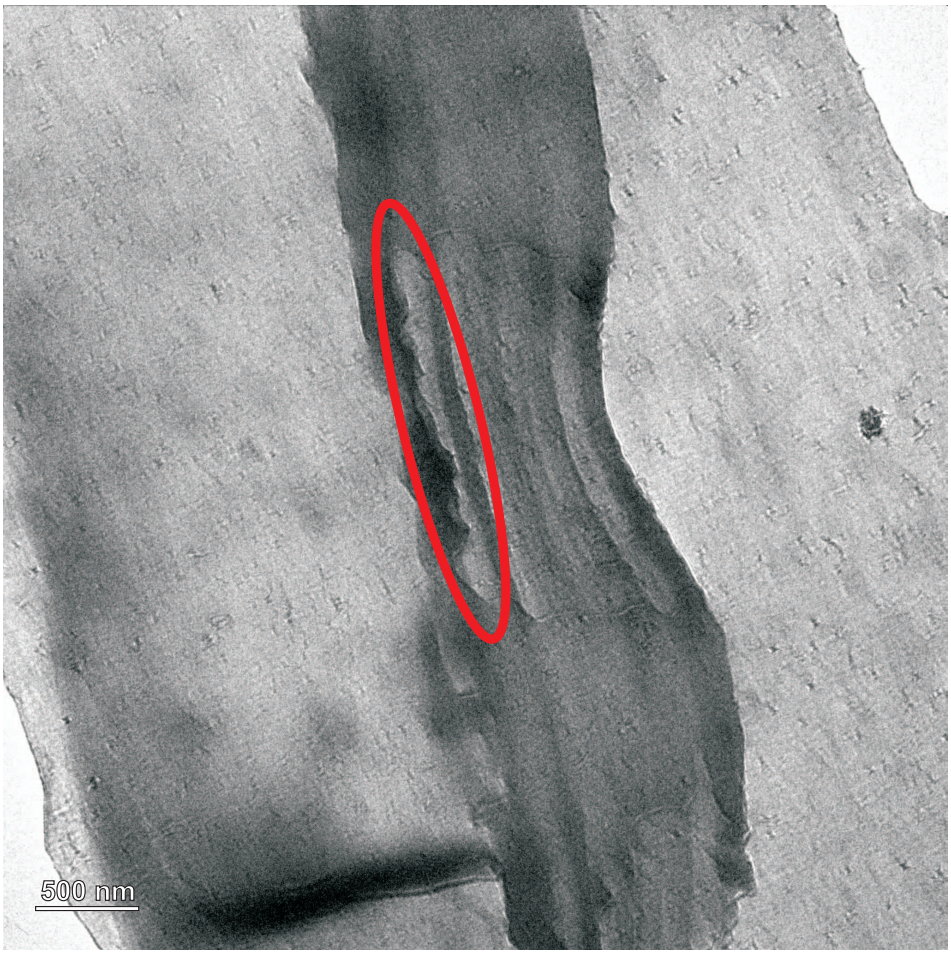

Figure 3.29: Transmission electron microscope (TEM) image of a 200 nm thick microtome cut form a PMAOC-C8 IOL stained with OsO_4. Voids can be seen in the image of which one is marked in red.

3.3.1 Change in Focal Length Measurement

For *in vitro* measurements of the UV light induced focal length change of an IOL, the following optical setup was used. To determine the location of the focal point along the

optical axis, a low intensity continuous wave beam from a helium-neon laser (632.8 nm) was used. The collimated laser beam was incident through the IOL to be tested. The IOL was mounted in an adjustable holder and thoroughly aligned so that the beam was centered on the lens and its principal planes were perpendicular to the beam axis. By means of an adjustable aperture the diameter of the parallel beam entering the lens could be adjusted. The diameter was chosen to be 3 mm in accordance with industry standards to measure the optical properties of IOLs. After focussing by the lens the beam was collected by a 40× microscope objective (NA 0.65) that was mounted on a CCD camera. The camera's image is used to determine the shape and diameter of the refracted light at a certain distance from the lens. The IOL holder is mounted on a linear axis with a resolution of 1 µm to allow a precise positioning of the IOL on the optical axis and determination of its relative distance from the camera system (Fig. 3.30). A picture is recorded and the distance of the IOL to the camera is decreased by only a few microns. This process is automatically repeated and controlled by the measurement software to get an array of several hundred pictures. Each picture is assigned to a certain z-axis position of the IOL. When the distance between the IOL and the camera system decreases towards the focal length, the spot detected on the camera becomes smaller. At the position were the spot size is smallest, the position of the focal point is determined. Further decrease of the IOL's distance to the camera leads again to an increase in the spot size. At the initial measurement of the unirradiated IOL the position of the z-axis position at which the focal point is found is arbitrarily set to zero. The z-resolution of this beam profile measurement system is determined by the resolution of the linear axis and the depth of sharpness of the microscope objective. With the system used here the focal position can be measured with a resolution of 10 µm. Since a two-dimensional image of the beam is obtained, the diameter and shape of the spot when the system is tuned to the focal length can be used as a measure of the imaging quality of the IOL.

To irradiate the IOL with UV light in order to induce the focal length change by changing the refractive index of the lens polymer, a UV laser beam is incident on the IOL. The HeNe laser is turned off and a mirror is translated into the optical axis at 45° to guide the UV laser beam onto the IOL. To avoid damage of the microscope objective and the CCD camera chip, a beam blocker is installed right behind the IOL during UV irradiation (Fig. 3.31). The key advantage of this irradiation procedure is that no loss of adjustment of the focal length measurement setup can occur. The 355 nm UV laser is operated at 10 kHz and the averaged power at the location of the IOL was measured to be 345 mW. After irradiating for a short time of 1 to 10 s, the mirror for the UV laser as

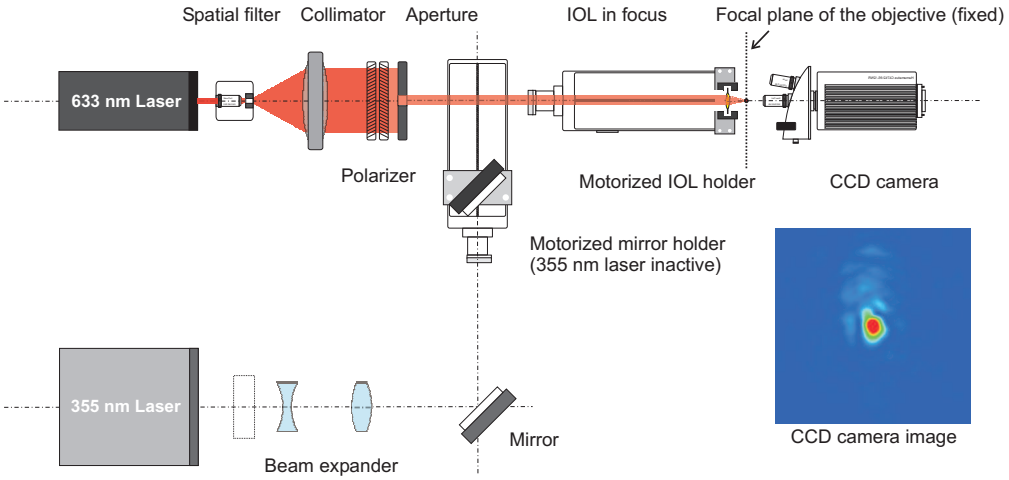

Figure 3.30: Experimental setup to measure the focal length of an IOL. The imaging of the the beam profile when the IOL is in focus is shown here.

well as the beam blocker are removed from the beam path of the HeNe laser. The spot that is imaged by the CCD camera has increased in diameter because the focal length of the IOL has changed as a result of the UV irradiation (Fig. 3.32). This process is also repeated with increasing photon energy doses irradiated on the lens. The progression of the focal length's change can be tracked from the beam images taken after each irradiation step. The UV light irradiation causes a dimerization of the coumarin molecules and the refractive index decreases. The lower refractive index leads in turn to an increased focal length. After the IOL has been sufficiently irradiated it is moved away from the CCD camera until the z-axis location of the new focus is found. The distance that the IOL needs to be moved from the initial position of the focus before the irradiation to the position of the new focus is defined as the focal length change.

The focal length measurements were conducted with three IOLs made of crosslinked PMAOC-C8 with glued in haptics. The IOLs were put in specially designed metal holders that fix the IOL only by clamping the hapitcs while no force is exerted on the optics part of the IOL (Fig. 3.33). The metal holder with the IOL is fixed in the measurement setup for the focal length measurements.

The measurements on the prototype IOLs showed that the described concept does not only hold true theoretically but actually works in an real lens. The focal length of the IOLs tested increased with increasing photon energy doses. Their behavior is therefore as expected from the thin film measurements (Tab. 3.7). However, the maximum focal

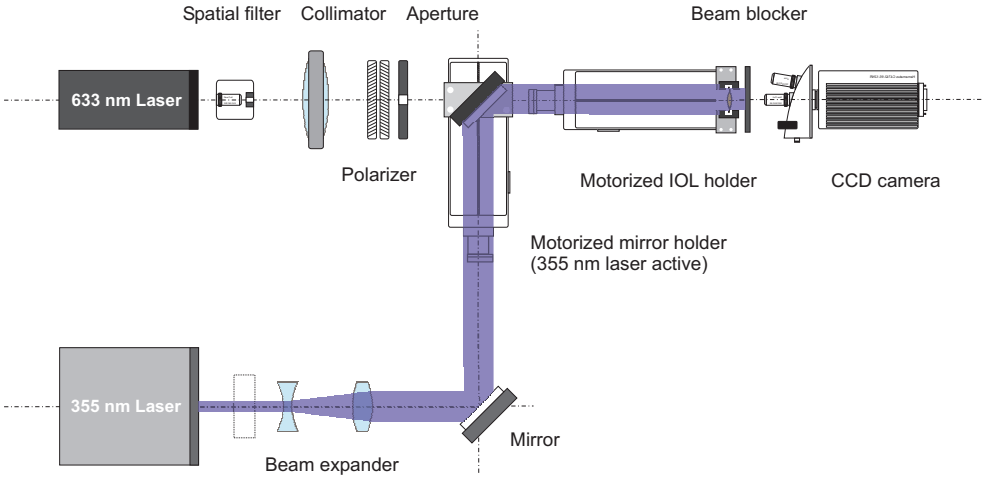

Figure 3.31: Experimental setup of the UV light irradiation of an IOL. The beam monitoring CCD camera is blocked to protect it from the high power UV laser.

length that could be achieved is not as high as the value calculated from the polymers maximum change in refractive index. This can be mainly attributed to the fact that the relatively thick IOL absorbs most of the UV light preferentially from the side that is exposed to the laser. Therefore, it is difficult and a very high total photon energy dose needs to be induced for a complete dimerization of the polymer in the regions close to the back side of the lens. Irradiation of both sides of the IOL is of course not possible because light can only be incident from one side, once the IOL is implanted into the eye. However, this problem can be overcome when the photoinduced dimerization of the coumarin molecules can be induced by a two-photon process. Using a two-photon process, the photoreaction only takes place in a very small confined focal volume that can be located at virtually any place inside the IOL. In a conventional one-photon process, the photoreaction may take place anywhere along the beam's path through the polymer leading to the absorption of photons. In a one-photon excited photochemical reaction it is practically impossible to control the location where the reaction takes place along the beam axis. Since this is a linear process most of the photons will be absorbed in the layers of the material that are closest to the beam's point of entry.

Using the described beam profile measurement technique, the shape and full width half at maximum diameter of the IOL's foci before and after irradiation were determined (Fig. 3.34). The data shows that the focus diameter is about 5 µm, a value that is almost the same as in commercially available IOLs. During the irradiation process, the focus quality was not negatively affected. This is very important because it proofs that

the imaging quality does not decrease as a result of the focal length tuning process. It further shows that the concept and materials reported here are suitable for IOL manufacturing.

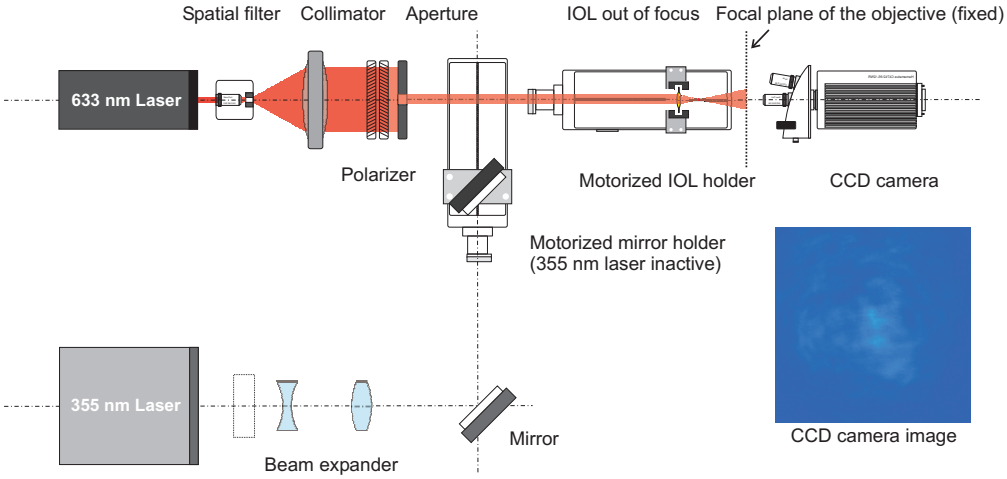

Figure 3.32: Experimental setup to measure the focal length of an IOL. The microscope objective is out of focus due to the UV induced focal length change of the IOL.

Figure 3.33: IOL in a specially designed metal holder for focal length measurements. The lens is clamped by its haptics and centered in the middle of the hole that can be seen in the black metal holder.

Table 3.7: Results of the photoinduced focal length change measurements on prototype IOLs.

IOL	Focal length change / mm	/ D	Photon energy dose / J mm^{-2}
1	0.19	−0.51	84
2	0.81	−2.51	419
3	0.22	−0.58	97

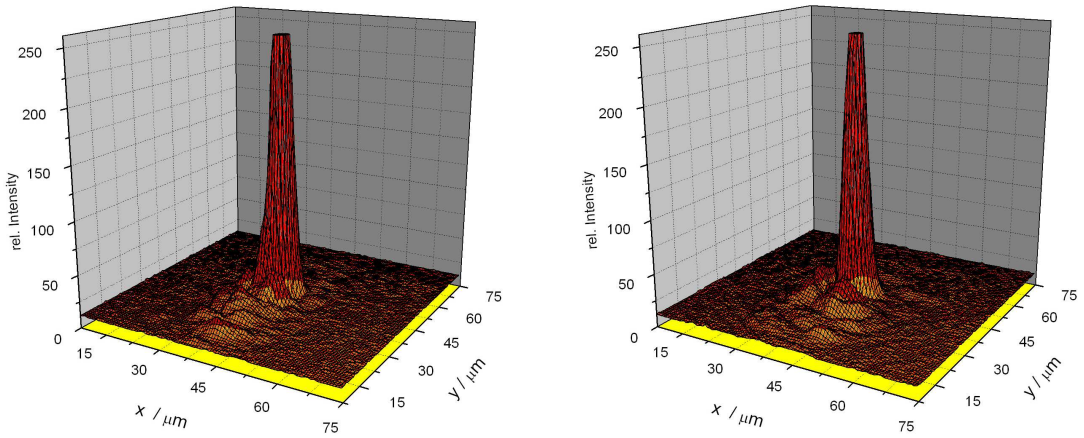

Figure 3.34: Focus profiles of the IOLs recorded with the beam measurement setup before (a) and after (b) UV irradiation.

4 Summary and Outlook

In this work significant improvements to the material properties of polymers for the fabrication of IOLs with the ability to postoperatively tune the refractive index in a non-invasive, photoinduced manner could be shown. From several possible photodimerizable linker systems the coumarin molecule was chosen for further investigation. Although, the simplest polymer containing coumarin side groups, PMAOC, showed a sufficient change in refractive index it is not usable because of other material properties not meeting the requirements for IOL fabrication. Therefore, improvements were necessary with respect to the material properties. Whereas copolymerization with BMA did not show the desired effects, the introduction of aliphatic spacers of varying length between the polymer backbone and the coumarin moieties was found to be the key to significant improvements. The glass transition temperature is significantly lowered and transparent work pieces are obtained. The flexibility of the materials can be tuned to the application's demands by altering the spacer length and/or adding various amounts of an acrylic crosslinker.

Photoinduced refractive index changes up to 0.03 were obtained. Changes in focal length of about 2 D can be obtained with IOLs made from the novel polymers described here. A high number of patients could be brought to optimal vision without external correction after cataract surgery using IOLs made of the polymers reported in this work. The light induced refractive tuning was demonstrated to work not only in polymer films but also IOL prototypes were manufactured and tested. The refractive index change of the polymer was shown to lead to the desired focal length change of the prototype IOLs.

The photochemical tuning of the IOLs focal length could be accomplished either by single-photon absorption (SPA) of UV-light or by two-photon absorption (TPA) of visible light, e.g., in the red spectral range. The two most important ocular structures that could be damaged during the photoinduced tuning of the IOL are the cornea and

the retina. *Zuclich* and *Connolly* reported that the damage threshold of rhesus monkey corneas is between 0.6 to 0.7 J mm^{-2} for 350 nm radiation in the near UV.[432] Excitation with 365 nm has been considered for focal tuning of IOLs.[433] About 90% of the maximal refractive index change in the polymers with alkyl spacer attached coumarin presented here can be achieved with energies within this limit. In principle, the focal length tuning of the implanted IOLs could be achieved by SPA-induced refractive index changes with intensities below the damage limit of the cornea. More sensitive is the retina. The damage energy threshold (also for rhesus monkeys) is about 0.05 J mm^{-2} for 350 nm which is about a factor of 10 less as compared to the damage threshold of the cornea.[434] When assessing the risk of retina damage it has to be noted that most of the UV light is absorbed in the IOL material itself, but an additional UV absorbing layer could be coated on the back side of the IOL. This UV coating would ensure that the UV light transmitted through the IOL stays well below the retina damage dose. However, an SPA process in the UV region is less interesting for implanted IOLs because of the UV absorbing nature of the cornea. It is more interesting to use an alternative approach: a TPA process allows for a photochemical process behind a UV absorbing barrier like the cornea by the combination of two photons in the visible range of the spectrum. Both the TPA-induced photodimerization of coumarin derivatives[435] as well as the TPA-triggered coumarin dimer cleavage has been demonstrated.[392]

The polymers presented here are the first that combine a high initial refractive index, a high photoinduced refractive index change, a low glass transition temperature, as well as a high transparency in the visible wavelength regime. The very low photoinduced density changes may also make the introduced materials interesting for optical data storage.[436]

Further work should concentrate on the investigation of the TPA-induced refractive index change of the polymers described here. Also, a further optimization of the bulk polymerization process could afford even more improved materials and solve the problem of undesired liquid uptake of the IOLs. A manufacturing process should be developed to allow the foldable low T_g polymers being machined into IOLs. On a wider scope derivatization of the linker system may further increase the change in refractive index and thereby focal length.

5 References

[1] G. Brian, H. Taylor, Cataract blindness - challenges for the 21st century, *Bull. World Health Organ.* **2001**, *79(3)*, 249–256.

[2] N. H. L. Ridley, Intraocular acrylic lenses, *Trans. Ophthalmol. Soc. UK* **1951**, *71*, 617–621.

[3] N. H. L. Ridley, Artifical intraocular lenses after cataract extraction, *St. Thomas' Hospital Reports* **1951**, *7 (2nd series)*, 12–14.

[4] N. H. L. Ridley, Intraocular acrylic lenses after cataract extraction, *Lancet* **1952**, *19*, 118–129.

[5] N. H. L. Ridley, Further observations on intraocular acrylic lenses in cataract surgery, *Trans. Am. Academy Ophthalmol. Otolaryngol.* **1953**, *57*, 98–106.

[6] N. H. L. Ridley, Further experiences of intraocular acrylic lens surgery, *Br. J. Ophthalmol.* **1954**, *38*, 156–162.

[7] N. H. L. Ridley, Intraocular acrylic lenses - 10 years development, *Br. J. Ophthalmol.* **1960**, *44*, 705–712.

[8] D. Apple, N. Mamalis, K. Loftfield, J. M. Googe, L. C. Novak, D. Kavka-Van Norman, S. E. Brandy, R. J. Olson, Complications of intraocular lenses. A histopathological review, *Surv. Ophthalmol.* **1984**, *29*, 1–54.

[9] D. J. Apple, K. D. Solomon, M. R. Tetz, E. I. Assia, E. Y. Holland, U. F. Legler, J. C. Tsai, V. E. Casteneda, J. P. Hoggatt, A. M. Kosick, Posterior capsule opacification, *Surv. Ophthalmol.* **1992**, *37*, 73–116.

[10] D. A. Schaumberg, M. R. Dana, W. G. Christen, R. J. Glynn, A systematic overview of the incidence of posterior capsule opacification, *Ophthalmology* **1998**, *105*, 1213–1221.

[11] M. E. Wilson, Intraocular lens implantation: has it become standard for children?, *Ophthalmology* **1996**, *103*, 1719–1720.

[12] S. K. Pandey, M. E. Wilson, R. H. Trivedi, A. M. Izak, T. A. Macky, L. Werner, D. J. Apple, Pediatric cataract surgery and intraocular lens implantation: current techniques, complications and management, *Int. Ophthalmol. Clin.* **2001**, *41*, 175–196.

[13] T. Kohnen, R. Pena-Cuesta, D. D. Koch, Secondary cataract formation following pediatric intraocular lens implantation: 6-month results, *Ger. J. Ophthalmol.* **1996**, *5*, 171–175.

[14] J. Zwaan, P. B. Mullaney, A. Awad, S. al Mefser, D. T. Wheeler, Pediatric intraocular lens implantation. Surgical results and complications in more than 300 patients, *Ophthalmology* **1998**, *105*, 112–118.

[15] P.-R. Preußner, J. Wahl, Konsistente numerische Berechnung der Optik des pseudophaken Auges, *Ophthalmologe* **2000**, *97*, 126–141.

[16] P. R. Preußner, J. Wahl, H. Lahdo, O. Findl, Konsistente IOL-Berechnung, *Ophthalmologe* **2001**, *98*, 300–304.

[17] J. S. Hillman, Intraocular lens power calculation - the selection of formula, *Trans. Ophthalmol. Soc. UK* **1985**, *104(7)*, 693–698.

[18] S. Longstaff, Factors affecting intraocular lens power calculation, *Trans. Ophthalmol. Soc. UK* **1986**, *105(6)*, 642–646.

[19] M. S. Dang, P. P. Raj, SPK II formula in the calculation of intraocular lens power, *Br. J. Ophthalmol.* **1989**, *73(10)*, 823–826.

[20] T. Olsen, Refraction factor in IOL power calculation, *J. Cataract Refract. Surg.* **1990**, *16(1)*, 129–130.

[21] W. Niederer, Analysis of parameters for calculating the intraocular lens, *Klin. Monatsbl. Augenheilkd.* **1994**, *204(5)*, 435–437.

[22] T. Olsen, L. Corydon, H. Gimbel, Intraocular lens power calculation with an improved anterior chamber depth prediction algorithm, *J. Cataract Refract. Surg.* **1995**, *21(3)*, 313–319.

[23] P. S. Raj, B. Ilango, A. Watson, Measurement of axial length in the calculation of intraocular lens power, *Eye* **1998**, *12(2)*, 227–229.

[24] J. T. Holladay, Standardizing constants for ultrasonic biometry, keratometry, and intraocular lens power calculations, *J. Cataract Refract. Surg.* **1997**, *23(9)*, 85–88.

[25] J. Nemeth, O. Fekete, N. Pesztenlehrer, Optical and ultrasound measurement of axial length and anterior chamber depth for intraocular lens power calculation, *J. Cataract Refract. Surg.* **2003**, *29(1)*, 85–88.

[26] P. C. Hoffmann, W. W. Hütz, H. B. Eckhardt, Bedeutung der Formelauswahl für die postoperative Refraktion nach Katarakt-Operation (Importance of IOL calculation formula for postoperative refraction after cataract surgery), *Klin. Monatsbl. Augenheilkd.* **1997**, *211*(3), 168–177.

[27] P.-R. Preußner, Accuracy limits in IOL calculation: current status, *Klin. Monatsbl. Augenheilkd.* **2007**, *224(12)*, 893–899.

[28] T. Olsen, Calculation of intraocular lens power: a review, *Acta Ophthalmol. Scand.* **2007**, *85(5)*, 472–485.

[29] V. Feiz, M. J. Mannis, IOL calculations, *Ophthalmology* **2007**, *114(5)*, 1028–1029.

[30] P.-R. Preußner, T. Olsen, P. Hoffmann, O. Findl, Intraocular lens calculation accuracy limits in normal eyes, *J. Cataract Refract. Surg.* **2008**, *34(5)*, 802–808.

[31] J.-K. Wang, C.-Y. Hu, S.-W. Chang, Intraocular lens power calculation using the IOLMaster and various formulas in eyes with long axial length, *J. Cataract Refract. Surg.* **2008**, *34(2)*, 262–267.

[32] E. A. Gavin, C. J. Hammond, Intraocular lens power calculation in short eyes, *Eye* **2008**, *22(7)*, 935–938.

[33] C. Tromans, P. M. Haigh, S. Biswas, I. C. Lloyd, Accuracy of intraocular lens power calculation in paediatric cataract surgery, *Br. J. Ophthalmol.* **2001**, *85(8)*, 939–941.

[34] D. Moore, Z. I. Ben, D. E. Neely, D. A. Plager, S. Ofner, D. T. Sprunger, G. J. Roberts, Accuracy of biometry in pediatric cataract extraction with primary intraocular lens implantation, *J. Cataract Refract. Surg.* **2008**, *34(11)*, 1940–1947.

[35] N. E. S. Norrby, L. W. Grossman, G. E. P., Accuracy in determining intraocular lens dioptric power assessed by interlaboratory tests, *J. Cataract Refract. Surg.* **1996**, *22*, 983–993.

[36] H. B. Fam, K. L. Lim, A comparative analysis of intraocular lens power calculation methods after myopic excimer laser surgery, *J. Refract. Surg.* **2008**, *24(4)*, 355–360.

[37] W. Haigis, Intraocular lens calculation after refractive surgery for myopia: Haigis-L formula, *J. Cataract Refract. Surg.* **2008**, *34(10)*, 1658–1663.

[38] S.-H. Lee, C.-Y. Tsai, S.-W. Liou, R.-F. Tsai, J.-D. Ho, Intraocular lens power calculation after automated lammellar keratoplasty for high myopia, *Cornea* **2008**, *27(9)*, 1086–1089.

[39] J. B. Randleman, J. B. Foster, D. N. Loupe, S. C. D., R. D. Stulting, Intraocular lens power calculations after refractive surgery: consensus-K technique, *J. Cataract Refract. Surg.* **2007**, *33(11)*, 1892–1898.

[40] T. M. Rabsilber, A. J. Reuland, M. P. Holzer, G. U. Auffarth, Intraocular lens power calculation using ray tracing following excimer laser surgery, *Eye* **2007**, *21*, 697–701.

[41] I. M. Hamdi, A. Artola, J. L. Alio, New frontiers for the perioperative data method for IOL calculation following corneal refractive surgeries, *Eur. J. Ophthalmol.* **2006**, *22(4)*, 809–815.

[42] G. J. C. Jin, A. S. Crandall, Y. Jin, Analysis of intraocular lens power calculation for eyes with previous myopic LASIK, *J. Refract. Surg.* **2006**, *22(4)*, 387–395.

[43] D. D. Koch, New options for IOL calculations after refractive surgery, *J. Cataract Refract. Surg.* **2006**, *32(3)*, 371–372.

[44] K. Pesudovs, D. B. Elliott, The evolution of cataract surgery, *Optometry today* **2001**, *10*(10), 30–32.

[45] T. H. Shastid, *American Encyclopedia and Dictionary of Ophthalmology*, The Cleveland Press, Chicago, **1913**.

[46] D. Albert, *Men of Vision: Lives of Notable Figures in Ophthalmology*, Harcourt, Orlando, **1993**.

[47] A. Sorsby, *Modern Ophthalmology*, Butterworths, London, **1963**.

[48] J. Daviel, A new method of curing cataract by extraction of the lens, *Memoires de L'Academie Royale de Chirirgie Paris* **1753**, *2*, 337–354.

[49] F. Blodi, *Management and Care of the Cataract Patient, in F.J. Weinstock, Ed. The History of Cataract Operation*, Blackwell Scientific Publications, Oxford, **1992**.

[50] K. Koller, The application of cocaine to the eye as an anaesthetic, *Wiener med. Bl.* **1884**, *23*, 1352–1355.

[51] E. Fuchs, A. Duane, *Text-book of Ophthalmology*, Lippincott Company, Philadelphia, **1908**.

[52] A. Mathewson, A case illustrating the natural history of cataract, *Trans Am Ophthalmol Soc.* **1884**, *3*, 694–696.

[53] I. Barraquer, Phakoerisis, *Am. J. Ophthalmol.* **1920**, *3*, 721–726.

[54] I. Barraquer, Phakoerisis. The advantages and important details of techniques, *Arch. Ophthalmol.* **1922**, *51*, 448–450.

[55] T. Krwawicz, Intracapsular extraction of intumescent cataract by application of low temperature, *Br. J. Ophthalmol.* **1961**, *83*, 279–283.

[56] C. D. Kelman, Phacoemulsification and aspiration: a new technique of cataract removal. A preliminary report, *Am. J. Ophthalmol.* **1967**, *64*, 23–35.

[57] G. W. Stachowiak, A. W. Batchelor, *Engineering tribology*, Butterworth-Heinemann, Boston, **2001**.

[58] R. F. Steinert, S. F. Brint, S. M. White, I. Fine, Astigmatism after small incision cataract surgery: a prospective, randomised, multicenter comparison of 4- and 6.5 mm incisions, *Ophthalmol.* **1991**, *98*, 417–424.

[59] J. M. Emery, K. A. Wilhelmus, S. Rosenberg, Complications of phacoemulsification, *Ophthalmology* **1978**, *85*, 141–150.

[60] W. T. Green, D. L. Boase, How clean is your capsule?, *Eye* **1989**, *3*, 678–684.

[61] K. Sundelin, J. Sjostrand, Posterior capsule opacification 5 years after extracapsular cataract extraction, *J. Cataract Refract. Surg.* **1999**, *25*, 246–250.

[62] E. J. Hollick, D. J. Spalton, P. G. Ursell, M. V. Pande, Lens epithelial cell regression on the posterior capsule with different intraocular lens materials, *Br. J. Ophthalmol.* **1998**, *82*, 1182–1188.

[63] M. R. Tetz, M. W. Ries, C. Lucas, Inhibition of posterior capsule opacification by an intraocular-lens-bound sustained drug delivery system: an experimental animal study and literature review, *J. Cataract Refract. Surg.* **1996**, *22*, 1070–1078.

[64] M. R. Tetz, G. U. Auffarth, M. Sperker, Photographic image analysis system of posterior capsule opacification, *J. Cataract Refract. Surg.* **1997**, *23*, 1515–1520.

[65] M. P. Nasisse, M. J. Dykstra, L. M. Cobo, Lens capsule opacification in aphakic and pseudophakic eyes, *Graefes Arch. Clin. Exp. Ophthalmol.* **1995**, *233*, 63–70.

[66] N. R. Powe, O. D. Schein, S. C. Gieser, Synthesis of the literature on visual acuity and complications following cataract extraction with intraocular lens implantation, *Arch. Ophthalmol.* **1994**, *112*, 239–252.

[67] P. L. Davis, Posterior capsule: do they always tighten? A 4-year prospective study, *Eur. J. Implant. Refract. Surg.* **1990**, *2*, 53–55.

[68] P. J. McDonnell, M. A. Zarbin, W. R. Green, Posterior capsule opacification in pseudophakic eyes, *Ophthalmology* **1983**, *90*, 1548–1553.

[69] W. R. Green, P. J. McDonnell, Opacification of the posterior capsule, *Trans. Ophthalmol. Soc. UK* **1985**, *104*, 727–739.

[70] R. L. Lindstrom, W. S. Harris, Management of the posterior capsule following posterior chamber lens implantation, *J. Am. Intraocul. Implant. Soc.* **1980**, *6*, 255–258.

[71] P. J. McDonnell, W. J. Stark, W. R. Green, Posterior capsule opacification: a specular microscopic study, *Ophthalmology* **1984**, *91*, 853–856.

[72] D. J. McIntyre, Posterior capsule opacification, *Trans. New. Orleans Acad. Ophthalmol.* **1988**, *36*, 163–167.

[73] J. L. Menezo, A. L. Cisneros-Lanuza, E. Ferrer-Galindo, Late capsular opacification, *Eur. J. Implant. Refract. Surg.* **1989**, *1*, 123–126.

[74] J. Moisseiev, E. Bartov, A. Schochat, M. Blumenthal, Longterm study of the prevalence of capsular opacification following extracapsular cataract extraction, *J. Cataract Refract. Surg.* **1989**, *15*, 531–533.

[75] K. R. Wilhelmus, J. M. Emery, Posterior capsule opacification following phacoemulsification, *Ophthalmic Surg.* **1980**, *11*, 264–267.

[76] J. K. Shugar, T. Schwartz, Interpseudophakos Elschnig pearls associated with late hyperopic shift: a complication of piggyback posterior chamber intraocular lens implantation, *J. Cataract Refract. Surg.* **1999**, *25*, 863–867.

[77] R. R. Holweger, B. Marefat, Intraocular pressure change after neodymium:YAG capsulotomy, *J. Cataract Refract. Surg.* **1997**, *23*, 115–121.

[78] K. Kato, D. Kurosaka, H. Bissen-Miyajima, Elschnig pearl formation along the posterior capsulotomy margin after neodymium YAG capsulotomy, *J. Cataract Refract. Surg.* **1997**, *23*, 1556–1560.

[79] I. D. Ladas, S. Baltatzis, D. Panagiotidis, Topical 2.0% dorzolamide vs oral acetazolamide for prevention of intraocular pressure rise after neodymium YAG laser posterior capsulotomy, *Arch. Ophthalmol.* **1997**, *115*, 1241–1244.

[80] B. V. Magno, M. B. Datiles, M. S. Lasa, Evaluation of visual function following neodymium YAG laser posterior capsulotomy, *Ophthalmology* **1997**, *104*, 1287–1293.

[81] J. M. Tielsch, M. W. Legro, S. D. Cassard, Risk factors for retinal detachment after cataract surgery. A population-based case-control study, *Ophthalmology* **1996**, *103*, 1537–1545.

[82] M. J. Tassignon, V. de Groot, R. M. Smets, Secondary closure of posterior continuous circular capsulorhexis, *Bull. Soc. Belge Ophthalmol.* **1996**, *261*, 87–91.

[83] C. E. Jahn, M. Emke, Long-term elevation of intraocular pressure after neodymium YAG laser posterior capsulotomy, *Ophthalmologica* **1996**, *210*, 85–89.

[84] N. Mamalis, B. Phillips, C. H. Kopp, Neodymium: YAG capsulotomy rates after phacoemulsification with silicone posterior chamber intraocular lenses, *J. Cataract. Refract. Surg.* **1996**, *22*, 1296–1302.

[85] T. J. Newland, G. U. Auffarth, T. A. Wesendahl, D. J. Apple, Neodymium:YAG laser damage on silicone intraocular lenses. a comparison of lesions on explanted lenses and experimentally produced lesions, *J. Cataract Refract. Surg.* **1994**, *20*, 527–533.

[86] D. S. Aron-Rosa, J. J. Aron, Effect of preoperative YAG laser anterior capsulotomy on the incidence of posterior capsule opacification: ten year follow-up., *J. Cataract Refract. Surg.* **1992**, *18*, 559–561.

[87] R. F. Steinert, C. A. Puliafito, S. R. Kumar, Cystoid macular edema, retinal detachment, and glaucoma after Nd:YAG laser posterior capsulotomy, *Am. J. Ophthalmol.* **1991**, *112*, 373–380.

[88] H. Erbil, S. Sinav, Intraocular lens damage in experimental Nd:YAG laser capsulotomy: a comparison of Perspex CQ and cross-linked PMMA lenses, *Ophthalmic Surg.* **1991**, *22*, 202–203.

[89] S. Fourman, J. Apisson, Late-onset elevation in intraocular pressure after neodymium-YAG laser posterior capsulotomy, *Arch. Ophthalmol.* **1991**, *109*, 511–513.

[90] R. Brancato, G. Leoni, G. Trabucchi, Study of laser damage to injection-molded diffractive intraocular lenses, *J. Cataract Refract. Surg.* **1991**, *17*, 639–641.

[91] D. W. Albert, E. C. Wade, R. K. Parrish, A prospective study of angiographic cystoid macular edema one year after Nd:YAG posterior capsulotomy, *Ann. Ophthalmol.* **1990**, *22*, 139–143.

[92] M. R. Capon, F. Docchio, G. Leoni, Comprehensive study of damage to intraocular lenses by single and multiple nanosecond neodymium YAG laser pulses, *J. Cataract Refract. Surg.* **1990**, *16*, 603–610.

[93] J. E. Downing, M. T. Alberhasky, Biconvex intraocular lenses and Nd:YAG capsulotomy: experimental comparison of surface damage with different poly(methyl methacrylate) formulations, *J. Cataract Refract. Surg.* **1990**, *16*, 732–736.

[94] J. J. Alpar, Experiences with the neodymium YAG laser: interruption of anterior hyaloid membrane of the vitreous and cystoid macular edema, *Ophthalmic Surg.* **1986**, *17*, 157–165.

[95] D. S. Aron-Rosa, Influence of picosecond and nanosecond YAG laser capsulotomy on intraocular pressure, *J. Am. Intraocul. Implant. Soc.* **1985**, *11*, 249–252.

[96] D. S. Aron-Rosa, J. J. Aron, H. C. Cohn, Use of a pulsed picosecond Nd:YAG laser in 6,664 cases, *J. Am. Intraocul. Implant. Soc.* **1984**, *10*, 35–39.

[97] D. Aron-Rosa, J. J. Aron, M. Griesemann, R. Thyzel, Use of the neodymium-YAG laser to open the posterior capsule after lens implant surgery: a preliminary report, *J. Am. Intraocul. Implant. Soc.* **1980**, *6*, 352–354.

[98] R. W. Snyder, M. G. Jani, M. Yarborough, G. R. Marcellino, R. J. Noecker, T. R. Kramer, J. Vidaurri, Erbium:YAG laser for cataract extraction, *Proc. SPIE* **1998**, *3246*, 172–184.

[99] D. Apple, J. Ram, A. Foster, Q. Peng, Elimination of cataract blindness: a global perspective entering the new millennium, *Surv. Ophthalmol.* **2000**, *45(Suppl. 1)*((Suppl. 1)), 1–204.

[100] M. Belpoliti, G. Maraini, Sugar alcohols in the lens epithelium of age related cataract, *Exp. Eye. Res.* **1993**, *56*, 3–6.

[101] J. D. Bhattacharjee, R. S. Sharma, N. K. Saini, K. K. Datta, Methods for estimating prevalence and incidence of senile cataract blindness in a district., *Indian J. Ophthalmol.* **1996**, *44*, 207–211.

[102] C. D. Cook, A. A. Stulting, Prevalence and incidence of blindness due to age-related cataract in the rural areas of South Africa, *S. Afr. Med. J.* **1995**, *85*, 26–27.

[103] J. Evans, D. C. Minassia, Epidemiology of age-related cataract, review article, *Comm. Eye Health* **1992**, *9*, 2–6.

[104] J. J. Harding, Pharmacological treatment strategies in age-related cataracts, *Drugs Aging* **1992**, *2*, 287–300.

[105] J. J. Harding, R. van Heyningen, Epidemiology and risk factors for cataract, *Eye* **1987**, *1*, 537–541.

[106] T. S. Hu, Q. Zhen, R. D. Sperduto, Age-related cataract in the Tibet Eye Study, *Arch. Ophthalmol.* **1989**, *107*, 666–669.

[107] S. Kashyap, J. Ram, A. Gupta, B. Ram, Systemic diseases in senile cataract - a study of 2480 patients, *Afro Asian J. Ophthalmol.* **1991**, *9*, 134–136.

[108] S. M. Lee, S. Y. Lin, C. L. Cheng, R. C. Liang, Progressive changes in secondary conformation and composition of the senile cataractous human lens capsules, *Acta Ophthalmol. Scand.* **1996**, *74*, 542–546.

[109] M. C. Leske, L. T. Chylack, S. Y. Wu, The lens opacities case control study group: risk factor for cataract, *Comm. Eye Health* **1992**, *10*, 12.

[110] M. C. Leske, R. D. Sperduto, The epidemiology of senile cataracts: a review, *Am. J. Epidemiol.* **1983**, *118*, 152–165.

[111] W. S. Mao, T. S. Hu, An epidemiologic survey of senile cataract in China, *Chin. Med. J.* **1982**, *95*, 813–818.

[112] S. K. West, C. T. Valmadrid, Epidemiology of risk factors for age-related cataract, *Surv. Ophthalmol.* **1995**, *39*, 323–324.

[113] S. K. West, Daylight, diet, and age-related cataract, *Optom. Vis. Sci.* **1993**, *70*, 869–872.

[114] M. A. Babizhayev, Failure to withstand oxidative stress induced by phospholipid hydroperoxides as a possible cause of the lens opacities in systemic diseases and ageing, *Biochim. Biophys. Acta* **1996**, *1315*, 87–99.

[115] H. Bloemendal, E. L. Benedetti, I. Dunia, Transgenic mice models for the study of cataractogenesis. A minireview, *Ophthalmic Res.* **1996**, *28*, 1–7.

[116] J. J. Harding, R. Blakytny, Pathophysiology of cataract, *Curr. Opin. Ophthalmol.* **1994**, *5*, 9–15.

[117] J. J. Harding, *Cataract: biochemistry, epidemiology and pharmacology*, Chapman and Hall, London, **1991**.

[118] J. A. Knight, Diseases related to oxygen-derived free radicals, *Ann. Clin. Lab. Sci.* **1995**, *25*, 111–121.

[119] H. Rink, A. A. el Layeh, J. Bours, M. Emarah, Basic biochemical parameters of one hundred cataractous lenses from Egyptian patients, *Ophthalmic Res.* **1995**, *27(Suppl.)*, 44–53.

[120] A. Taylor, T. Nowell, Oxidative stress and antioxidant function in relation to risk for cataract, *Adv. Pharmacol.* **1997**, *38*, 515–536.

[121] J. M. Benitez del Castillo, T. del Rio, J. Garcia-Sanchez, Effects of estrogen use on lens transmittance in postmenopausal women, *Ophthalmology* **1997**, *104*, 970–973.

[122] V. N. Cushnir, O. S. Slepova, T. B. Cruglova, The role of HBV-infection in development of cataracts in children and adults, *Oftalmologia* **1997**, *41*, 318–322.

[123] S. P. Dhir, R. Detels, E. R. Alexander, The role of environmental factors in cataract, pterygium and trachoma, *Am. J. Ophthalmol.* **1967**, *64*, 128–135.

[124] R. J. Glynn, W. G. Christen, J. E. Manson, Body mass index. An indipendant predictor of cataract, *Arch. Ophthalmol.* **1995**, *113*, 1131–1137.

[125] R. Lim, P. Mitchell, R. G. Cumming, Cataract associations with pinguecula and pterygium: the Blue Mountains eye study, *Am. J. Ophthalmol.* **1998**, *126*, 717–719.

[126] J. C. Livesey, L. W. Wiens, D. J. von Seggern, Inhibition of radiation cataractogenesis by WR-77913, *Radiat. Res.* **1995**, *141*, 99–104.

[127] D. C. Minassian, J. Baasanhu, G. J. Johnson, G. Burendei, The relationship between cataract and climatic droplet keratopathy in Mongolia, *Acta Ophthalmol.* **1994**, *72*, 490–495.

[128] H. R. Taylor, The environment and the lens, *Br. J. Ophthalmol.* **1980**, *64*, 303–310.

[129] R. van Heyningen, J. J. Harding, A case-control study of cataract in Oxfordshire: some risk factors, *Br. J. Ophthalmol.* **1988**, *72*, 804–808.

[130] O. Weinreb, A. Dovrat, Transglutaminase involvement in UV-A damage to the eye lens, *Exp. Eye Res.* **1996**, *63*, 591–597.

[131] M. Balaji, K. Sasikala, T. Ravindran, Copper levels in human mixed, nuclear brunescence, and posterior subcapsular cataract, *Br. J. Ophthalmol.* **1992**, *76*, 668–669.

[132] Y. Belkacemi, M. Ozsahin, F. Pene, Cataractogenesis after total body irradiation, *Int. J. Radiat. Oncol. Biol. Phys.* **1996**, *35*, 53–60.

[133] J. Blondin, V. Baragi, E. R. Schwartz, Dietary vitamin C prevents eye lens protein damage, *Invest. Ophthalmol. Vis. Sci.* **1986**, *27(Suppl)*, 9.

[134] A. J. Bron, N. A. Sparrow, J.and Brown, The lens in diabetes, *Eye* **1993**, *7*, 260–275.

[135] Y. Ohta, H. Okada, Y. Majima, I. Ishiguro, Anticataract action of vitamin E: its estimation using an in vitro steroid cataract models, *Ophthalmic Res.* **1996**, *28(Suppl.)*, 16–25.

[136] S. Vitale, S. West, J. Hallfrisch, Plasma antioxidants and risk of cortical and nuclear cataract, *Epidemiology* **1993**, *4*, 195–203.

[137] R. E. Neale, J. L. Purdie, A. C. Hirst, L. W. andGreen, Sun exposure as a risk factor for nuclear cataract, *Epidemiology* **2003**, *14(6)*, 707–712.

[138] T. W. Bochow, S. K. West, A. Azar, Ultraviolett light exposure and risk of posterior subcapsular cataracts, *Arch. Ophthalmol.* **1989**, *107*, 369–372.

[139] L. B. Brilliant, N. C. Grasset, R. P. Pokhrel, Associations among cataract prevalence, sunlight hours, and altitude in the Himalayas, *Am. J. Epidemiol.* **1983**, *118*, 250–264.

[140] M. Burton, E. Fergusson, A. Hart, The prevalence of cataract in two villages of northern Pakistan with different levels of ultraviolett radiation, *Eye* **1997**, *11*, 95–101.

[141] K. J. Cruickshanks, B. E. Klein, R. Klein, Ultraviolett light exposure and lens opacities: the Beaver Dam eye study, *Am. J. Public Health* **1992**, *82*, 1658–1662.

[142] K. J. Dilley, Ultraviolet light and human cataract, *Nature* **1975**, *257*, 71–72.

[143] C. Forker, A. Wegener, J. Graw, Effects of UV-B radiation on a hereditary suture cataract in mice, *Exp. Eye Res.* **1997**, *64*, 405–411.

[144] W. C. Li, A. Spector, Lens epithelial cell apoptosis is an early event in the development of UVB-induced cataract, *Free Radic. Biol. Med.* **1996**, *20*, 301–311.

[145] F. S. Rosenthal, C. Phoon, A. E. Bakalian, H. R. Taylor, The ocular dose of ultraviolett radiation to outdoor workers, *Invest. Ophthalmol. Vis. Sci.* **1988**, *29*, 649–656.

[146] H. R. Taylor, S. West, B. Munoz, The long-term effect of visible light on the eye, *Arch. Ophthalmol.* **1992**, *110*, 99–104.

[147] H. R. Taylor, S. K. West, F. S. Rosenthal, Effect of ultraviolet radiation on cataract formation, *N. Engl. J. Med.* **1988**, *319*, 1429–1433.

[148] S. K. West, D. D. Duncan, B. Munoz, Sunlight exposure and risk of lens opacities in a population-based study: the salisbury eye evaluation project, *J. Am. Med. Assoc.* **1998**, *280*, 714–718.

[149] A. Chatterjee, V. C. Rambo, S. Franken, Vision survey in Himalayan area, *Am. J. Ophthalmol.* **1968**, *66*, 113–116.

[150] K. J. Awan, Smoking: the evil, the eye sight, the eye openers, *Pakistan J. Ophthalmol.* **1992**, *9*, 29–30.

[151] W. G. Christen, J. E. Manson, J. M. Seddon, A prospective study of cigarette smoking and risk of cataract in men, *J. Am. Med. Assoc.* **1992**, *268*, 989–993.

[152] R. G. Cumming, P. Mitchell, Alcohol, smoking, and cataracts: the Blue Mountains eye study, *Arch. Ophthalmol.* **1997**, *115*, 1296–1303.

[153] S. E. Hankinson, W. C. Wilett, G. A. Colditz, A prospective study of cigarette smoking and risk of cataract surgery in women, *J. Am. Med. Assoc.* **1992**, *268*, 994–998.

[154] J. J. Harding, Cigarettes and cataract: cadmium or a lack of vitamin C?, *Br. J. Ophthalmol.* **1995**, *79*, 199–200.

[155] R. T. Ravenholt, Cigarette smoking and risk of cataracts, *J. Am. Med. Assoc.* **1993**, *269*, 747–748.

[156] J. J. Harding, R. van Heyningen, Beer, cigarettes and military work as risk factors for cataract, *Dev. Ophthalmol.* **1989**, *17*, 13–16.

[157] R. Hiller, R. D. Sperduto, M. J. Podgor, Cigarette smoking and the risk of development of lens opacities: the Farmingham studies, *Arch. Ophthalmol.* **1997**, *115*, 113–118.

[158] B. E. Klein, R. Klein, K. L. Linton, T. Franke, Cigarette smoking and lens opacities: the Beaver Dam eye study, *Am. J. Prev. Med.* **1993**, *9*, 27–30.

[159] S. Ramakrishnan, K. N. Sulochana, T. Selvaraj, Smoking of beedies and cataract: cadmium and vitamin C in the lens and blood, *Br. J. Ophthalmol.* **1995**, *79*, 202–206.

[160] S. West, Does smoke get in your eyes?, *J. Am. Med. Assoc.* **1992**, *268*, 1025–1026.

[161] S. West, B. Munoz, E. A. Emmett, H. R. Taylor, Cigarette smoking and risk of nuclear cataracts, *Arch. Ophthalmol.* **1989**, *107*, 1166–1169.

[162] S. West, B. Munoz, O. D. Schein, Cigarette smoking and risk for progression of nuclear opacities, *Arch. Ophthalmol.* **1995**, *113*, 1377–1380.

[163] S. West, B. Munoz, S. Vitale, Watermen study II: smoking and nuclear opacities, *Invest. Ophthalmol. Vis. Sci.* **1992**, *33*, 1097.

[164] D. C. Minassian, V. Mehra, J. D. Verrey, Dehydrational crises: a major risk factor in blinding cataract, *Br. J. Ophthalmol.* **1989**, *79*, 100–105.

[165] J. J. Harding, K. Rixon, Is diarrhoea a major cause of cataract in some tropical countries?, *Metab. Pediatr. Ophthalmol.* **1981**, *5*, 161–166.

[166] S. E. Hankinson, M. J. Stampfer, J. M. Seddon, Nutrient intake and cataract extraction in woman: a prospective study, *Brit. Med. J.* **1992**, *305*, 335–339.

[167] R. Hiller, R. D. Sperduto, F. Ederer, Epidemiologic association with cataract in the 1971-1972 national health nutrition examination survey, *Am. J. Epidemiol.* **1983**, *118*, 239–249.

[168] J. M. Weintraub, W. C. Willett, B. Rosner, G. A. Colditz, J. M. Seddon, S. E. Hankinson, A prospective study of the relationship between body mass index and cataract extraction among US women and men, *Nature* **2002**, *26(12)*, 1588–1595.

[169] P. F. Jacques, S. C. Hartz, L. T. Chylack jr., Nutritional status in persons with and without senile cataract: blood vitamin and mineral levels, *Am. J. Clin. Nutr.* **1988**, *48*, 152–158.

[170] B. A. Underwood, P. Arthur, The contribution of vitamin A to public health, *FASEB J.* **1996**, *10(9)*, 1040–1048.

[171] A. Kassoff, A. Ruby, R. R. Margherio, M. L. Klein, R. F. Dreyer, A. Capone Jr., M. Lambert, T. Meredith, D. H. Orth, J. M. Seddon, et al., A randomized, placebo-controlled, clinical trial of high-dose supplementation with vitamins C and E and beta carotene for age-related cataract and vision loss, *Arch. Ophthalmol.* **2001**, *119*, 1439–1452.

[172] B. Munoz, U. Tajchman, T. Bochow, S. West, Alcohol use and risk of posterior subcapsular opacities, *Arch. Ophthalmol.* **1993**, *111*, 110–112.

[173] J. J. Harding, R. van Heyningen, Drugs, including alcohol, that act as risk factors for cataract, and possible protection against cataract by aspirin-like analgesics and cyclopenthiazide, *Br. J. Ophthalmol.* **1988**, *72*, 809–814.

[174] C. I. Phillips, R. M. Clayton, J. Cuthbert, Human cataract risk factors: significance of absention from, and high consumption of, ethanol (U-curve) and non-significance of smoking, *Ophthalmic Res.* **1996**, *28*, 237–247.

[175] L. L. Ritter, B. E. Klein, R. Klein, J. A. Mares-Perlman, Alcohol use and lens opacities in the beaver dam eye study, *Arch. Ophthalmol.* **1993**, *111*, 113–117.

[176] K. Stromland, K. Sundelin, and ophthalmologic observations in offspring of alcohol abusing mothers, *Acta Paediatr.* **1996**, *85*, 1463–1468.

[177] F. I. Caird, A. Pirie, T. G. Ramsell, *Diabetes and the eye*, Blackwell Scientific Publications, Oxford, **1969**.

[178] J. J. Harding, M. Egerton, R. van Heyningen, R. S. Harding, Diabetes, glaucoma, sex, and cataract: analysis of combined data from two case control studies, *Br. J. Ophthalmol.* **1993**, *77*, 2–6.

[179] M. C. Leske, S. Y. Wu, A. Hennis, Diabetes, hypertension, and central obesity as cataract risk factors in a black population. The barbados eye study, *Ophthalmology* **1999**, *106*, 35–41.

[180] R. van Heyningen, J. J. Harding, Risk factors for cataract: diabetes, myopia and sex, *Colloq. INSERM* **1986**, *147*, 381–385.

[181] B. Klein, R. Klein, K. Lee, L. Grady, Statin use and incident nuclear cataract, *J. Am. Med. Assoc.* **2006**, *295(23)*, 2752–2758.

[182] B. Olmedilla, F. Granado, I. Blanco, M. Vaquero, Lutein, but not alpha-tocopherol, supplementation improves visual function in patients with age-related cataracts: a 2-y double-blind, placebo-controlled pilot study, *Nutrition* **2003**, *19(1)*, 21–24.

[183] H. T. V. Vu, L. Robman, A. Hodge, C. A. McCarty, H. R. Taylor, Lutein and zeaxanthin and the risk of cataract: the melbourne visual impairment project, *Invest. Ophthalmol. Vis. Sci.* **2006**, *47(9)*, 3783–3786.

[184] C. Delcourt, I. Carrière, M. Delage, P. Barberger-Gateau, W. Schalch, Plasma lutein and zeaxanthin and other carotenoids as modifiable risk factors for age-related maculopathy and cataract: the POLA study, *Invest. Ophthalmol. Vis. Sci.* **2006**, *47(6)*, 2329–2335.

[185] J. D. Ribaya-Mercado, J. B. Blumberg, Lutein and zeaxanthin and their potential roles in disease prevention, *J. Am. Coll. Nutr.* **2004**, *23(6)*, 567S–587S.

[186] A. Z. Fursova, O. G. Gesarevich, A. M. Gonchar, N. A. Trofimova, N. G. Kolosova, Dietary supplementation with bilberry extract prevents macular degeneration and cataracts in senesce-accelerated OXYS rats, *Adv. Gerontol.* **2005**, *16*, 76–79.

[187] H. Hess, J. J. Knapka, D. A. Newsome, Dietary prevention of cataracts in the pink-eyed RCS rat., *Lag. Anim. Sci.* **1985**, *35*, 47–53.

[188] J. Yamakoshi, M. Saito, S. Kataoka, S. Tokutake, Procyanidin-rich extract from grape seeds prevents cataract formation in hereditary cataractous (ICR/f) rats, *J. Agric. Food Chem.* **2002**, *50(17)*, 4983–4988.

[189] G. Bravetti, Preventive medical treatment of senile cataract with vitamin E and anthocyanosides: clinical evaluation, *Ann. Ottalmol. Clin. Ocul.* **1989**, *115*, 109.

[190] D. L. Williams, P. Munday, The effect of a topical antioxidant formulation including N-acetyl carnosine on canine cataract: a preliminary study, *Vet. Ophthalmol.* **2006**, *9(5)*, 311–316.

[191] Y. Guo, H. Yan, Preventive effect of carnosine on cataract development, *Yan Ke Xue Bao* **2006**, *22(2)*, 85–88.

[192] B. Thylefors, A global initiative for the elemination of avoidable blindness, *Am. J. Ophthalmol.* **1998**, *125*, 90–93.

[193] A. L. Robin, G. Natchiar, R. D. Thulasiraj, G. Venkataswamy, A long-term approach to eliminate cataract blindness, *Ophthalmology* **1997**, *104*, 571–572.

[194] J. C. Javitt, F. Wang, S. K. West, Blindness due to cataract: epidemiology and prevention, *Ann. Rev. Pub. Health* **1996**, *17*, 159–177.

[195] C. Kupfer, The international agency for the prevention of blindness, *Am. J. Ophthalmol.* **1994**, *117*, 253–257.

[196] A. M. Nasr, E. I. Traboulsi, Treatment or prevention?, *Middle East J. Ophthalmol.* **1993**, *1*, 3.

[197] G. J. Johnson, Audit of results of cataract surgery, *Comm. Eye Health* **1992**, *10*, 1–2.

[198] S. K. West, H. A. Quigley, Cataract blindness: what to do?, *Arch. Ophthalmol.* **1991**, *109*, 1665–1666.

[199] A. J. Bron, N. A. Brown, J. M. Sparrow, G. A. Shun-Shin, Medical treatment of cataract, *Eye* **1987**, *1*, 542–550.

[200] C. Kupfer, A decade of progress in the prevention of blindness, *Am. J. Ophthalmol.* **1987**, *104*, 80–83.

[201] C. Kupfer, Bowman lecture. The conquest of cataract: a global challenge, *Trans. Ophthalmol. Soc. UK* **1985**, *104*, 1–10.

[202] P. F. Kador, Overview of the current attempts toward the medical treatment of cataract, *Ophthalmology* **1983**, *90*, 352–364.

[203] G. Venkataswamy, Can cataract surgery be marketed like hamburgers in developing countries?, *Arch. Ophthalmol.* **1993**, *111*, 580.

[204] J. M. Seddon, The differential burden of blindness in the United States, *N. Engl. J. Med.* **1991**, *325*, 1440–1442.

[205] B. Zhang, S. Gao, W. Tao, An epidemiological survey of cataract in China, *Dev. Ophthalmol.* **1997**, *27*, 89–94.

[206] T. Snellingen, D. J. Apple, The south Asian cataract management study. Part I. The first 662 cataract surgeries: a preliminary report, *Br. J. Ophthalmol.* **1995**, *79*, 1029–1035.

[207] S. P. Zhu, J. J. Xu, Q. Yu, An epidemiologic survey of blindness and low vision in persons over 45 years old in Doumen county, *Chung Hua Yen Ko Tsa Chih* **1994**, *30*, 386–388.

[208] C. Hu, J. L. Zhao, Q. N. Zhang, Establishment of a primary eye care network and creation of a cataract-free zone in Shunyi county of Beijing, *Chung Hua Yen Ko Tsa Chih* **1994**, *30*, 134–137.

[209] Y. S. Cai, Y. S. Hao, Is outpatient cataract surgery available alternative in China?, *Asia Pac. J. Ophthalmol.* **1993**, *5*, 49.

[210] W. Mao, J. Xu, Z. Wu, Survey and treatment of the blind in Xinhui, Guangdong, China, *Yen Ko Hsueh Pao* **1992**, *8*, 147–151.

[211] X. J. Song, An epidemiological survey of blindness and low vision in Hebei province, *Chung Hua Yen Ko Tsa Chih* **1992**, *28*, 105–107.

[212] J. J. Xu, Q. Yu, An epidemiological survey and treatment of blindness in Kaipin county of Guangdong province, *Chung Hua Yen Ko Tsa Chih* **1992**, *28*, 265–266.

[213] S. Y. Zhang, The 1987 national epidemiological survey of blindness and low vision in China, *Chung Hua Yen Ko Tsa Chih* **1992**, *28*, 260–264.

[214] S. Y. Zhang, L. H. Zou, Y. Q. Gao, National epidemiological survey of blindness and low vision in China, *Chin. Med. J.* **1992**, *105*, 603–608.

[215] B. C. Sun, Prevention of blindness in China, *Asia Pac. J. Ophthalmol.* **1991**, *3*, 60–61.

[216] X. L. Su, S. R. Liu, Changing prevalence of blindness in 30 years in Guangdong Province, *Chung Hua Yen Ko Tsa Chih* **1990**, *26*, 108–110.

[217] J. X. Zhang, A survey of blindness and low vision in Shanxi province, *Chung Hua Yen Ko Tsa Chih* **1990**, *26*, 39–42.

[218] M. Hogeweg, Y. Sapkota, A. Foster, Acceptability of aphakic correction. Results from Karnali eye camps in Nepal, *Acta Ophthalmol.* **1992**, *70*, 407–412.

[219] E. G. Hale, I. M. Strachan, Non-surgical factors in the correction of aphakia, *Trans. Ophthalmol. Soc. UK* **1981**, *101*, 62–64.

[220] A. I. Ivashina, Aniseikonia for near vision with unilateral aphakia corrected by intraocular lenses, *Ann. Ophthalmol.* **1981**, *13*, 1309–1311.

[221] O. H. Dabezies Jr., Defects of vision through aphakic spectacle lenses, *Ophthalmology* **1979**, *86*, 352–379.

[222] H. Gernet, The binocular confusion in unilateral aphakia, *Ann. Ophthalmol.* **1979**, *11*, 617–621.

[223] A. E. Sloane, Perspectives on management of aphakia after 40 years, *Ophthalmic Surg.* **1977**, *8*, 75–77.

[224] J. F. H. Hilbourne, Social and other aspects of adjustments to single eye cataract extraction in elderly patients, *Trans. Ophthalmol. Soc. UK* **1975**, *9*, 254–259.

[225] P. J. Fenton, Temps: temporary protective aphakic spectacles, *Trans. Ophthalmol. Soc. UK* **1969**, *88*, 451–460.

[226] C. S. McLemore, Aphakic correction from an aphake's point of view, *Arch. Ophthalmol.* **1965**, *74*, 443.

[227] R. C. Troutman, Artiphakia and aniseikonia, *Am. J. Ophthalmol.* **1963**, *56*, 602–639.

[228] A. Linksz, Aniseikonia; with notes on the Jackson-Lancaster controversy. The XV Jackson memorial lecture, *Am. J. Ophthalmol* **1959**, *48*, 441–462.

[229] A. C. Woods, The adjustment to aphakia, *Am. J. Ophthalmol.* **1952**, *35*, 118–122.

[230] B. Thylefors, A global initiative for the elimination of avoidable blindness, *J. Comm. Eye Health* **1998**, *11(25)*, 1–3.

[231] W. J. Stark, G. P. Kracher, C. L. Cowan, Extended wear contact lenses and intraocular lenses for aphakic corrections, *Am. J. Ophthalmol.* **1979**, *88*, 532–542.

[232] J. T. Wilensky, *Intraocular Lenses*, Appleton-Century-Crofts, New York, **1975**.

[233] N. H. L. Ridley, Intra-ocular lenses - past, present and future, *Trans. Ophthalmol. Soc. UK* **1964**, *84*, 5–14.

[234] D. P. Choyce, Correction of unilateral aphakia by means of an acrylic anterior chamber lens, *Ophthalmology* **1960**, *49*, 417–420.

[235] D. P. Choyce, The correction of uniocular aphakia by means of all-acrylic anterior chamber implants, *Am. J. Ophthalmol.* **1960**, *49*, 417–439.

[236] D. P. Choyce, Correction of uni-ocularaphakia by means of anterior chamber acrylic implants, *Trans. Ophthalmol. Soc. UK* **1958**, *78*, 459–470.

[237] C. D. Binkhorst, The iridocapsular (two-loop) lens and the iris-clip (four-loop) lens in pseudophakia, *Trans. Am. Acad. Ophthalmol.* **1973**, *77*, 589–617.

[238] L. G. Vargas, Q. Peng, M. Escobar-Gomez, J. M. Schmidbauer, D. J. Apple, Overview of modern foldable intraocular lenses and clinically relevant anatomy and histology of the crystalline lens, *Int. Ophthalmol. Clin.* **2001**, *41(3)*, 1–15.

[239] P.-R. Preußner, J. Wahl, D. Weitzel, S. Berthold, K. Kriechbaum, O. Findl, Predicting postoperative intraocular lens position and refraction, *J. Cataract Refract. Surg.* **2004**, *30(10)*, 2077–2083.

[240] B. Dick, B. Schwenn O. Stoffelns, P. N., Adhesion of liquid perfluorocarbone to different IOL materials. A light microscopic investigation, *Ophthalmologe* **1998**, *95(5)*(95), 301–306.

[241] H. C. Seward, Folding intraocular lenses: materials and methods, *Br. J. Ophthalmol.* **1997**, *81(5)*, 340–341.

[242] R. G. A. Faragher, S. P. Denyer, S. Dropoova, P. R. Gard, B. Hall, G. W. Hanlon, S. A. Jones, A. W. Lloyd, S. V. Makhalovsky, C. J. Olliff, M. Riding, P. H. Rosen, Novel base materials for intraocular lenses, *Eur. J. Pharm. Sci.* **1996**, *4(Suppl. 1)*, 175.

[243] D. Leaming, Practice styles and preferences of ASCRS members: 1995 survey, *J. Cataract Refract. Surg.* **1996**, *22*, 931–939.

[244] D. P. Hainsworth, S. I. Chen, T. A. Cox, G. J. Jaffe, Condensation on polymethylmethacrylate, acrylic polymer, and silicone intraocular lenses after fluid-air exchange in rabbits, *Ophthalmology* **1996**, *103*, 1410–1418.

[245] G. D. Barett, *The evolution of implants, in P. Sourdille, Ed. Evolution of microsurgery*, S. Karger, Basel, **1991**.

[246] T. Oshika, Y. Suzuki, H. Kizaki, S. Yaguchi, Two year clinical study of a soft acrylic intraocular lens, *J. Cataract Refract. Surg.* **1996**, *22*, 104–109.

[247] P. B. Percivals, A. J. Jafree, Preliminary results with a new hydrogel intraocular lens, *Eye* **1994**, *8*, 672–675.

[248] G. D. Barrett, A new hydrogel intraocular lens design, *J. Cataract Refract. Surg.* **1994**, *20*, 18–25.

[249] J. S. Cumming, Postoperative complications and uncorrected acuities after implantation of plate haptic silicone and three-piece silicone IOLs, *J. Cataract Refract. Surg.* **1993**, *19*, 263–275.

[250] K. P. Thompson, Intraocular lens for restoring accommodation and allows adjustment of optical power, U.S. Patent 5 607 472, **1997**.

[251] C. D. Kelman, Cataract, emulsification and aspiration, *Trans. Ophthalmol. Soc. UK* **1970**, *90*, 13–22.

[252] A. Gullstrand, *Die Dioptrik des Auges, in H. von Helmholtz, Ed. Handbuch der physiologischen Optik*, Springer Verlag, Hamburg, 3rd ed., **1909**.

[253] M. D. Bailey, G. L. Mitchell, D. K. Dhaliwal, B. S. Boxer Wachler, K. Zadnik, Patient satisfaction and visual symptoms after laser in situ keratomileusis, *Ophthalmology* **2003**, *110(7)*, 1371–1378.

[254] C. N. McGhee, J. P. Craig, N. Sachdev, K. H. Weed, A. Brown, Functional, psychological, and satisfaction outcomes of laser in situ keratomileusis for high myopia, *J. Cataract Refract. Surg.* **2000**, *26(4)*, 497–509.

[255] P. A. Tipler, *Electricity and magnetism, light & elementary modern physics*, 5th ed., Freeman, New York, **2004**.

[256] G. Wyszecki, W. S. Stiles, *Color science: concepts and methods, quantitative data and formulae*, 2nd ed., Wiley, New York, **1982**.

[257] J. E. Greivenkamp, *Field guide to geometrical optics*, SPIE Press, Bellingham, **2004**.

[258] E. Hecht, *Optics*, 2nd ed., Addison-Wesley, Reading, **1987**.

[259] A. Lembares, X.-H. Hu, G. W. Kalmus, Absorption Spectra of Corneas in the Far Ultraviolet Region, *Invest. Ophthalmol. Vis. Sci.* **1997**, *38(6)*, 1283–1287.

[260] E. A. Boettner, J. R. Wolter, Transmission of the ocular media, *Invest. Ophthalmol.* **1962**, *1(6)*, 776–783.

[261] W. Ambach, M. Blumthaler, T. Schöpf, E. Ambach, F. Katzgraber, F. Daxecker, A. Daxer, Spectral transmission of the optical media of the human eye with respect to keratitis and cataract formation, *Doc. Ophthalmol.* **1994**, *88*, 165–173.

[262] J. D. Jackson, *Classical Electrodynamics*, 3rd ed., Wiley, New York, **1999**.

[263] R. King, *Fundamental electromagnetic theory*, 2nd ed., Dover Publications, New York, **1963**.

[264] J. Träger, H.-C. Kim, M. Schraub, N. Hampp, *Photo Reactions Induced by Two-photon Absorption in M. Lackner, Ed. Lasers in Chemistry Vol. 2*, Wiley-VCH, Weinheim, **2008**.

[265] W. Demtröder, *Experimentalphysik, Vol. 2: Elektrizität und Optik*, 2nd ed., Springer, Berlin, **1999**.

[266] M. Born, *Optik*, 3rd ed., Springer, Berlin, **1972**.

[267] D. W. van Krevelen, *Properties of Polymers: Their Correlation with Chemical Structure, Their Numerical Estimation and Prediction from Additive Group Contributions*, 3rd ed., Elsevier, Amsterdam, **1990**.

[268] H. A. Lorentz, Über die Beziehung zwischen der Fortpflanzungsgeschwindigkeit des Lichtes und der Körperdichte, *Ann. Phys.* **1880**, *9*, 641–665.

[269] L. V. Lorenz, Über die Refractionsconstante, *Ann. Phys.* **1880**, *11*, 70–103.

[270] T. Kada, A. Obara, T. Watanabe, S. Miyata, Fabrication of refractive index distributions in polymer using a photochemical reaction, *J. Appl. Phys.* **2000**, *87(2)*, 638–642.

[271] A. I. Vogel, *Practical Organic Chemistry*, Longmans, London, **1956**.

[272] D. W. van Krevelen, *in J. Bicerano, Ed. Computational Modeling of Polymers*, Marcel Dekker, New York, **1992**.

[273] J. C. Seferis, *in J. Brandrup, E.H. Immergut, Eds. Polymer Handbook*, Wiley, New York, 3rd ed., **1989**.

[274] C.-J. Yang, S. A. Jenekhe, Group Contribution to Molar Refraction and Refractive Index of Conjugated Polymers, *Chem. Mater.* **1995**, *7(7)*, 1276–1285.

[275] J. H. Gladstone, T. P. Dale, Researches on the Refraction, Dispersion, and Sensitiveness of Liquids, *Philos. Trans. R. Soc. Lond. A* **1863**, *153*, 317–344.

[276] T. P. Dale, J. H. Gladstone, On the Influence of Temperature on the Refraction of Light, *Philos. Trans. R. Soc. Lond. A* **1858**, *148*, 887–894.

[277] A. I. Vogel, W. T. Cresswell, G. H. Jeffery, J. Leicester, Bond refractions and bond parachors, *Chem. Ind.* **1950**, 358.

[278] A. I. Vogel, W. T. Cresswell, G. H. Jeffery, J. Leicester, Calculation of the refractive indices of liquid organic compounds: bond molecular refraction coefficients, *Chem. Ind.* **1951**, 376.

[279] J. A. Osaheni, S. A. Jenekhe, Effects of Molecular Structure on the Electroactive and Optical Properties of Conjugated Rigid-Rod Poly(benzobisazoles), *Chem. Mater.* **1995**, *7(4)*, 672–682.

[280] W.-C. Chen, S. A. Jenekhe, J. S. Meth, H. Vanherzeele, Refractive Index and Nonlinear Optical Properties of Polyaniline Derivatives, *J. Polym. Sci. B: Polym. Phys.* **1994**, *32(1)*, 195–200.

[281] C. J. Yang, S. A. Jenekhe, Effects of Structure on Refractive Index of Conjugated Polyimines, *Chem. Mater.* **1994**, *6(2)*, 196–203.

[282] A. K. Agrawal, S. A. Jenekhe, Thin-film processing and optical properties of conjugated rigid-rod polyquinolines for nonlinear optical applications, *Chem. Mater.* **1992**, *4(1)*, 95–104.

[283] C. Wochnowski, S. Metev, G. Sepold, UV-laser-assisted modification of the optical properties of poly(methyl methacrylate), *Appl. Surf. Sci.* **2000**, *154-155*, 706–711.

[284] R. A. George, D. A. Martin, E. G. Wilson, The ultraviolet spectra of polyethylene and long-chain paraffins, *J. Phys. C: Solid State Phys.* **1972**, *5(8)*, 871–878.

[285] S. Onari, Vacuum Ultraviolet Absorption Spectra of Synthesized Polymer Film, *J. Phys. Soc. Jpn.* **1969**, *26(8)*, 500–504.

[286] A. Holländer, J. E. Klemberg-Sapieha, M. E. Wertheimer, Vacuum-ultraviolet induced oxidation of the polymers polyethylene and polypropylene, *J. Polym. Sci. A: Polym. Chem.* **1995**, *33(12)*, 2013–2025.

[287] A. Holländer, J. E. Klemberg-Sapieha, M. E. Wertheimer, The Influence of Vacuum-Ultraviolett Radiation on Poly(ethylene terephthalate), *J. Polym. Sci. A: Polym. Chem.* **1996**, *34(8)*, 1511–1516.

[288] J. F. Rabek, *Photodegradation of Polymers: Physical Characteristics and Applications*, Springer, Berlin, **1996**.

[289] C. Wochnowski, K. Meteva, S. Metev, Laser Photochemical Modification of Polymers and Applications in Optical Information Technology, *Proc. SPIE* **2003**, *4830*, 396–402.

[290] A. K. Baker, P. E. Dyer, Refractive-index modification of polymethylmethacrylate (PMMA) thin films by KrF-laser irradiation, *Appl. Phys. A.* **1993**, *57(6)*, 543–544.

[291] J. Yu, X. Tao, H. Tam, M. Suleyman Demokan, Modulation of refractive index and thickness of poly(methyl methacrylate) thin films with UV irradiation and heat treatment, *Appl. Surf. Sci.* **2005**, *252*, 1283–1292.

[292] A. Torikai, T. Hattori, T. Eguchi, Wavelength effect on the photoinduced reaction of polymethylmethacrylate, *J. Polym. Sci. A: Polym. Chem.* **1995**, *33(11)*, 1867–1871.

[293] T. Mitsuoka, A. Torikai, K. Fueki, Wavelength sensitivity of the photodegradation of poly(methyl methacrylate), *J. Appl. Polym. Sci.* **1993**, *47(6)*, 1027–1032.

[294] T. Kada, T. Hiramatsu, K. Ogino, C. Liang, H. Machida, K. Kiso, S. Miyata, Fabrication of Refractive Index Profiles in Poly (Methyl Methacrylate) using Ultraviolet Rays Irradiation, *Jpn. J. Appl. Phys.* **2002**, *41(2a)*, 876–880.

[295] D. S. Dunn, A. J. Ouderkirk, Laser-induced refractive index change in polymers, *AIP Conference Proc.* **1989**, *191(Adv. Laser Sci. IV)*, 375–378.

[296] T. Goto, J. Kato, T. Yamashita, Transient refractive index change behavior of poly(N-isopropylacrylamide) gels via laser induced photo-thermal conversion process, *J. Photopolym. Sci. Technol.* **2004**, *17(2)*, 285–290.

[297] L. Ding, R. Blackwell, J. F. Künzler, W. H. Knox, Large refractive index change in silicone-based and non-silicone-based hydrogel polymers induced by femtosecond laser micromachining, *Opt. Express* **2006**, *14(24)*, 11901–11909.

[298] N. Takeshima, Y. Narita, S. Tanaka, Y. Kuroiwa, K. Hirao, Fabrication of high-efficiency diffraction gratings in glass, *Opt. Lett.* **2005**, *30*, 352–354.

[299] N. Takeshima, Y. Kuroiwa, Y. Narita, S. Tanaka, K. Hirao, Fabrication of aperiodic structure with a high refractive-index difference by femtosecond laser pulses, *Opt. Express* **2004**, *12*, 4019–4024.

[300] Y. Kawaguchi, Y. Moroishi, T. Inoue, Radiation sensitive refractive index changing composition and refractive index changing method, U.S. Patent Application US 2003/0139486 A1, **2003**.

[301] Y. Kawaguchi, Y. Moroishi, T. Inoue, K. Mune, Photochemically refractive-index-changing polymer, photochemically refractive-index-changing polymer composition, and method of refractive index regulation, U.S. Patent Application US 2007/0066705 A1, **2007**.

[302] Y. Kawaguchi, Y. Moroishi, T. Inoue, Optical refractive index-modifying polymer composition, hologram recording material and method of controlling refractive index, U.S. Patent Application US 2007/0128523 A1, **2007**.

[303] B. Bilen, Y. Skarlatos, G. Aktas, M. N. Inci, T. Dispinar, M. M. Kose, A. Sanyal, In situ measurement of humidity induced changes in the refractive index and thickness of polyethylene glycol thin films, *J. Appl. Phys.* **2007**, *102*, 073534.

[304] O. Lyutakov, V. Švorčík, I. Huttel, J. Siegel, N. Kasálková, P. Slepička, Refractive index of polymethylmethacrylate oriented by fluid temperature under electical field, *J. Mater. Sci.: Mater. Electron.* **2008**, *19*, 1064–1068.

[305] L. Nikolova, T. Todorov, Volume Amplitude Holograms in Photodichroic Materials, *Opt. Acta* **1977**, *24(12)*, 1179–1192.

[306] T. Todorov, N. Tomova, L. Nikolova, High-sensitivity material with reversible photoinduced anisotropy, *Opt. Commun.* **1983**, *47(2)*, 123–126.

[307] T. Todorov, L. Nikolova, N. Tomova, Polarization holography 1: A new high-efficiency organic material with reversible photoinduced birefringence, *Appl. Opt.* **1984**, *23(23)*, 4309–4312.

[308] T. Todorov, L. Nikolova, N. Tomova, Polarization holography 2: Polarization holographic gratings in photoanisotropic materials with and without intrinsic birefringence, *Appl. Opt.* **1984**, *23(24)*, 4588–4591.

[309] T. Todorov, L. Nikolova, K. Stoyanova, N. Tomova, Polarization holography 3: Some applications of polarization holographic recording, *Appl. Opt.* **1985**, *24(6)*, 785–788.

[310] C. J. G. Kirkby, R. Cush, I. Bennion, Optical nonlinearity and bistability in organic photochromic thin films, *Opt. Commun.* **1983**, *56(4)*, 288–292.

[311] D. Oesterhelt, C. Bräuchle, N. Hampp, Bacteriorhodopsin: A Biological Material for Information Processing, *Quart. Rev. Biophys.* **1991**, *24*, 425–478.

[312] T. Lueckemeyer, H. Franke, Profiles in Volume Phase Holograms in Dichlorobis(cyclopentadienyl)titanium dichloride, *Appl. Phys. B: Lasers Opt.* **1988**, *46(2)*, 203–208.

[313] N. Tanio, M. Irie, Photooptical Switching of Polymer Waveguide Containing Photochromic Diarylenes, *Jpn. J. Appl. Phys.* **1994**, *33(3a)*, 1550–1553.

[314] N. Tanio, M. Irie, Refractive Index of Organic Photochromic Dye-Amorphous Polymer Composites, *Jpn. J. Appl. Phys.* **1994**, *33(7a)*, 3942–3946.

[315] F. Ebisawa, M. Hoshino, K. Sukegawa, Self-holding photochromic polymer Mach-Zehnder optical switch, *Appl. Phys. Lett.* **1994**, *65(23)*, 2919–2921.

[316] K. W. Beeson, K. A. Horn, M. J. McFarland, A. Nahata, C. Wu, J. T. Yardley, *in S.R. Marder, J.E. Sohn and G.D. Stucky, Eds. Materials for nonlinear optics: Chemical perspectives, ACS Symposium Series No.455*, American Chemical Society, washington d.c. ed., **1991**, p. Chap. 20.

[317] K. Kinoshita, K. Horie, S. Morino, T. Nishikubo, Large photoinduced refractive index changes of a polymer containing photochromic norbornadiene groups, *Appl. Phys. Lett.* **1997**, *70(22)*, 2940–2942.

[318] S. Murase, K. Kinoshita, K. Horie, S. Morino, Photo-optical Control with Large Refractive Index Changes by Photodimerization of Poly(vinyl cinnamate) Film, *Macromolecules* **1997**, *30(25)*, 8088–8090.

[319] A. Nagata, T. Sakaguchi, T. Ichihashi, M. Miya, K. Ohta, Refractive index decrease during photocrosslinking in photopolymers suitable for holographic recording, *Macromol. Rapid. Commun.* **1997**, *18(2)*, 191–196.

[320] S. Murase, K. Horie, Large Photoinduced Refractive Index Changes of Transparent Polymer Films Containing Photoeliminable Diazo and Azido Groups, *Macromolecules* **1999**, *32(4)*, 1103–1110.

[321] S. R. Marder, N. Peyghambarian, B. Kippelen, B. Volodin, E. Hendrickx, Process of changing the refractive index of a composite containing a polymer and a compnd having large dipole moment and polarizability and applications thereof, U.S. Patent 6 090 332, **2000**.

[322] Y. Shi, W. H. Steier, L. Yu, M. Chen, L. R. Dalton, Large stable photoinduced refractive index change in a nonlinear optical polyester polymer with disperse red side groups, *Appl. Phys. Lett.* **1991**, *58(11)*, 1131–1133.

[323] H. Kurihara, A. Shishido, T. Ikeda, Evaluation of photoinduced change in refractive index of a polymer film doped with an azobenzene liquid crystal by means of a prism-coupling method, *J. Appl. Phys.* **2005**, *98*, 083510(5pp).

[324] Y. Yang, J. Yin, Z. Cao, Q. Shen, X. Chen, Real-time investigation photobleaching process using non-scanning ATR method: Measurement of the refractive index and the thickness of the polymer, *Mater. Lett.* **2006**, *60*, 2470–2474.

[325] W.-H. Lee, P. H. Voisin, Method of using diazotype photographic materials with preexposure treatment to form uniform sites of refractive index, U.S. Patent 4 508 808, **1985**.

[326] E. Ortyl, S. Kucharski, Refractive Index Modulation in Polymeric Photochromic Films, *Cent. Eur. J. Chem.* **2003**, *2*, 137–159.

[327] E. Ortyl, S. Kucharski, T. Gotszalk, Refractive index modulation in the polyurethane films containing diazo sulfonamide chromophores, *Thin Solid Films* **2005**, *479*, 288–296.

[328] T. Ikeda, Photochemical Modulation of Refractive Index by Means of Photsensitive Liquid Crystals, *Mol. Cryst. Liq. Cryst.* **2001**, *364*, 187–197.

[329] M. Hoshino, F. Ebisawa, T. Yoshida, K. Sukegawa, Refractive index change in photochromic diarylethene derivatives and its application to optical switching devices, *J. Photochem. Photobiol. A: Chem.* **1997**, *105*, 75–81.

[330] K. Horie, S. Murase, S. Takahashi, M. Teramoto, H. Furukawa, Photochemically-Induced Refractive Index and Fluorescence Patterning on Polymer Films, *Macromol. Symp.* **2003**, *195*, 201–208.

[331] E. Kim, Y.-K. Choi, M.-H. Lee, Photoinduced Refractive Index Change of a Photochromic Diarylethene Polymer, *Macromolecules* **1999**, *32(15)*, 4855–4860.

[332] K. Sasaki, T. Nagamura, Ultrafast wide range all-optical switch using complex refractive-index changes in a composite film of silver and polymer containing photochromic dye, *J. Appl. Phys.* **1998**, *83(6)*, 2894–2900.

[333] K. Sasaki, T. Nagamura, Ultrafast all-optical switch using complex refractive index changes of thin films containing photochromic dye, *Appl. Phys. Lett.* **1997**, *71(4)*, 434–436.

[334] K. Tanaka, K. Shima, H. Kondoh, T. Igarashi, T. Sakurai, Photocontrol of the Refractive Index of Poly(methyl methacrylate) with Nitrone Additive, *J. Appl. Polym. Sci.* **2004**, *93*, 2517–2520.

[335] T. Nagamura, T. Hamada, Novel all optical light modulation based on complex refractive index changes of organic dye-doped polymer film upon photoexcitation, *Appl. Phys. Lett.* **1996**, *69(9)*, 1191–1193.

[336] T. Nagamura, K. Sasaki, F. Iizuka, T. Adachi, I. Yoshida, Ultrafast all-optical spatial light modulation based on complex refractive index changes of copper phthalocyanine-doped polymer film upon photoexcitation in guided mode geometry, *Opt. Commun.* **2002**, *205*, 107–112.

[337] M. Leclerc, Polyfluorenes: Twenty years of progress, *J. Polym. Sci. A: Polym. Chem.* **2001**, *39(17)*, 2867–2873.

[338] P. N. Stavrinou, G. Ryu, M. Campoy-Quiles, D. D. C. Bradley, The change in refractive index of poly(9,9-dioctylfluorene) due to adoption of the β-phase chain confirmation, *J. Phys.: Condens. Matter* **2007**, *19*, 466107(14pp).

[339] T. Nagamura, R. Matsumoto, A. Naito, Y. Nagai, Highly sensitive ultrafast all-optical light modulation by complex refractive-index changes in guided mode geometry composed of a photoresponsive polymer and a low-refractive index polymer., *Appl. Phys. Lett.* **2005**, *87*, 041107(3pp).

[340] Y. Kashiyama, J. He, S. Machida, K. Horie, Large Photoinduced Refractive Index Change in a Polyimide Film by Charge-Transfer Complex Formation with a Polymer-Bound Phenylazide Fragment, *Macromol. Rapid Commun.* **2001**, *22*, 185–188.

[341] J. Kato, K. Yuasa, H. Matsushita, Y. Maekawa, K. Enomoto, T. Ishii, K. Itoh, T. Yamashita, Refractive Index Change and Color Imaging of Acid-Chromic Polymer Films Using EB-Induced Acid Generation, *J. Photopolym. Sci. Technol.* **2006**, *19(1)*, 105–110.

[342] K. Lee, E. Miller, N. S. Sariciftci, J. C. Hummelen, F. Wudl, A. J. Heeger, Photoinduced absorption and photoinduced reflectance in conducting polymer/methanofullerene films: Nonlinear-optical changes in the complex index of refraction, *Phys. Rev. B* **1996**, *54(15)*, 10525–10529.

[343] E. K. Miller, K. Lee, K. Hasharoni, J. C. Hummelen, F. Wudl, A. J. Heeger, Photo-induced changes in the complex index of refraction in conjugated polymer/fullerene belends, *J. Chem. Phys.* **1998**, *108(4)*, 1390–1394.

[344] U. Streppel, P. Dannberg, C. Waechter, D. Michaelis, R. Kowarschik, A. Braeuer, Influence and utilization of UV-induced refractive index changes of photopolymers for the fabrication of 3D micro-optical elements, *Proc. SPIE* **2003**, *4991*, 321–332.

[345] Y. Kato, K. Horie, Photoinduced Refractive Index Change of Polymer Films Containing Mesoionic Sulfur-Substituted Phenyloxatriazolones, *Macromol. Chem. Phys.* **2002**, *203(16)*, 2290–2295.

[346] A. Theis, H. Ritter, F. Bhme, C. Klinger, S. Mittler, B. Menges, Photosensitive Mesoionic Main-Chain Polymers: Synthesis and Anisotropic Changes of the Refractive Index on Irradiation of Spin-Coated Films, *Chem. Mater.* **2002**, *14(5)*, 2109–2112.

[347] T. Höfler, T. Grießer, X. Gstrein, G. Trimmel, G. Jakopic, W. Kern, UV reactive polymers for refractive index modulation based on the photo-Fries rearrangement, *Polymer* **2007**, *48*, 1930–1939.

[348] G. W. Sluggett, N. J. Turro, H. D. Roth, Rh(III)-Photosensitized Interconversion of Norbornadiene and Quadricyclane, *J. Phys. Chem. A* **1997**, *101*, 8834–8838.

[349] G. Langer, T. Kavc, W. Kern, G. Kranzelbinder, E. Toussaere, Refractive Index Changes in Polymers Induced by Deep UV Irradiation and Subsequent Gas Phase Modification, *Macromol. Chem. Phys.* **2001**, *202*, 3459–3467.

[350] W. Schöfberger, N. Zaami, K. A. Mahler, G. Langer, G. Jakopic, A. Pogantsch, W. Kern, F. Stelzer, Photoinduced Changes of the Refractive Index in Substituted Fluorenyl-*p*-phenylene Copolymers, *Macromol. Chem. Phys.* **2003**, *204*, 779–786.

[351] T. Kavc, W. Kern, C. Zenz, G. Leising, G. Kranzelbinder, E. Toussaere, Phase Gratings in Photoreactive Polymers: A Way to Optically Pumped Organic Lasers, *Monatsh. Chem.* **2001**, *132*, 531–540.

[352] T. Fujinami, M. A. Mehta, Y. Yamada, M. Hiramatsu, I. Hirano, Potential Switching of Optical Properties in Polymer Electrolytes, *J. Polym. Sci. B: Polym. Phys.* **1997**, *35*, 2057–2062.

[353] K. Harada, K. Munakata, M. Itoh, T. Yatagai, Y. Honda, S. Umegaki, High-speed light modulation using complex refractive-index changes of electro-optic polymers, *Appl. Phys. Lett.* **2000**, *77(23)*, 3683–3685.

[354] M. Osterfeld, H. Franke, Monitoring electric field induced refractive index changes in liquid crystals with polymer lightguides, *Mol. Cryst. Liq. Cryst.* **1990**, *183*, 321–328.

[355] S. L. Subota, V. Y. Reshetnyak, S. P. Pavliuchenko, T. J. Sluckin, Numerical Modeling of Tunable Liquid-Crystal-Polymer-Network Lens, *Mol. Cryst. Liq. Cryst.* **2008**, *489*, 366–379.

[356] O. Diels, K. Alder, Synthesen in der hydroaromatischen Reihe, *Justus Liebigs Ann. Chem.* **1928**, *460(1)*, 98–122.

[357] O. Diels, K. Alder, Synthesen in der hydroaromatischen Reihe. III. Mitteilung: Synthese von Terpenen, Camphern, hydroaromatischen und heterocyclischen Systemen, *Justus Liebigs Ann. Chem.* **1929**, *470(1)*, 62–103.

[358] O. Diels, K. Alder, Synthesen in der hydroaromatischen Reihe, IV. Mitteilung: Über die Anlagerung von Maleinsäure-anhydrid an arylierte Diene, Triene und Fulvene, *Ber. Dtsch. Chem. Ges.* **1929**, *62(8)*, 2081–2087.

[359] O. Diels, K. Alder, Synthesen in der hydroaromatischen Reihe, V. Mitteilung: Über Δ^4-Tetrahydro-*o*-phthalsäure, *Ber. Dtsch. Chem. Ges.* **1929**, *62(8)*, 2087–2090.

[360] R. B. Woodward, R. Hoffmann, Stereochemistry of Electrocyclic Reactions, *J. Am. Chem. Soc.* **1965**, *87(2)*, 395–397.

[361] F. A. Carey, R. J. Sundberg, *Advanced Organic Chemistry, Part A: Structure and Mechanisms*, 5$^{\text{th}}$ ed., Springer, New York, **2008**.

[362] G. O. Schenck, I. von Wilucki, C. H. Krauch, Photosensibilisierte Cyclodimerisation von Cumarin, *Chem. Ber.* **1962**, *95(6)*, 1409–1412.

[363] C. H. Krauch, S. Farid, G. O. Schenck, Photo-C4-Cyclodimerisation von Cumarin, *Chem. Ber.* **1966**, *99(2)*, 625–633.

[364] T. Wolff, H. Görner, Photodimerization of coumarin revisted: Effect of solvent polarity on the triplet reactivity and product pattern, *Phys. Chem. Chem. Phys.* **2004**, *6*((2)), 368–376.

[365] A. W. K. de Jong, Über die Einwirkung des Lichtes auf die Zimtsäuren und über die Konstitution der Truxillsäuren, *Ber. Dtsch. Chem. Ges.* **1922**, *55(2)*, 463–474.

[366] H. Stobbe, F. K. Steinberger, Lichtreaktionen der trans-und cis-Zimtsäuren, *Ber. Dtsch. Chem. Ges.* **1922**, *55(8)*, 2225–2245.

[367] A. W. K. de Jong, Über die Konstitution der Truxill- und Truxinsäuren und über die Einwirkung des Sonnenlichtes auf die Zimtsäuren und Zimtsäure-Salze, *Ber. Dtsch. Chem. Ges.* **1923**, *56(4)*, 818–832.

[368] H. Stobbe, A. Lehfeldt, Polymerisationen und Depolymerisationen durch Licht verschiedener Wellenlänge, II.: α- und β-trans-Zimtsäure, allo-Zimtsäure und ihre Dimeren, *Ber. Dtsch. Chem. Ges.* **1925**, *58(10)*, 2415–2427.

[369] X. Coqueret, A. El Achari, A. Hajaiej, A. Lablache-Combier, C. Loucheux, L. Randrianarisoa, Some aspects of the reactivity of photo-dimerizable esters grafted onto silicone main chain polymers, *Makromol. Chem.* **1991**, *192(7)*, 1517–1534.

[370] P. L. Egerton, E. M. Hyde, J. Trigg, A. Payne, P. Beynon, M. V. Mijovic, A. Reiser, Photocycloaddition in liquid ethyl cinnamate and in ethyl cinnamate glasses. The photoreaction as a probe into the micromorphology of the solid, *J. Am. Chem. Soc.* **1981**, *103(13)*, 3859–3863.

[371] J. Rennert, Photodimer formation in the condensed phase, *Photogr. Sci. Eng.* **1971**, *15(1)*, 60–63.

[372] P. L. Egerton, E. Pitts, A. Reiser, Photocycloaddition in solid poly(vinyl cinnamate). The photoreactive polymer matrix as an ensemble of chromophore sites, *Macromolecules* **1981**, *14(1)*, 95–100.

[373] L. M. Minsk, J. G. Smith, W. P. Van Deusen, J. F. Wright, Photosensitive polymers. I. Cinnamate esters of poly(vinyl alcohol) and cellulose, *J. Appl. Polym. Sci.* **1959**, *2(6)*, 302–307.

[374] E. M. Robertson, W. P. van Deusen, L. M. Minsk, Photosensitive polymers. II. Sensitization of poly(vinyl cinnamate), *J. Appl. Polym. Sci.* **1959**, *2(6)*, 308–311.

[375] M. D. Cohen, G. M. J. Schmidt, F. I. Sonntag, Topochemistry. Part II. The Photochemistry of trans-Cinnamic Acid, *J. Chem. Soc.* **1964**, 2000–2013.

[376] H. Stobbe, K. Bremer, Zur Photochemie der Zimtsäuren, der Chalkone und ihrer Derivate. (II. Mitteilung Über Truxill- und Truxinketone), *J. Prakt. Chem.* **1929**, *123(1)*, 1–60.

[377] R. Stoermer, K. Cruse, Die Sonderstellung der ε-Truxillsäure; Truxillketone (XIX. Mitteil.), *Ber. Dtsch. Chem. Ges.* **1935**, *68(11)*, 2117–2124.

[378] R. Stoermer, H. Starck, H.-E. Anker, Ring-Erweiterungen im Gebiet der Truxinsäuren (XXII. Mitteil.), *Ber. Dtsch. Chem. Ges.* **1937**, *70(3)*, 483–498.

[379] R. E. Lutz, R. H. Jordan, cis-Benzalacetophenone, *J. Am. Chem. Soc.* **1950**, *72(9)*, 4090–4091.

[380] L. P. Kuhn, R. E. Lutz, C. R. Bauer, A Spectroscopic Study of cis- and trans-Dibenzoylethylenes and Related Compounds, *J. Am. Chem. Soc.* **1950**, *72(11)*, 5058–5063.

[381] F. M. E. Abdel-Megeid, A. K. Bose, M. A.-F. Elkaschef, A. Elsayed, K.-E. M. Mokhtar, S. D. Sharma, Benzophenone-sensitized Irradiation of Chalkone, *Indian J. Chem.* **1975**, *13*, 482–484.

[382] J. Träger, S. Härtner, J. Heinzer, H.-C. Kim, N. Hampp, Two-photon-induced cycloreversion reaction of chalcone photodimers, *Chem. Phys. Lett.* **2008**, *455*, 307–310.

[383] M. B. Smith, J. March, *March's advanced organic chemistry*, 5th ed., Wiley, New York, **2001**.

[384] F. D. Lewis, T. Wu, E. L. Burch, D. M. Bassani, J.-S. Yang, S. Schneider, W. Jäger, R. L. Letsinger, Hybrid Oligonucleotides Containing Stilbene Units. Excimer Fluorescence and Photodimerization, *J. Am. Chem. Soc.* **1995**, *117*, 8785–8792.

[385] D. G. Amirsakis, A. M. Elizarov, M. A. Garcia-Garibay, P. T. Glink, J. F. Stoddart, A. J. P. White, D. J. Williams, Diastereospecific Photochemical Dimerization of a Stilbene-Containing Daisy Chain Monomer in Solution as well as in the Solid State, *Angew. Chem. Int. Ed.* **2003**, *42(10)*, 1126–1132.

[386] G. Ciamician, P. Silber, Chemische Lichtwirkung, *Ber. Dtsch. Chem. Ges.* **1902**, *35*, 4128–4131.

[387] G. S. Hammond, C. A. Stout, A. A. Lamola, Mechanisms of Photochemical Reactions in Solution. XXV. The Photodimerization of Coumarin, *J. Am. Chem. Soc.* **1964**, *86*(15), 3103–3106.

[388] H. Morrison, C. H., T. McDowell, Solvent Effects on the Photodimerization of Coumarin, *J. Am. Chem. Soc.* **1966**, *88(23)*((23)), 5415–5419.

[389] F. D. Lewis, S. V. Barancyk, Lewis Acid Catalysis of Photochemical Reactions. 8. Photodimerization and Cross-Cycloaddition of Coumarin, *J. Am. Chem. Soc.* **1989**, *111*, 8653–8661.

[390] S. C. Shim, B. M. Jeong, Y. H. Paik, Photodimerization of 5,7-Dimethoxycoumarin, *Bull. Korean Chem. Soc.* **1992**, *13(6)*((6)), 684–688.

[391] T. J. Brett, J. M. Alexander, J. J. Stezowski, Chemical insight from crystallographic disorder-structural studies of supramolecular photochemical systems. Part 3. The β-cyclodextrin-7-hydroxy-4-methylcoumarin inclusion complex: direct observations of photodimerization by X-ray crystallography, *J. Chem. Soc., Perkin Trans. 2* **2000**, 1105–1111.

[392] H.-C. Kim, S. Kreiling, A. Greiner, N. Hampp, Two-photon-induced cycloreversion reaction of coumarin photodimers, *Chem. Phys. Lett.* **2003**, *372(5-6)*, 899–903.

[393] K. Gnanaguru, K. Ramasubbu N. Venkatesan, R. V., A Study on the Photochemical Dimerization of Coumarins in the Solid State, *J. Org. Chem* **1985**, *50(13)*(50), 2337–2346.

[394] S. Perny, J. Le Barny, P. Delaire, T. Buffeteau, C. Sourisseau, I. Dozov, S. Forget, P. Martinot-Lagarde, Photoinduced orientation in poly(vinylcinnamate) and poly(7-methacryloyloxycumarin) thin films and the consequences on liquid crystal alignment, *Liq. Cryst.* **2000**, *27(3)*(3), 329–340.

[395] D. D. Perrin, W. L. F. Armarego, *Purification of laboratory chemicals*, 4$^{\text{th}}$ ed., Butterworth-Heinemann, Oxford, **2000**.

[396] P. Haaland, M. J., The art and science of thin film coating: A progress report, *Solid State Technol.* **1995**, *38(4)*, 83–89.

[397] S. F. Kistler, S. P. M., *Liquid Film Coating*, 3$^{\text{rd}}$ ed., Chapman & Hall, London, **1997**.

[398] D. E. Bornside, C. W. Macosko, L. E. Scriven, On the Modeling of Spin Coating, *J. Imag. Technol.* **1987**, *13(4)*, 122–130.

[399] D. J. Whitehouse, *Surfaces and their measurement*, Kogan Page Science, London, **2002**.

[400] D. J. Whitehouse, *Handbook of surface and nanometrology*, Institute of Physics Publishing, Bristol, **2003**.

[401] P. K. Tien, R. Ulrich, R. J. Martin, Modes of Propagating Light Waves in Thin Depositied Semiconductor Films, *Appl. Phys. Lett.* **1969**, *14(9)*, 291–294.

[402] P. K. Tien, Light Waves in Thin Films and Integrated Optics, *Appl. Opt.* **1971**, *10(11)*, 2395–2413.

[403] R. Ulrich, R. Torge, Measurement of Thin Film Parameters with a Prism Coupler, *Appl. Opt.* **1973**, *12(12)*, 2901–2908.

[404] J. H. Harris, R. Shubert, J. N. Polky, Beam Coupling to Films, *J. Opt. Soc. Am.* **1970**, *60(8)*, 1007–1016.

[405] P. K. Tien, R. Ulrich, Theory of Prism-Film Coupler and Thin-Film Light Guides, *J. Opt. Soc. Am.* **1970**, *60(10)*, 1325–1337.

[406] R. Ulrich, Theory of the Prism-Film Coupler by Plane-Wave Analysis, *J. Opt. Soc. Am.* **1970**, *60(10)*, 1337–1350.

[407] F. Goos, H. Hänchen, Ein neuer und fundamentaler Versuch zur Totalreflexion, *Ann. Phys.* **1943**, *436(7-8)*, 333–346.

[408] *Model 2010 Prism Coupler Operating and Maintanance Guide*, Metricon Corp., Pennington, **1991**.

[409] R.-P. Herr, F. Herzog, A. Schuster, Cumarin and Quinoline Derivatives for Preparing Liquid Crystal Orientation Layers, Int. Patent Application WO 1996/10049, **1996**.

[410] M. Obi, S. Morino, K. Ichimura, The reversion of Photoalignment of a Liquid Crystal induced by a Polymethacrylate with Coumarin Side Chains, *Macromol. Rapid Commun.* **1998**, *19(12)*(12), 643–646.

[411] S.-K. Kang, W.-S. Kim, B.-H. Moon, An Effective Method for the Preparation of ω-Bromoalkanols from α,ω-Diols, *Synthesis* **1985**, 1161–1162.

[412] J. M. Chong, M. A. Heuft, P. Rabbat, Solvent Effects on the Monobromination of α,ω-Diols: A Convenient Preparation of ω-Bromoalkanols, *J. Org. Chem.* **2000**, *65(18)*, 5837–5838.

[413] Y. Chen, K. H. Chen, Synthesis and Reversible Photocleavage of Novel Polyurethanes Containing Coumarin Dimer Components, *J. Polym. Sci. A: Polym. Chem.* **1997**, *35*, 613–624.

[414] R. P. Wayne, *Principles and applications of photochemistry*, Oxford University Press, Oxford, **1988**.

[415] T. W. Greene, P. G. M. Wuts, *Protective Groups in Organic Syntesis*, 3rd ed., Wiley, New York, **1999**.

[416] H. E. Winberg, F. S. Fawcett, [2.2]Paracyclophane, *Org. Synth.* **1962**, *42*, 83–87.

[417] H. J. Reich, D. J. Cram, Macro rings. XXXVI. Ring expansion, racemization, and isomer interconversions in the [2.2]paracyclophane system through a diradical intermediate, *J. Am. Chem. Soc.* **1969**, *91(13)*, 3517–3526.

[418] P. Kramer, A. K. Sharma, E. E. Hennecke, H. Yasuda, Polymerization of para-xylylene derivatives (parylene polymerization). I. Deposition kinetics for parylene N and parylene C, *J. Polym. Sci. A: Polym. Chem.* **2003**, *22(2)*, 475–491.

[419] R. H. Kahn, W. E. Burkel, Propagation of pseudo-intimal linings of vascular prostheses, *In Vitro* **1973**, *8(6)*, 451–458.

[420] E. S. Nuwayser, P. B. Mansfield, A. Wechezak, W. E. Kahn, W. E. Burkel, J. B. Boatman, Cultured linings for vascular assist devices, *Trans. Am. Soc. Artif. Intern. Organs* **1973**, *19*, 168–174.

[421] F. R. Tittmann, W. F. Beach, *Parylene coated polypropylene microfibers as cell seeding substrates, in M. Szycher, W.J. Robinson Eds. Synthetic Biomedical Polymers: Concepts and Applications*, Technomic Pub. Co., Westport, **1980**.

[422] *Certificates of Compliance, USP Biological Tests*, NAMSA Incorporated, Northwood.

[423] N. Stark, Literature Review: Biological Safety of Parylene C, *Med. Plast. Biomater.* **1996**, *3(2)*, 30–35.

[424] E. M. Schmidt, J. S. McIntosh, M. J. Bak, Long-Term Implants of Parylene C Coated Microelectrodes, *Med. Bio. Eng. Comp.* **1988**, *26*, 96–101.

[425] F. G. Yamagishi, Investigation of Plasma-Polymerized Films as Primers for Parylene C Coatings on Neural Prothesis Material, *Thin Solid Films* **1991**, *202*, 39–50.

[426] A. Thornton, Conformal Coatings for Pacemaker Applications, *NBS Spec. Publ.* **1979**, *400(50)*, 109–113.

[427] D. Devanathan, R. Carr, Polymeric Conformal Coatings for Implantable Electronic Devices, *IEEE Trans. Biomed. Engin.* **1980**, *27(11)*, 671–675.

[428] J. S. Seixas de Melo, R. S. Becker, A. L. Macanita, Photophysical Behavior of Coumarins as a Function of Substitution and Solvent: Expermiental Evidence for the Existence of a Lowest Lying $^1(n, \pi^*)$ State, *J. Phys. Chem.* **1994**, *98(24)*(24), 6054–6058.

[429] J. Brandrup, E. H. Immergut, E. A. Grulke, A. Abe, D. R. Bloch, *Polymer Handbook*, 4th ed., Wiley, New York, **2003**.

[430] H.-G. Elias, *Makromoleküle*, 6th ed., Wiley-VCH, Weinheim, **2003**.

[431] K. Kato, The osmium tetroxide procedure for light and electron microscopy of ABS plastics, *Polym. Eng. Sci.* **1967**, *7(1)*, 38–39.

[432] J. A. Zuclich, J. S. Connolly, Ocular damage induced by near-ultraviolet laser radiation, *Invest. Ophthalmol.* **1976**, *15(9)*, 760–764, investigative Ophthalmology.

[433] D. M. Schwartz, Light-adjustable lens, *Trans. Am. Ophthalmol. Soc.* **2003**, *101*, 417–436.

[434] W. T. Ham Jr., H. A. Mueller, J. J. Ruffolo Jr., D. Guerry III, R. K. Guerry, Action spectrum for retinal injury from near-ultraviolet radiation in the aphakic monkey, *Am. J. Ophthalmol.* **1982**, *93*(3), 299–306.

[435] K. D. Belfield, M. V. Bondar, Y. Liu, O. V. Przhonska, Photophysical and photochemical properties of 5,7-dimethoxycoumarin under one- and two-photon excitation, *J. Phys. Org. Chem.* **2003**, *16*, 69–78.

[436] S. Härtner, H.-C. Kim, N. Hampp, Photodimerized 7-hydroxycoumarin with improved solubility in PMMA: Single-photon and two-photon-induced photocleavage in solution and PMMA films, *J. Photochem. Photobiol. A: Chem.* **2007**, *187*, 242–246.

6 List of Abbreviations

ACN	acetonitrile
ASCRS	The American Society of Cataract and Refractive Surgery
BMA	butyl methacrylate
BMI	body mass index
BTE	bis(thiophen-3-yl)ethene
c_0	speed of light in vacuum ($2.99792458 \cdot 10^8\ \mathrm{m\,s^{-1}}$)
c_m	speed of light in a given medium
CSR	cataract surgery rate
D	diopter
	(the reciprocal of the focal length measured in meters)
DMF	*N*,*N*′-dimethylformamide
ϵ_0	magnetic constant
ECCE	extra-capsular cataract extraction
EGDMA	ethylene glycol dimethacrylate
eq.	equivalent
FDA	U.S. Food and Drug Administration
HEMA	hydroxyethyl methacrylate
HOMO	highest occupied molecular orbital
HPLC	high performance liquid chromatography
HRMS	high resolution mass spectra
ICCE	intra-capsular cataract extraction
IOL	intraocular lens
LASIK	laser-assisted in situ keratomileusis
LUMO	lowest unoccupied molecular orbital
μ_0	magnetic constant
$\bar{M}_\mathrm{n}$	number average molar mass
$\bar{M}_\mathrm{w}$	weight average molar mass
MAOC	7-methacryloyloxycoumarin

OD	optical density
PCO	posterior capsule opacification
PDI	polydispersity index ($\bar{M}_w / \bar{M}_n$)
PEG	poly(ethylene glycol)
PET	poly(ethylene terephthalate)
PHEMA	poly(hydroxyethyl methacrylate)
PMAOC	poly(7-methacryloyloxycoumarin)
PMAOChalc	poly(4′-methacryloyloxychalcone)
PMAOS	poly(4-methacryloyloxystilbene)
PMMA	poly(methyl methacrylate)
ppm	parts per million
PTFE	poly(tetrafluoroethene)
PVCi	poly(vinyl cinnamate)
rpm	revolutions per minute
SI	Le Système International d'Unitéas (engl. The International System of Units)
SOMO	single occupied molecular orbital
TEM	transmission electron microscope
YAG	yttrium aluminium garnet

Danksagung

An dieser Stelle möchte ich mich bei all jenen bedanken, die mich bei Erreichen meiner wissenschaftlichen Ziele und bei der Erstellung dieser Arbeit unterstützt haben.

Herrn Prof. Dr. Norbert Hampp danke ich für das interessante Thema, das er mir zur selbständigen Bearbeitung überlassen hat. Weiterhin danke ich Herrn Prof. Hampp dafür, dass er mir die Möglichkeit gab an zahlreichen internationalen Fachtagungen und Messen teilzunehmen, welchen meinen Horizont erweiterten.

Herrn Prof. Dr. Marcus Motzkus danke ich für die freundlichen Übernahme des Zweitgutachtens.

Ich danke allen Mitgliedern des Arbeitskreises für die gute Arbeitsatmosphäre, ihre Diskussionsbereitschaft, Fachkompetenz und ihren guten Humor.

Der ganzen ACTIOL-Abteilung danke ich für die schöne Zeit. Macht weiter so, Ihr seid einfach die beste Mannschaft. Besonderer Dank gilt meinen „Mädels“. Jasmin Heinzer und Janina Förster danke ich für die gewissenhafte Durchführung von Synthesen und Polymerisationen, das Säulen und die Durchführung unzähliger Messungen. Sandra Noll danke ich besonders für die HPLC, LC/MS und GC/MS Messungen, für die äußerst rasche Ausführung der vielen Bestellungen, sowie für die Hilfe in organisatorischen Dingen. Natalia Galka danke ich für die schönen Grafiken, die sie mit Inkscape angefertigt hat und dass ich jetzt weiß was eine Mohr-Westphal’sche Waage ist.

Danke Hee-Cheol Kim für die Hilfe bei optischen und technischen Aufbauten, für die Erstellung von LabView Programmen und die hilfreiche Diskussion. Martin Schraub danke ich für die fruchtvolle Diskussion in Fragen der organischen Synthese.

Roelf-Peter Baumann danke ich für die gewissenhafte Durchsicht dieser Arbeit und weiterer Manuskripte und für die vielen Vorschläge und Hilfestellungen zur Verbesse-

rung des Englischen. Diese Danksagung gilt als Gutschein für einmal Kübelböck-Film schauen.

Sven Kirchberg danke ich für die rasche Beantwortung meiner vielen Fragen zu LaTeX und Linux.

Herrn Uwe Justus danke ich für die Durchführung der GPC Analysen.

Frank Noll danke ich für die Besorgung diverser Publikationen über Subito.

Ich danke den Studenten Silke Ruck, Kirstin Wenck, Wolfgang Große, Martin Schraub, Stephanie Jung, Andreas Authmann, Andreas Haedler, Gunther Zimmermann und Armin Sandek die im Rahmen der Vertiefungsprojekte des Physikalisch-, Organisch- und Polymerchemischen Fortgeschrittenen-Praktikums einen Beitrag zur Forschung an den optische adaptierbaren IOLs geleistet haben. Den zahlreichen Studenten aus dem Fortgeschrittenen Praktikum der Organischen Chemie danke ich, dass sie uns in Form Auftragspräparaten mit diversen Chemikalien versorgt haben.

Denn Mitarbeitern der Feinmechanik- und Elektronikwerkstatt danke für ihre Hilfe und präzise Anfertigung einiger Teile und Geräte sowie für die produktiven Arbeiten zu den Messeexponaten.

Frau Jutta Hennen, für das bearbeiten der bürokratischen Angelegenheiten, Sie haben einem wirklich viel abgenommen.

Meinen Eltern danke ich, dass sie mich während des Studiums und der Doktorarbeit mit vollstem Vertrauen unterstützt haben.